Anomalous Transport Phenomena on Various Types of Electronic States in Semiconductors

by

Akira Fujimoto

Dissertation on Physics

January 2001

Graduate School of Science

Osaka University

Toyonaka, Osaka

Abstract

The problem of transport property in the semiconductor is in all ages a research subject which contains a lot of bottomless mysteries. Especially the metal-insulator (MI) transition in doped semiconductors has been one of the important subjects over the past years. Below the critical donor concentration for the MI transition, the wavefunction of electrons strongly localizes at a donor site and the electrical conduction is mainly dominated by the hopping process of electrons. In this case the resistivity increases exponentially with decreasing temperature, and the magnetoresistance (MR) is positive due to the shrinkage of the wavefunction of electrons and consequently to the reduced hopping probability. Above the critical donor concentration for the MI transition, on the other hand, the type of the electrical conduction is in the weak localization (WL) regime, and at low temperatures the MR is negative arising from the destructive quantum interference effect. However, in case of the system with strong spin-orbit (SO) interaction, the MR is positive in the weak fields, resulting from the anti-localization (AL) effect.

In this study galvanomagnetic measurements were carried out to investigate the various kinds of electronic conduction as mentioned above for various types of semiconductors such as the bulk crystals and the δ-doped samples of Si:Sb, and thin film InSb, with the donor concentration close to the MI transition. The SO interaction increases with the atomic number Z of the donor as $(Z - Z')^4$, where Z' is the atomic number of the host material. The anomalous transport characteristics in Si:Sb, which are different from those of Si:P and Si:As, are expected, because the atomic number of Sb is much larger than the others. The transport properties of the bulk Si:Sb are analyzed in the light of the hopping as well as the WL regime. The δ-doped samples have a two-dimensional electronic nature and the scattering probability of electrons by doped impurities is much larger than that in the bulk samples. Consequently the AL effect becomes conspicuous. We found that for thin film InSb on GaAs substrate a carrier accumulation layer is formed at the interface between two materials, and it exhibits peculiar behavior. For the temperature dependence of the Hall coefficient the

anomalous peak is observed around 140K, and the MR at low temperatures is positive and shows a steep rise up to 0.3T. We discuss the electronic states in the interface which can explain our experimental results.

We conclude that the present experimental results for temperature and magnetic field dependence of the resistivity and the Hall coefficient originate in the electronic states which strike up hopping conduction, WL effect, electron-electron interaction and SO interaction at low temperatures.

Contents

1 Introduction

The metal-insulator (MI) transition in doped semiconductors has been one of the important subjects in numerous experimental and theoretical investigations over the past years. Fritzsche and Lark-Horovitz [1] have found a negative magnetoresistance effect in p-InSb for the first time in 1955, and Sasaki and Kanai [2] have observed the same effect on Ge:Sb in 1956. However it had taken over 20 years to make clear the physical meaning on the negative magnetoresistance.

For heavily doped semiconductors the wavefunction of the adjoining donor electrons overlap as the donor concentration increases, and thus the transition from the insulator to the metallic phase occurs. Mott [3] has suggested that the transition occurs when the effective Bohr radius of an isolated donor a_B and the Thomas-Fermi's screening length become equal, that is, $N_c^{1/3}a_B \simeq 0.25$ is satisfied, where N_c is a critical concentration of the MI transition. The criterion $N_c^{1/3}a_B \simeq 0.26 \pm 0.05$ has been confirmed from various experiments [4].

As for the MI transition due to the electron correlation effects, it is understood that the transition from insulator to metal occurs when the lower Hubbard band (LHB) (D^0band) and the upper Hubbard band (UHB) (D^-band) overlap [5]. On the other hand, Anderson [6] has proposed that the transition from metal to insulator occurs due to the electron localization. The MI transition occurs when the Fermi energy E_F moves from localized states to extended states, in short, E_F comes at a mobility edge E_C. Because of the existence of two origins, i.e., electron correlation effects (Mott-Hubbard type) and potential fluctuation arising from randomly distributed impurities (Anderson type), it has been more difficult to theoretically figure out the problem of MI transition. There still remains some ambiguity as to whether the MI transition is primarily a Mott-Hubbard type or an Anderson type. The latter mechanism was principally claimed for many-valley semiconductors in which the exchange effect as well as the correlation between carriers stands out.

In addition, the spin-orbit (SO) interaction in the interference effect has been shown to have a drastic influence on the weak localization (WL). In the systems with

the strong SO interaction, the positive magnetoresistance (MR) in the WL regime appears, which is known as the anti-localization (AL) effect. The AL effect has been mainly studied for the metallic thin films over many years [7][8]. On Si:Sb samples with the impurity concentration near the MI transition, Long and Pepper [9] have reported the low-temperature anomaly of the resistivity. Paying attention to the fact that such an anomaly had been never observed in Si:P and Si:As, Kaveh and Mott have argued that the anomaly is based on the scattering effect related to the SO interaction due to the heavy Sb atoms in Si [10].

In the present study we have investigated the temperature and the magnetic field dependence of resistance for various kinds of samples and clarified the mechanism of MI transition and the relevant transport properties. Moreover we discuss the SO interaction effect in the WL regime. We have employed various kinds of samples, such as the bulk samples of Si:Sb, the Si samples with an Sb δ-doped layer and the thin films of InSb on GaAs substrates. We have especially paid attention to the dimensionality of the electronic system and the difference between the bulk crystals and the δ-doped sample. Through the present experiments the positive magnetoresistance (MR) was observed, which is caused by the AL effect due to the SO interaction in the δ-doped sample, but not for the bulk samples. The extraordinary positive MR in the weak magnetic field was observed for a thin-film InSb sample in this study. However such phenomena are not observed for the bulk samples of InSb [11][12][13]. We have found that the MR sensitively reflects the differences of the electronic system.

We have measured the MR of Si:Sb with the Sb concentration just below the critical concentration for MI transition. It is made clear that the resistivity at low temperatures for the sample is dominated by the Efros-Shklovskii (ES)-type variable-range hopping (VRH), which arises from the long-range Coulomb interaction, and then the density of states $N(E)$ has a quadratic dependence on E near E_F. We have investigated the characteristic behavior of the MR under various electric current density and found that the MR strongly depends on the electric current density. For the sample with a non-metallic nature the positive MR is observed in the low current

density region. A crossover from positive- to negative-MR is found as the current density increases. It is considered that these phenomena originate from the rise of the electron temperature and are closely related to the transport in the UHB [14][15].

For the metallic Si:Sb sample whose donor concentration is extremely close to the critical concentration of the MI transition, we have observed a crossover from $d\sigma/dT < 0$ to $d\sigma/dT > 0$ by the application of a magnetic field. It is considered that the term of Hartree type due to direct interaction between electrons becomes larger with increasing magnetic field. The experimental results have been analyzed with the theory of electron-electron (e-e) interaction as well as the theory of VRH. It was found that the result contradicts with the theory of VRH; Moreover the conductivity is ascertained to show stronger dependence on temperature and magnetic field than that expected from the theory of e-e interaction [16].

In addition we have investigated the two-dimensional (2D) electron system of Si:Sb. We have employed some samples with Sb δ-doped layer. In this system the typical 2D electronic system is produced by the quantum confinement effect in the layer. In the δ-doped layer, doped impurities themselves greatly influence the movement of the 2D electrons, which differs from the modulation-doped heterostructures such as GaAs/AlGaAs. We report on the magnetoconductance (MC) of the above-mentioned δ-doped sample, comparing with a bulk Sb doped sample. When the magnetic field was applied perpendicularly to the doping layer with 0.11 monolayer of Sb atoms, the positive MC due to the destruction of the quantum interference effect appears. Interestingly, in very weak fields negative MC appears due to the SO interaction, and the positive MR is observed in parallel fields [17].

On the other hand, for the metallic Si:Sb sample whose donor concentration is 3.7 times of the critical concentration for MI transition, the positive magnetoconductivity is observed between 4.2K and 3.1K. The characteristic feature caused by the AL due to the SO interaction is not explicitly seen. Temperature dependence of conductivity in the absence of magnetic field for the δ-doped sample shows a logarithmic behavior at lower temperatures and that for the bulk sample has the tendency in

proportion to T^1. The obtained results are discussed within the framework of the WL theories.

We have investigated two kinds of samples of InSb, which are thin films grown on GaAs substrate by molecular beam epitaxy (MBE) method. They have enough donor concentration to exceed the critical concentration for MI transition. One of them shows Shubnikov-de Haas oscillation for the MR at low temperatures, and the other shows the peculiar behavior. The temperature dependence of Hall coefficient has a maximum around 140K, which indicates that there are two kinds of electrons with different mobilities, and the resistivity does not show the striking temperature dependence with decreasing temperatures. The MR in the perpendicular configuration shows a drastic rise in the weak magnetic field, then decreases with increasing magnetic field and finally increases again. The obtained results are understood by taking into account the transport by interface carriers in addition to bulk carriers. It is reported that for InSb films grown on GaAs substrate an accumulation interface layer with certain space charges frequently exists. In addition, we found that the MR in InSb film shows the angle dependence for the direction of the applied magnetic field and the rapid rise in the weak magnetic fields even in the parallel configuration. It is considered that the MR mainly arises from the SO interaction in the interface.

2 Theoretical Backgrounds

2.1 Mott's intuitive explanation

In covalent crystals a monatomic donor is generally considered as an impurity like a hydrogen atom. When a donor concentration is small, an electron is bound by a donor at low temperatures and the electron cannot move the whole crystal. In this case the system shows non-metallic nature. For heavily doped semiconductors, on the other hand, the wavefunction of adjacent donor electrons overlap and the electrons can move the whole area of crystal as the donor concentration increases, and as a result a metallic nature appears.

The strength of Coulomb potential for the donor in crystal is much smaller than that for a hydrogen atom. Electrons which gather in the circumference of the positive charge, shield the charge of the positive charge. The screened Coulomb potential thus is expressed with Thomas-Fermi theory,

$$\Phi(r) = -\frac{e}{r}\exp(-\frac{r}{\lambda_{TF}}), \tag{1}$$

where r is the distance between a donor electron and the positive charge located at center and λ_{TF} is the Thomas-Fermi screening length, which is expressed as

$$\lambda_{TF} = (\frac{\kappa E_F}{6\pi n e^2})^{1/2}, \tag{2}$$

where κ is the dielectric constant and n is the carrier concentration. Mott considered that a metal-insulator (MI) transition occurs when the effective Bohr radius $a_D = \kappa\hbar^2/m_e e^2$ is equal to the Thomas-Fermi screening length. Therefore the following formula can be derived.

$$n_C^{1/3} a_D \simeq 0.25, \tag{3}$$

here n_c is the critical concentration for MI transition.

For the samples as InSb with an extremely small effective mass, the effective Bohr radius is very large. Though the wavefunction of the donor electron shrinks under the magnetic field and thereby the effective Bohr radius becomes small, the MI transition induced by the magnetic field occurs in the strong magnetic field. Here the

parameter γ is introduced.

$$\gamma = \frac{\hbar\omega_c}{2Ry} = \frac{a_B}{l_B}, \tag{4}$$

where $\omega_c = eB/m_e$ the cyclotron frequency, Ry the effective donor Rydberg constant and $l_B = (\hbar/eB)^{1/2}$ is the cyclotron radius. As the magnetic field increases, the characteristic size of the wavefunctions of electrons becomes smaller. $a_{//} = a_B/\ln\gamma$ shows the effective Bohr radius in the direction parallel to the field and $a_\perp = 2l_B$ shows one in the perpendicular direction [18]. Thus the volume of the electron wavefunction given by $(a_\perp)^2 a_{//} = 4a_B^3/(\gamma\ln\gamma)$ decreases as B is raised. Once the overlap between the wavefunctions is sufficiently reduced, the MI transition is expected to occur according to the following condition

$$n(a_\perp)^2 a_{//} \simeq \delta^3, \tag{5}$$

where $\delta = 0.25$ is a constant. Various values of δ have been reported by a lot of researchers. For example, Ishida and Otsuka [11] have investigated the critical concentration N_D, as a function of magnetic field and found the critical concentration N_D^c expressed as $N_D^c(a_\perp)^2 a_{//} \simeq (0.26)^3$. This relation was found for magnetic fields up to 1.3T at which a value of $a_\perp/a_{//}$ is ~ 0.55.

2.2 Anderson Localization

Anderson has considered that no diffusion at all can take place in his model "impurity band" [6]. Assuming that the impurity band has the width of level distribution W, which is much larger than $|V|$, where $|V|$ is the transfer energy between two levels. As shown in Fig.2.2.1, when the energy difference between two levels $\Delta E = |E_1 - E_2|$ is sufficiently small compared with $|V|$, the wavefunctions have nearly the same amplitudes on both side. On the other hand, if $\Delta E \gg |V|$, the ratio of the amplitudes is given by $|V|/\Delta E(\ll 1)$. It implies that the inequality

$$\Delta E < |V| \tag{6}$$

should hold for the wavefunctions to extend to neighboring sites. The probability, which the energy level on the nearest neighbor site is in the energy region (6), is given

by $|V|/W$. The $|V|/W$ gives the probability that the wavefunction extends to the neighbor site.

$$P_1 \sim \begin{cases} 1 & (|V| > W) \\ |V|/W & (|V| < W), \end{cases} \tag{7}$$

where P_1 represents the probability that the wavefunction extends to the nearest neighbor site. Using the same argument repeatedly, one finds the probability that the wavefunction extends to the n-th neighbor site is given by

$$P_n \sim L_n(\frac{|V|}{W})^n, \tag{8}$$

where L_n is the number of n-th neighbor site. Since $L_n \propto n^d$ in d dimensions, P_n tends to zero as $n \to \infty$. It means that if $W \gg |V|$ the wavefunctions are all localized and the system of electrons becomes an insulator. Since it is metallic in the limit $W \to 0$, there should be a critical value $(W/|V|)_{cr}$ such that if $W/|V| < (W/|V|)_{cr}$ the system is metallic and it is an insulator otherwise. When randomness (or $W/|V|$) increases, there appears the MI transition at some point.

2.3 Transport in the Impurity Band and Hubbard Model

Fritzsche [1] has explained the experimental results of the temperature dependence of conductivity on Sb-doped Ge (Ge:Sb) using the following formula

$$\sigma = \sigma_1 \exp(-\frac{\epsilon_1}{k_B T}) + \sigma_2 \exp(-\frac{\epsilon_2}{k_B T}) + \sigma_3 \exp(-\frac{\epsilon_3}{k_B T}), \tag{9}$$

where ϵ_1 represents the activation energy of an electron between the Fermi level in the impurity band and the conduction band and ϵ_3 the hopping energy to jump to the nearest donor site. He has suggested that ϵ_2 is the energy between the D^0 and the D^- states. Afterwards Hubbard [5] has theoretically introduced the following Hamiltonian to describe this electronic system.

$$\mathcal{H} = \sum_{ij} \sum_{\sigma} t_{ij} c_{i\sigma}^{+} c_{j\sigma} + \frac{U}{2} \sum_{i} \sum_{\sigma} \tilde{n}_{i\sigma} \tilde{n}_{i-\sigma}. \tag{10}$$

The first term means that an electron in j-th donor site transfers into the i-th site at a transition rate t_{ij}, where $c_{i\sigma}^{+}$ and $c_{j\sigma}$ are the creation operators of electron with

a spin state σ at j site and the annihilation one, respectively. The second term is all the sum of the Coulomb repulsion energy U between electrons with up-spin and down-spin in the same site, where $\tilde{n}_{i\sigma} = c^{+}_{i\sigma}c_{i\sigma}$. With the hydrogenic 1s wavefunction

$$\Psi_{1s}(r) = (\pi a_D^3)^{-1/2} \exp(-\frac{r}{a_D}), \tag{11}$$

one can calculate the value of U as

$$U = \frac{5}{8}\frac{e^2}{\kappa a_D}. \tag{12}$$

$U(= I - A)$ can be defined as the energy required to transfer an electron from one neutral donor to another one, where I is the ionization energy and A the electron affinity. The Hubbard gap corresponds to the ϵ_2 introduced by Fritzsche. In fact, the value of Hubbard gap is calculated taking the exchange interaction besides the U into account. The band which consists of D^- (D^0) states is called upper (lower) Hubbard band. When ϵ_2 disappears, the upper Hubbard band and the lower one overlap, and then MI transition occurs.

2.4 Scaling Theory

For a long time, it is one of the outstanding problems how the conductivity at 0 K changes as the impurity concentration increases in semiconductor. Mott [19] has considered that a finite jump of the conductivity occurs at the critical concentration. According to him, in the metallic regime the conductivity is given by the used Drude formula,

$$\sigma = \frac{ne^2\tau}{m_e}. \tag{13}$$

Using the Fermi wave number k_F and the mean free path $l = v_F\tau$, where v_F is the Fermi velocity, the conductivity (eq.(13)) is written as

$$\sigma \sim \frac{e^2}{\hbar}k_F^{d-1}l, \tag{14}$$

here d is the dimension of the system. In dirty metal, l might be short, but can never be shorter than the lattice constant. Therefore the relation $k_F l \geq 1$ should be

established. This suggests that the metallic conductivity has a minimum value.

$$\begin{aligned} \sigma_{min} &\sim \frac{e^2}{\hbar} k_F^{d-2} \\ &= \frac{0.03e^2}{\hbar a}. \end{aligned} \tag{15}$$

After the advent of the scaling theory, the concept of Mott's minimum metallic conductivity was denied. A useful method to deduce the conductivity is the numerical calculation using computers. However, the calculation is limited to the system with a finite size L. Thouless *et al.* [20] have investigated the difference of energy between the some systems which have the various length.

Abrahams, Anderson, Licciardello and Ramakrishnan have proposed the scaling theory [21]. They have considered how the dimensionless conductance $g(L)$ changes as the system size L varies. The following equation is defined as the scaling function.

$$\beta(g(L)) = \frac{d \ln g(L)}{d \ln L}. \tag{16}$$

When $\beta(g(L))$ is positive (negative), the wavefunction of electrons is always extended (localized). The qualitative behavior can be clarified by considering two limiting cases as L increases, that is, $g \to \infty$ and $g \to 0$. In the limit $g \to \infty$, the system behaves as a metal so that the conductivity σ can be defined independently of the system size. Then $g(L)$ is given by

$$g(L) \propto \sigma L^{d-2}, \tag{17}$$

where d represents a dimension of the system. From eqs.(16) and (17),

$$\beta(g) \simeq d - 2. \tag{18}$$

In the limit $g \to 0$, the system tends to be an insulator and the conductance vanishes exponentially as

$$g(L) \sim \exp(-c\frac{L}{L_A}), \tag{19}$$

where c is a constant of the order of unity. Then one gets

$$\beta(g) \propto \frac{1}{\ln g}. \tag{20}$$

The behavior of $\beta(g)$ for $d = 1, 2, 3$ is shown in Fig 2.4.1. The following conclusion is made. (1) In one and two dimensions (2D) the wavefunction of electrons is always localized. For 2D system, however, the conclusion is not always correct, if the electron-electron interaction is considered. (2) In three dimensional (3D) system the MI transition takes place depending on the circumstances.

Especially in the case of 2D system of the large g, the conductivity decreases logarithmically as the system size increases, i.e., one may assume $\beta(g)$ tends to zero as

$$\beta(g) \simeq -\frac{\alpha}{g}. \tag{21}$$

Then eq.(21) is integrated as

$$g(L) \simeq g_0 - \alpha \ln(\frac{L}{L_0}), \tag{22}$$

where g_0 is the initial value of g, i.e., $g_0 = g(L_0)$. The logarithmic decrease of g shows a precursor effect of localization.

In case of large conductance g for 3D system, the function $\beta(g)$ is expressed as

$$\beta(g) \sim 1 - \frac{\alpha'}{g}. \tag{23}$$

where α' is a constant of the order of unity. Putting eq.(23) into eq.(16), the following equation is obtained.

$$\frac{dg}{g - \alpha'} = \frac{dL}{L} \tag{24}$$

Assuming that the conductance in the limit of $L \to \infty$ is given by $g = \sigma_0 L$, the conductivity σ is expressed as

$$\sigma \simeq \sigma_0 + \frac{\alpha'}{L}. \tag{25}$$

For the metallic region in 3D system, the conductivity decreases as the size of the system increases. The term, which depends on the size, corresponds to the weak localization effect.

At a first glance, it seems that the size dependence of conductivity such as eqs.(22) and (25) can never be observed in macroscopic systems. In real systems electrons interact with one another and with phonons. At finite temperatures electrons

are scattered inelastically by these interactions. If the inelastic scattering occurs before electron reaches the boundary of the region of localization, the memory of the phase of the wavefunction is lost there. Then the electron starts again the quantum diffusion from that point. In this way, the electron can arrive at the boundary of the system by the help of the inelastic scattering. The conductivity is given by eqs.(22) and (25) with replacement of L by the length L_ϵ to which an electron propagates by diffusion within the inelastic relaxation time τ_ϵ. Denoting the diffusion constant by $D(= v_F^2\tau/d)$, L_ϵ is given by the diffusion equation as

$$L_\epsilon = \sqrt{D\tau_\epsilon}. \tag{26}$$

The probability of the inelastic scattering $1/\tau_\epsilon$ vanishes at zero temperatures, and is given at finite temperatures as

$$\frac{1}{\tau_\epsilon} \propto T^p \quad (p > 0). \tag{27}$$

Substituting eqs.(26) and (27) in eqs.(22) and (25)

$$\Delta\sigma_2(T) \propto p \ln T \quad \text{(2D)}, \tag{28}$$

and

$$\Delta\sigma_3(T) \propto T^{p/2} \quad \text{(3D)}, \tag{29}$$

one finds the conductivity for 2D decreases logarithmically with decreasing temperature. According to the calculation of conductivity with Kubo formula, the quantum correction for the conductivity is given by

$$\Delta\sigma_2(T) = -\frac{e^2}{2\pi^2\hbar}\ln(\frac{\tau_\epsilon}{\tau}) = \frac{pe^2}{2\pi^2\hbar}\ln T. \tag{30}$$

2.5 Weak Localization

In the simple case, a progressive wave $e^{i\boldsymbol{k}\cdot\boldsymbol{r}}$ attributed to an electron interferes with the scattering wave $e^{-i\boldsymbol{k}\cdot\boldsymbol{r}}$ when the backward scattering occurs strongly. Due to the superposition of these two waves, the standing wave is generated and electrons localize. The interference effect is the precursor of the formation of the localized states for electrons.

2.5.1 Bergmann's Treatment

Since the Scaling theory was proposed, a large number of studies on electron localization have been carried out. Bergmann [7] suggested that conductivity should be reduced due to the multiple scattering of electrons by impurities. The electron with the wave-vector $\boldsymbol{k}$ is scattered into a state $\boldsymbol{k}_1'$, then into a state $\boldsymbol{k}_2'$, and finally into a state $-\boldsymbol{k}$. This scattering sequence,

$$\boldsymbol{k} \rightarrow \boldsymbol{k}_1' \rightarrow \boldsymbol{k}_2' \rightarrow \cdots \rightarrow -\boldsymbol{k}, \tag{31}$$

is drawn in Fig.2.5.1 There is an equal probability for the electron with $\boldsymbol{k}$ to be scattered from $\boldsymbol{k}$ to $-\boldsymbol{k}$ through another process.

$$\boldsymbol{k} \rightarrow \boldsymbol{k}_1'' \rightarrow \boldsymbol{k}_2'' \rightarrow \cdots \rightarrow -\boldsymbol{k}. \tag{32}$$

For the two processes the amplitude in the final state is the same. If the amplitudes A_R and A_L in the final state are in-phase, the total intensity is given by

$$|A_R + A_L|^2 = |A_R|^2 + |A_L|^2 + A_R^* A_L + A_R A_L^* = 4|A|^2. \tag{33}$$

As a result of quantum interference, both $A_R^* A_L$ and $A_R A_L^*$ are $|A|^2$. If the two amplitudes were out-of-phase, the total intensity becomes $2|A|^2$. This means that the scattering intensity is larger than that of the classical scattering by $2|A|^2$. In case that the spin-orbit (SO) interaction is strong, the total intensity is $|A|^2$.

2.5.2 Expression for Magnetoconductance

Under the magnetic field, the component of vector potential

$$\exp(i\frac{e}{\hbar}\int A \cdot r), \tag{34}$$

is added to the phase factor of electron wavefunction, and thus the magnetic field breaks the time reversal symmetry of the system. Then the phase shift between two waves induced by the magnetic field is $2e\Phi/\hbar$. Accordingly the quantum interference effect is destroyed by application of the magnetic field, and the electron localization

effect is defused and conductivity increases. Therefore negative magnetoresistance (MR) can be experimentally observed.

In other words, the effect of the weak localization is caused by the interference of two electron waves which are scattered by impurities but propagate in the opposite directions along the same closed trajectory, and return to the origin with equal phases. Therefore, it leads to a suppression of conductivity.

For two dimensional (2D) system, Hikami, Larkin and Nagaoka [22] have developed the theory with ladder diagram, including the SO interaction. In the weak magnetic field

$$\Delta\sigma(B) = \frac{e^2}{2\pi^2\hbar}[\frac{3}{2}\Psi(\frac{1}{2}+\frac{l_B^2}{4D\tau_1}) - \ln\frac{l_B^2}{4D\tau_1} - \frac{1}{2}\Psi(\frac{1}{2}+\frac{l_B^2}{4D\tau_\epsilon}) - \ln\frac{l_B^2}{4D\tau_\epsilon}] \tag{35}$$

and

$$\frac{1}{\tau_1} = \frac{4}{\tau_{so}} + \frac{1}{\tau_\epsilon}, \tag{36}$$

where l_B is the cyclotron radius, and the magnetic scattering τ_s is ignored. If the SO interaction is weak,

$$\Delta\sigma(B) = \frac{e^2}{2\pi^2\hbar}\Psi(\frac{1}{2}+\frac{l_B^2}{4D\tau_\epsilon} - \ln\frac{l_B^2}{4D\tau_\epsilon}). \tag{37}$$

Especially they have expanded eq.(37) for $4D\tau_\epsilon/l_B^2 << 1$

$$\Delta\sigma(B) = \frac{e^2}{48\pi^2\hbar}(\frac{4DeB\tau_\epsilon}{\hbar})^2 \tag{38}$$

for $4D\tau_\epsilon/l_B^2 >> 1$

$$\Delta\sigma(B) = \frac{e^2}{2\pi^2\hbar}\ln(\frac{4DeB\tau_\epsilon}{\hbar}). \tag{39}$$

For three dimensional (3D) system, Kawabata [23] has developed the theory with use of Feynman graph method under the condition that $k_F l > 1$, $\omega_c\tau < 1$ and $l/l_B < 1$, where k_F is the Fermi wavenumber, $l = v_F\tau$: the mean free path and $\omega_c = eB/m_e$: the cyclotron angular frequency. Then he defines $\Delta\sigma$ as its difference from the value at $H = T = 0$.

$$\Delta\sigma(H,T) = \Delta\sigma_a(H,T) + \Delta\sigma_b(T), \tag{40}$$

where $\Delta\sigma_1(H,T)$ is the magnetoconductivity (MC) and expressed as

$$\Delta\sigma_a(H,T) = \frac{e^2}{2\pi^2\hbar l_B}F(\delta), \tag{41}$$

with

$$F(\delta) = \sum_{N=0}^{\infty} (2[\sqrt{N+1+\delta} - \sqrt{N+\delta}] - \frac{1}{\sqrt{N+1/2+\delta}}), \tag{42}$$

where $\delta = l_B^2/l_\epsilon^2$ and $l_\epsilon = 2\sqrt{D\tau_\epsilon}$: inelastic scattering length. For $\delta \ll 1$ (at high magnetic field or low temperature), he expands the right-hand side of eq.(42) in δ as

$$F(\delta) = 0.605 - 2\sqrt{\delta} + 2.39\delta. \tag{43}$$

and the leading term of $\Delta\sigma_1$ is

$$\Delta\sigma_a(H,0) = 2.90\sqrt{H}. \tag{44}$$

For $\delta \gg 1$ (at low magnetic field), he expands the right-hand side of eq.(42) in power of $1/(N+1/2+\delta)$, and

$$F(\delta) = \frac{1}{32}\sum_{N=0}^{\infty}(N+\frac{1}{2}+\delta)^{-5/2} = \frac{\delta^{-3/2}}{48}, \tag{45}$$

then

$$\Delta\sigma_a(H,T) = \sigma_0(\frac{\tau_\epsilon}{\tau})^{3/2}(\frac{eH\tau}{m_e c})^2 = CH^2. \tag{46}$$

From the experimental data on MC the inelastic scattering time τ_ϵ and the SO scattering one τ_{so} are estimated. And one can see a crossover from B^2-dependence to $\sqrt{B}$-one of the conductivity [24].

2.5.3 Physical Viewpoint of Weak Localization

The physical viewpoint of weak localization is discussed from now. It is crucial that the impurity potential,

$$V(\boldsymbol{r}) = \sum_{i=1} v(\boldsymbol{r} - \boldsymbol{R}_i), \tag{47}$$

has the time reversal symmetry. Here $v(\boldsymbol{r})$ is the respective impurity potentials and $\boldsymbol{r}_i$ the position of the impurity. Due to the symmetry, the matrix element for the scattering from $|\boldsymbol{k}>$ to $|\boldsymbol{k}'>$ should be the same as that from $|-\boldsymbol{k}'>$ to $|-\boldsymbol{k}>$: i.e.,

$$< \boldsymbol{k}'|V|\boldsymbol{k} > = < -\boldsymbol{k}|V|-\boldsymbol{k}' > . \tag{48}$$

The same symmetry holds for all matrix elements of higher order. The third order matrix element is illustrated in Fig.2.5.2.

If one puts $\boldsymbol{k}'=-\boldsymbol{k}$ here, both of the two different processes contribute to the backward scattering. Usually scattered waves of different scattering processes are incoherent due to the random distribution of impurities, and do not interfere with one another. In this case, however, two scattered waves of the reversed processes have the same phase due to the time reversal symmetry, and the interference takes place. The backward scattering is strengthened by the quantum interference, which results in the decrease of the conductivity. The detailed derivation is described in § 6 Appendix.

2.6 Spin-orbit interaction

The matrix element of the spin-orbit (SO) scattering is given by

$$< \boldsymbol{k}', \sigma' | V_{so} | \boldsymbol{k}, \sigma >= iu \sum_i e^{i(\boldsymbol{k}-\boldsymbol{k}')\cdot \boldsymbol{R}_i} (\boldsymbol{k} \times \boldsymbol{k}') \cdot \boldsymbol{s}_{\sigma\sigma'}, \tag{49}$$

where $\boldsymbol{s}$ denotes the spin matrix of electrons. In this case, the relation of the time reversal symmetry is given by,

$$< \boldsymbol{k}', \sigma' | V_{so} | \boldsymbol{k}, \sigma >=< -\boldsymbol{k}, \sigma | V_{so} | -\boldsymbol{k}', \sigma' > . \tag{50}$$

In order to explore whether the quantum interference effect is concerned, one has to know the phase relation between

$$< \boldsymbol{k}', \sigma' | V_{so} | \boldsymbol{k}, \sigma > \text{ and } < -\boldsymbol{k}, \sigma' | \mathrm{V_{so}} | -\boldsymbol{k}', \sigma > . \tag{51}$$

And one finds

$$< \boldsymbol{k}', \sigma' | V_{so} | \boldsymbol{k}, \sigma >= - < -\boldsymbol{k}, \sigma' | V_{so} | -\boldsymbol{k}', \sigma > . \tag{52}$$

The above relation means that two waves scattered backward by the reversed processes have the opposite phase and disappear by superposition. As a result, the backward scattering is weakened in this case, which leads to the increase of the conductivity (anti-localization). Due to the SO interaction, magnetoresistance (MR) is positive.

On Si:Sb samples with the impurity concentration near the metal-insulator transition, the low-temperature anomaly for the resistivity [9] has been reported and ascribed to the effect due to the SO interaction [10]. The interaction increases with the atomic number Z of the donor as $(Z-Z')^4$, where Z' is the atomic number of the host material, i.e., 14 for silicon. The anomaly for the resistivity has not been observed in Si:P ($Z = 15$ for P) and Si:As ($Z = 33$ for As).

It is recognized that two types of SO interaction can be identified. One is due to the random impurity potentials of individual scattering centers, which leads to the anti-localization (AL) effect. The other occurs in the systems which lack inversion symmetry. So far Greene *et al.* [25] has reported that the low-field MR of InSb-CdTe heterojunction is positive, which illustrates the importance of the zero-field spin splitting for the space-charge layer in narrow gap semiconductor. For GaAs/AlGaAs MOSFET the positive MR due to the SO scattering is observed [26], which arises from the crystal-field-induced spin splitting.

In order to investigate the AL effect due to the SO interaction, so far, metallic thin films have been employed. Bergmann has reported on positive MR with thin Mg-films covered with some amounts of Au atoms [27]. The superposition with Au increases SO scattering and the magnitude of positive MR is larger with increasing the amount of Au. Komori *et al.* [28] have examined the magnetoconductance (MC) for the Cu films, Cu-Ag films and Cu-Au films. It is indicated that the MC is mainly due to the localization effect with SO interaction.

2.7 Electron-electron interaction

When electrons localize due to the random potential, the electron-electron (e-e) interaction has a great influence on the electron localization. These interactions are classified into two different channels.

(1) The Cooper channel, which is also called the particle-particle channel, describes the interaction between electrons of antiparallel wavenumber. The effect produces a positive MR due to the orbital interference.

(2) The diffusion channel, which is also called particle-hole channel, describes the interaction between electrons of parallel wavenumber. The Zeeman effect leads to a positive MR [29].

For two-dimensional (2D) system Fukuyama [30] has examined the correction terms in the transport coefficient of e-e interaction. The interaction theory leads to the following result of the total relaxation time,

$$\frac{1}{\tau_{tot}} = \frac{1}{\tau}[1 + \frac{g}{2\pi\epsilon_F\tau}\ln\frac{1}{4\pi\tau T}], \tag{53}$$

$$g = g_1 + g_2 - 2(g_3 + g_4), \tag{54}$$

where τ is the relaxation time due to impurity scattering and g_i ($i = 1, 2, 3$ and 4) are dimensionless coupling constants characterizing four distinct processes as for e-e interaction. g_1 and g_3 (g_2 and g_4) processes are derived by the diffusion (Cooper) channel interaction. And g_1 and g_2 (g_3 and g_4) processes represent the exchange (Hartree) interaction. Temperature and magnetic field dependence of conductance reflect these interactions.

For three-dimensional (3D) system, Altshuler and Aronov [31] has developed the theory under the condition $k_F l > 1$, where k_F is the Fermi wavenumber and l the mean free path. As for the temperature dependence of conductivity, $T^{1/2}$ correction, resulting from e-e interaction in the presence of strong impurity scattering, was calculated as

$$\Delta\sigma_I(n, T) = m(n)T^{1/2}, \tag{55}$$

where $m(n)$ depends on the impurity concentration and reflects the exchange and the Hartree interaction. Moreover, the importance of e-e interaction for the density of states (DOS) $N(E)$ near the Fermi energy E_F has been suggested. Altshuler and Aronov showed DOS have square-root dependence,

$$N(E) = N(E_F)(1 + (\frac{|E - E_F|}{\Delta})^{1/2}), \tag{56}$$

where $\Delta \simeq \hbar D/l^2$, D the diffusion constant and l the mean free path.

Altshuler *et al.* have suggested an expression of the magnetoconductivity due

to the DOS corrections caused by the Cooper channel interaction [32] for the 2D and 3D cases. The formula is expressed as,

$$\Delta\sigma(B,T) = -\alpha\frac{e^2}{2\pi^2\hbar}g(B,T)\sqrt{\frac{eB}{\hbar}}\varphi_3(\frac{2DeB}{\pi k_B T}), \tag{57}$$

where α is a constant and $g(B,T)$ is the renormalized coupling constant. This expression is in the weak magnetic field regime for a one-valley semiconductor. Another form of $g(B,T)$ has been calculated by McLean and Tsuzuki [33] who give

$$g^{-1}(B,T) = \ln(\frac{T_F}{T}) + \Psi(\frac{1}{2}) - \Psi(\frac{1}{2} + \frac{DeB}{2\pi k_B T}), \tag{58}$$

where $\Psi(x)$ is the digamma function. The function φ_3 is defined for long phase coherence times by

$$\varphi_3(x) = \sqrt{\frac{\pi}{2x}}\int_0^\infty \frac{\sqrt{t}}{\sinh^2 t}(1 - \frac{xt}{\sinh(xt)})dt. \tag{59}$$

Especially,

$$\varphi_3(x) = \begin{cases} 1.90 & x \gg 1, \\ \frac{5\pi}{64}\zeta(\frac{5}{2})x^{3/2}/4 & x \ll 1, \end{cases} \tag{60}$$

where $\zeta(y)$ is the Riemann zeta function. For 2D Altshuler *et al.* have expressed as

$$\Delta\sigma_I(B,T) = -\alpha\frac{e^2}{2\pi^2\hbar}g(B,T)\varphi_2(\frac{2DeB}{\pi k_B T}), \tag{61}$$

and

$$\varphi_2(x) = \int_0^\infty \frac{t}{\sinh^2 t}(1 - \frac{xt}{\sinh(xt)})dt. \tag{62}$$

Especially,

$$\varphi_2(x) = \begin{cases} \ln x & x \gg 1 \\ \zeta(3)x^2/4 & x \ll 1, \end{cases} \tag{63}$$

is expressed.

2.8 Review of the Temperature Dependence of Conductivity

For three-dimensional (3D) system in the absence of magnetic field,

$$\sigma(T) = \sigma_3(0) + mT^{1/2} + BT^{p/2}, \tag{64}$$

where $\sigma_3(0)$ is the zero-temperature conductivity for 3D system. The second term and the third one are due to the electron-electron (e-e) interactions and the localization,

respectively. The localization generally gives $\Delta\sigma \sim T^{p/2}$ when an inelastic scattering time τ_ϵ varies as T^{-p}. The e-e interaction theory gives the following formula for the coefficient m taking mass anisotropy into account [34].

$$m = S_0 \frac{e^2}{2\pi^2\hbar} 0.46 (k_B/D\hbar)^{1/2} (\frac{4}{3} - 4F) \tag{65}$$

and

$$F = \frac{1}{\pi} \int_0^\pi \frac{dq}{1 + (2k_F/q_s)\sin(q/2)}, \tag{66}$$

where F is the Hartree factor, which is introduced by Altshuler *et al.* [35]. Taking the correlation effect into account [36][37], F is simply expressed as $F = [\ln(1+x)]/x$. Here, $x = (2k_F/K)^2$, k_F the Fermi wavenumber and K the Thomas-Fermi screening wave vector. q_s the reciprocal screening length given by Ando *et al.* [38]. The factor 4/3 results from the exchange term. And

$$S_0 = \frac{1}{\nu} \sum_{i=1}^{\nu} m_e [\frac{\sin^2\theta_i}{m_t} + \frac{\cos^2\theta_i}{m_l}], \tag{67}$$

where $m_e = (m_t^2 m_l)^{1/3}$, θ_i is the angle between the current and the axis of the spheroidal energy surface of the ith valley and ν the number of the valleys.

For two-dimensional (2D) system

$$\sigma(T) = \sigma_2(0) + \Delta\sigma(T), \tag{68}$$

where $\sigma_2(0)$ is the zero-temperature conductance for 2D system.

$$\Delta\sigma(T) = \alpha_T \frac{e^2}{2\pi^2\hbar} \ln T, \tag{69}$$

where $\alpha_T = p + g$ and the inelastic scattering time can be written $\tau_\epsilon \propto T^{-p}$. g is defined in §2.7.

2.9 Hopping Conduction

2.9.1 Nearest-Neighbor Hopping Conduction

Below the critical concentration for the metal-insulator (MI) transition, electrons localize on the sites of impurities at low temperatures, but they can hop from one

localized state to another by absorbing phonons. The concept was first introduced by Miller and Abrahams [39] and they supposed that an electron on an occupied site would normally jump to a nearest site with energy ΔE above it. The hopping probability W is then given by the form

$$W \propto \nu_{ph} \exp(-2\alpha R - \frac{\Delta E}{k_B T}), \tag{70}$$

where ν_{ph} depends on the strength of the interaction with phonons, R the distance between the electrons on the localized states and $\alpha = \xi^{-1}$, where ξ is the localization length. The first term represents the transition probability which depends on the overlap of wavefunctions expressed by $\exp(-\alpha R)$. If αR is small, this term can be ignored, and then the conductivity in the system is expressed as

$$\sigma = \sigma_3 \exp(-\frac{\epsilon_3}{k_B T}), \tag{71}$$

where σ_3 is a prefactor and $\Delta E = \epsilon_3$. This process is sometimes called the nearest-neighbor hopping (NNH) conduction against the variable-range hopping (VRH) conduction at sufficiently low temperatures which is explained in the following section.

2.9.2 Mott's Variable-Range Hopping Conduction

Let me consider the case that αR is not small and the interaction between electrons is not taken into account. An electron just below the Fermi level jumps into a state just above it. In this transfer the energy of ΔE as expressed in eq.(70) is necessary. As the electron jumps farther, the choice of states that the electron encounters is greater, and in general electron will jump to a state for which ΔE is as small as possible. The electron jumps a distance R, and it is necessary that there is a state at least within the distance R in order to hop to another state.

$$\frac{4\pi R^3}{3} \Delta E N(E_F) \simeq 1. \tag{72}$$

The above relation is an expression for three-dimensional (3D) systems. Here $N(E_F)$ is the density of states (DOS) at the Fermi energy E_F. One puts eq.(72) into eq.(70),

so the conductivity is proportional to

$$\exp[-2\alpha R - \frac{3}{4\pi k_B T R^3 N(E_F)}]. \tag{73}$$

And one calculates R_{max} to maximize eq.(73)

$$R_{max} = (\frac{8\pi\alpha k_B T N(E_F)}{9})^{-1/4}, \tag{74}$$

then $\sigma(T)$ is expressed as

$$\sigma(T) = \sigma_0 \exp[-(\frac{T_0}{T})^{\nu}], \tag{75}$$

where $\nu = 1/4$ is given for 3D systems. And

$$k_B T_0 = 18.1 \frac{\alpha^3}{N(E_F)}, \tag{76}$$

where α is the reciprocal of the localization length. The temperature dependence of conductivity, which obeys Mott's law, has been reported on various systems such as amorphous silicon [40] and impurity semiconductors [41][42]. An electron jumps from a state below the Fermi level to a nearby state for NNH conduction and to a distant state for which ΔE is as small as possible in the case of VRH conduction.

2.9.3 Efros-Shklovskii Type Variable-Range Hopping Conduction

Considering the Coulomb interaction between localized electrons, a soft Coulomb gap in the DOS near the Fermi level is created. The temperature dependence of conductivity reflects the gap. The concept has been introduced by Efros and Shklovskii [43]. They have considered the transfer of an electron from filled donor i to an empty donor j, where the state i and j are occupied and vacant, respectively. The transfer should increase the energy Δ_{ij} of the system.

$$\Delta_{ij} = E_j - E_i - \frac{e^2}{\kappa R}, \tag{77}$$

where κ is the dielectric constant, $E_i < E_F$ and $E_j > E_F$ and the third term describes the Coulomb interaction of the created electron-hole pair. E_i and E_j are assumed to be at the energy interval of small width ϵ centered at the Fermi level E_F. Assuming

$N(E_F) = N_0$, a mean distance R between the states is determined by the condition $N_0 R^3 \epsilon \simeq 1$ and R equals $(N_0\epsilon)^{-1/3}$. If $\epsilon << \Delta_c \equiv e^3 N_0^{1/2}/\kappa^{3/2}$, the interaction energy of the states $e^2/\kappa R = (e^2/\kappa)(N_0\epsilon)^{1/3}$ exceeds ϵ and eq.(77) breaks down. Thus a constant density of states contradicts the eq.(77) and $N(E)$ at $|E - E_F| < \Delta_c$ decreases with $|E - E_F|$ and should vanish at the Fermi level. In other words, the mean distance between the states in the interval ϵ has to be of the order of $e^2/\kappa\epsilon$

$$N(\epsilon)(\frac{e^2}{\kappa\epsilon})^3 \epsilon \simeq 1, \tag{78}$$

therefore,

$$N(\epsilon) = \eta \frac{\kappa^3 \epsilon^2}{e^6}, \tag{79}$$

where η is a numerical coefficient. For the two dimensional (2D) case, one finds

$$N(\epsilon) = \eta' \frac{\kappa^2 |\epsilon|}{e^4}. \tag{80}$$

Using eq.(79) and by analogy with the Mott law derivation one obtains

$$\sigma(T) = \sigma_0 \exp[-(\frac{T_0}{T})^{1/2}], \tag{81}$$

where $T_0 = e^2/\kappa a$. The same result is valid for the 2D system. The Coulomb gap Δ_c depends on the dielectric constant and will vanish as $\kappa \to \infty$ in the vicinity of the metal-insulator transition. Therefore the conduction according to the Mott's law will be expected.

In order to tell the hopping exponent ν in eq.(75), whether it is 1/4 or 1/2, Zabrodskii [44] has clarified the difference of the exponent with a good analysis. When eq.(75) is satisfied, one has

$$\ln w = -\nu \ln T + const. \tag{82}$$

and

$$w = -\frac{\partial \ln \rho}{\partial \ln T}, \tag{83}$$

where ρ is the reciprocal of the conductivity σ. The slope of curve in eq.(82) yields the hopping exponent ν. Zabrodskii has found that all curves for a series of n-Ge in the range of compensations $0.3 < K < 0.8$ approach a straight line with the slope $\nu = 0.5$ with decreasing temperatures.

2.9.4 Magnetoresistance in Variable-Range Hopping Conduction

The positive magnetoresistance (MR) observed in VRH regime has been attributed to the shrinkage of the wavefunction of electrons and consequently to the reduced hopping probability. The theory of positive MR for VRH conduction has been developed for two cases, namely, for a constant and for a quadratic density of states in the vicinity of Fermi level. In the low magnetic field region, the positive MR is expressed by Shklovskii [45] as

$$\ln \frac{\rho(B)}{\rho(0)} = t\frac{e^2B^2a^4}{\hbar^2}(\frac{T^*}{T})^y, \tag{84}$$

where $y = 3/4$ for Mott type and $y = 1/2$ for Efros-Shklovskii (ES) type. t is a numerical coefficient and B the magnetic field. The eq.(84) is derived from the resistor network model proposed by Miller and Abrahams [39]. Here $y = 3\nu$ holds, where ν is defined in eq.(75). When we determine the dominant hopping process, Mott's type or ES type, it is better to investigate the experimental data in the presence of magnetic field than those in the absence of it, because the difference of the hopping exponent appears clearly.

2.10 Two-Band Model

Now the electric current flows in the x-direction and a magnetic field is applied to the z-direction, then equation of motion on the electron is written using the velocity v and the electric field E.

$$\begin{aligned} m(\frac{d}{dt}+\frac{1}{\tau})v_x &= -e(E_x + Bv_y), \\ m(\frac{d}{dt}+\frac{1}{\tau})v_y &= -e(E_y - Bv_x), \\ m(\frac{d}{dt}+\frac{1}{\tau})v_z &= -eE_z. \end{aligned} \tag{85}$$

Then the respective components of the conductivity tensor σ are expressed as

$$\begin{aligned} \sigma_{xx} &= \sigma_{yy} = \frac{1}{1+(\omega_c\tau)^2}\sigma_0, \\ \sigma_{xy} &= -\sigma_{yx} = \frac{-\omega_c\tau}{1+(\omega_c\tau)^2}\sigma_0, \\ \sigma_{zz} &= \sigma_0, \end{aligned} \tag{86}$$

where

$$\sigma_0 = \frac{ne^2\tau}{m_e}, \tag{87}$$

and the cyclotron frequency is written as

$$\omega_c = \frac{eB}{m_e}. \tag{88}$$

We can set $J_y = 0$ for the measurements on Hall coefficient.

$$E_y = \frac{\sigma_{xy}}{\sigma_{yy}E_x} = \frac{\sigma_{xy}}{\sigma_{xx}}, \tag{89}$$

therefore,

$$J_x = \frac{\sigma_{xx}^2 + \sigma_{xy}^2}{\sigma_{xx}}E_x. \tag{90}$$

The Hall coefficient and the conductivity for the x-direction under a magnetic field are given by

$$R_H = \frac{E_y}{BJ_x} = \frac{1}{B}\frac{\sigma_{xy}}{\sigma_{xx}^2 + \sigma_{xy}^2} \tag{91}$$

and

$$\sigma = \frac{\sigma_{xx}^2 + \sigma_{xy}^2}{\sigma_{xx}}. \tag{92}$$

When two types of carriers of which carrier concentration and mobility are described as n_1, n_2, μ_1 and μ_2, the conductivity and the Hall coefficient are expressed as

$$\sigma = \sum_i n_i e\mu_i = n_1 e\mu_1 + n_2 e\mu_2 \tag{93}$$

and

$$\begin{aligned} R_H &= \frac{1}{B}\frac{\sum_i \sigma_{ixy}}{(\sum_i \sigma_{ixx})^2 + (\sigma_{ixy})^2}, \\ &= \frac{(n_1\mu_1^2 + n_2\mu_2^2) + \mu_1^2\mu_2^2(n_1+n_2)B^2}{(n_1\mu_1 + n_2\mu_2)^2 + \mu_1^2\mu_2^2(n_1+n_2)^2B^2}\frac{1}{e}, \\ &= \frac{(1+xb^2) + b^2\mu_1^2(1+x)B^2}{(1+xb)^2 + b^2\mu_1^2(1+x)^2B^2}\frac{1}{n_1 e}, \end{aligned} \tag{94}$$

where $x = n_2/n_1$ and $b = \mu_2/\mu_1$. In the case of the weak magnetic field, R_H is approximated by the following equation

$$R_H = \frac{1}{e}\frac{(n_1\mu_1^2 + n_2\mu_2^2)}{(n_1\mu_1 + n_2\mu_2)^2}. \tag{95}$$

3 Experimental procedures

3.1 Sample Preparation

3.1.1 Si:Sb bulk samples

In this study we have employed some Sb-doped Si samples with the impurity concentration of above and below the critical concentration for the metal-insulator (MI) transition grown by the Czochralski method. The critical concentration for the MI transition, $N_c = (3.0 \pm 0.2) \times 10^{18} \mathrm{cm}^{-3}$, is adopted from the work of Castner *et al.* [46]. We have determined the donor concentration through the Hall coefficient measurements at 300K. The Characteristics of the samples are shown in Table.1. In addition, we used sample C#, which has the almost same impurity concentration as that of sample C. The conductivity at low temperatures for sample C# is smaller than that for sample C.

Table 1: Characteristics of samples

Sample	N_D ($\times 10^{18}\mathrm{cm}^{-3}$)	Crystalline Plane	ρ_{300K} ($\times 10^{-2}\Omega$ cm)	Relation between N_D and N_C
A	1.4	$< 100 >$	2.06	$0.47N_C$
B	2.4	$< 100 >$	1.37	$0.80N_C$
C	3.0	$< 111 >$	1.07	$1.0N_C$
D	7.6	$< 111 >$	0.716	$2.5N_C$
E	11	$< 111 >$	0.556	$3.7N_C$

3.1.2 δ-doped Si:Sb

Three samples with Sb δ-doped layer were supplied by Prof. Fukatsu *et al.* [47]. The samples are grown on Si $< 100 >$ substrates by Si molecular beam epitaxy (MBE) method. After removal of the native oxide by heating the substrate up to 850°C for at least 30 min, a Si buffer layer was grown at 800-850 °C. An Sb adlayer was subsequently deposited on a 2×1 reconstructed surface at 100-650°C. Finally,

a capping layer was formed at 550°C by solid phase regrowth of an amorphous Si overlayer. The sample characteristics are listed in Table 2. Atomic distribution of Sb in three samples by way of the secondary-ion mass spectrometry(SIMS) is shown in ref.[47]. It is confirmed that the doped layer remains stable until the sample is annealed and the broadening of Sb distribution is less than 20nm. 1 monolayer (ML) corresponds to 6.78×10^{14} atoms per cm^2 on Si $< 100 >$ and the respective concentration is shown in Table 2.

Table 2: Characteristics of samples

Sample	Capping layer thickness ($\AA$)	Sb coverage (ML)	Buffer layer thickness ($\AA$)	Concentration (cm^{-2})
F	800	1.0	2000	6.8×10^{14}
G	1200	0.11	3560	7.5×10^{13}
H	800	0.06	500	4.1×10^{13}

3.1.3 InSb Thin Film

We have obtained two kinds of InSb thin film samples from Dr. Shibasaki of Asahi Chemical Industry Co., Ltd [48]. These samples were fabricated by the MBE method. The substrates are semi-insulating $< 100 >$ GaAs. The InSb thin films were grown directly on GaAs substrates, taking no thought of the large lattice mismatch of about 14%. The lattice constants GaAs and InSb are 5.65 $\AA$ and 6.48$\AA$, respectively. According to him, InSb/GaAs hetero interface has a lot of dislocations after the thin film growth, especially less than 0.5μm, and the electric properties of them depend on the film thickness. When the film thickness reaches about 1μm, it is possible to fabricate a stable sample at room temperature, where the mobility is $\sim$54000cm^2/Vs and the sheet resistance is 55$\sim$60Ω. The InSb thin films with high electron mobility are expected as magnetic sensors such as Hall elements. Two samples studied in this work are a non-doped sample and Sn-doped one, whose thickness is about 1μm. The parameters of the measured samples are shown in Table.3.

Table 3: Parameters of samples; Resistivity, carrier concentration and mobility at 300K are shown.

Sample	Film thickness (μm)	Dopant	Resistivity (Ωcm)	Concentration (cm^{-3})	Mobility (cm^2/Vs)
I457	~ 1	undoped	3.86×10^{-3}	1.1×10^{17}	1.5×10^{4}
I472	~ 1	Sn	3.43×10^{-3}	1.5×10^{17}	1.2×10^{4}

3.2 Experimental Setups

In the present study we have employed various measurement systems. Measurements down to about 0.4K were carried out using ^{3}He cryostat system, which mainly consists of ^{3}He pot and ^{4}He. After the ^{4}He pot reaches around 4K, it is pumped and the ^{3}He pot is cooled with pumped ^{4}He. Applying the heater to put ^{3}He gas out of charcoal, ^{3}He condenses in the ^{3}He pot. By evaporating ^{3}He, the system reaches around 0.3K. When we used the system, an ac resistance bridge was used for the resistance measurements in order to avoid the self-heating effect of samples.

The dc resistivity and Hall coefficient measurements at 4.2K were performed for directly immersed in liquid He. As for Hall measurement, Hall coefficient is obtained by averaging out the results measured for the two directions of the magnetic field. We have employed a Keithley 220 Programmable Current Source and Keithley Model 2001 multimeter. For Hall and magnetoresistance (MR) measurements we employed a superconducting magnet.

For the measurements above 4.2K, the sample was mounted in a helium refrigerator JMTR-4/300K under a computer control. For MR measurements in high magnetic field up to 10T we used a superconducting magnet JMTD-10T100M. They were produced by KOBELCO.

For Si:Sb bulk and δ-doped samples, the ohmic contacts were fabricated through the following procedures. The etchant for the sample is CP4 solution, which consists of nitric acid, hydrotiuoric acid and acetic acid in the proportions of HNO_3:HF:CH_3COOH= 5:3:3 by volume. The sample was placed in a chamber of 10^{-5}Torr and Au:Sb was evaporated onto it. Ohmic contacts were formed by annealing in Ar+H_2 atmosphere

at 400°C for 30 min. Indium metal was soldered onto the contacts area, where Ag wire was connected.

As for Si:Sb bulk samples, van der Pauw method was employed when the electrical measurements were performed. On the other hand, in the case of δ-doped Si:Sb sample and InSb thin films, the usual four contact measurements were carried out. The electrodes of δ-doped samples were put on the side of the sample, so electrons conduct in not only δ-doped layer but also the substrates at higher temperatures.

4 Experimental Results and Discussion

4.1 Results for Sb-doped Si bulk samples

On Si:Sb samples with the impurity concentration near the metal-insulator(MI) transition, Long and Pepper[9] have reported the low-temperature anomaly of the resistivity. Paying attention to the fact that such an anomaly had never been observed in Si:P and Si:As, Kaveh and Mott have argued the anomaly qualitatively based on the scattering effect related to the spin-orbit (SO) interaction due to the heavy Sb atoms in Si [10]. The strength of SO interaction depends on atomic number and generally in heavy elements it is stronger than that in light elements. As the other problem on the MI transition, there still remains some ambiguity as to whether the MI transition is primarily a Mott-Hubbard type or an Anderson type. The latter type transition is principally claimed for many-valley semiconductors. We want to make them clear through the experiments on Si:Sb bulk samples.

Figure 4.1.1 shows the temperature dependence of the resistivity for five samples with different impurity concentration. Sample A and B with the donor concentration below the critical one for the MI transition demonstrate that the resistivity increases with decreasing temperatures. The increase in the resistivity is mainly caused by the decrease of the conduction electrons (ϵ_1-conduction), and the details are described later. Sample D and E with the donor concentration above the critical one for the MI transition show a metallic conduction. In general the number of carriers does not depend on the temperature in a metallic regime and the change of the resistivity attributes to the temperature dependence of mobility, which results from the acoustic phonon and the impurity scatterings. The resistivity of sample C shows the maximum, which is described below in detail.

Figure 4.1.2 shows the temperature dependence of the Hall coefficient for samples concerned except for sample E, because the Hall coefficient for sample E was too small to measure due to the large number of carriers. For sample A and B the Hall coefficient increases as the temperature decreases, that means the decrease of thermally activated carriers from the donors to conduction band. Temperature vari-

ation of the Hall coefficient for Sample B is gentler than that of Sample A, which originates in the difference of the activation energy of donors called as ϵ_1. The Hall coefficients for sample C and D decrease with decreasing temperature, which arises from the temperature dependence of the Hall factor. The impurity concentration for Sample C just coincides with the critical one for the MI transition. Judging from the temperature dependence of the Hall coefficient, sample C is considered to be a metallic sample rather than an insulating one.

4.1.1 Results for the sample with the impurity concentration below MI transition

The temperature dependence of the conductivity between 20 and 300 K is shown against T^{-1} in Fig.4.1.3. It is found that the conductivity σ is approximated by the sum of two exponential terms with each characteristic activation energy of $\epsilon_1 = 10.3$meV and $\epsilon_2 = 2.2$meV, where ϵ_1 represents the activation energy of an electron from the Fermi level located in the lower Hubbard band (LHB) to the conduction band, and ϵ_2 corresponds to that to the extended states in the upper Hubbard band (UHB) as mentioned in § 2.2. On the other hand, from the temperature dependence of the conductivity for sample A, we found $\epsilon_1 = 13.6$meV. Characteristic conduction showing up ϵ_2 and ϵ_3 are not found in present temperature range of measurements. The difference of the activation energy ϵ_1 between two samples comes from the difference in the energy between the LHB and the tail states of conduction band. The energy ϵ_2 has been reported in ref.[49] for Si:P, and ϵ_2 distributes between 0.324 and 1.73 meV in the range of donor concentration between 2.07 and 2.63×10^{18}cm^{-3}. The deviation from the slope of ϵ_2 in Fig.4.1.3 is caused by the variable-range hopping (VRH) conduction at lower temperatures.

Figure 4.1.4 shows a plot of carrier concentration as a function of the reciprocal of the temperature T^{-1}. This is a typical analysis based on the one-band model and the slope of the graph corresponds to the activation energy between the conduction band and the impurity one. The activation energy obtained from the slope is 8.7 meV for sample A and 0.52 meV for sample B.

The first purpose of this study is to examine which type is predominant for the VRH conduction at low temperatures, Mott type or Efros-Shklovskii (ES) one. The temperature dependence of the resistivity for sample B is shown in Fig.4.1.5 in the absence of magnetic field. This dependence appears to obey the ES-type VRH law in the temperature range between 2.8 and 4.2 K, which is confirmed by plotting the logarithmic derivative $w = -\partial \ln \rho / \partial \ln T$ (eq.(83)) as a function of the temperature on a double logarithmic scale as shown in the inset of Fig.4.1.5. The slope of curve yields the hopping exponent ν of eq.(75). Here $\nu = 0.47$ and $T_0 = 320$K (for eq.(75)) are extracted from our experimental data, leading to $a = 41\mathring{A}$ with $\kappa = 35$, for which we refer to [46]. And the temperature dependence of conductivity between 3.8 and 10 K is shown in Fig.4.1.6 in order to confirm the difference between the nearest-neighbor hopping and VRH. It illustrates the better fit of $T^{-1/2}$-dependence.

On the occasion of fastening down which type, Mott type or ES type, is predominant for the VRH conduction at low temperatures, the magnetoresistance (MR) measurement is a better way because the temperature dependence (3/4 or 3/2) of MR is stronger than that (1/4 or 1/2) in the absence of magnetic field. The MR data at various temperatures (T$\leq$ 4.2K) are shown in Fig.4.1.7. The MR is always positive and increases with decreasing the temperature. It is found that $\ln \rho(B)/\rho(0)$ is proportional to B^2 in agreement with eq.(84). $\log[\ln \rho(1.5\mathrm{T})/\rho(0)]$ against $\log T$ is plotted in Fig.4.1.8. The slope of this graph yields $y = 1.6$ (eq.(84)). This value is rather closer to 3/2 than 3/4. Accordingly this results indicate that ES-type of VRH is predominant at low temperatures. The similar results were obtained on Si:P [50] and Ge:As [51].

Figure 4.1.9 shows the I-V characteristics and Fig.4.1.10 the electric current density dependence of the Hall coefficient at various temperatures for sample A. When the temperature is higher than 40 K, the I-V characteristics follows Ohm's law, but as the temperature decreases the deviation from Ohm's law becomes remarkable. These phenomena come from the excitation of electrons into higher energy states by electric fields.

Similarly, the dependence of the resistivity and the Hall coefficient at 4.2K on the electric current density for sample B are shown in Fig.4.1.11. In the low current density the resistivity follows Ohm's law. It is found that the resistivity decreases with increasing the current density owing to the rise in the electron temperature.

The variation of the MR $\rho(B)$ at 4.2K with the current density is shown in Fig.4.1.12. The positive MR is observed in the low current region. For the insulating sample, the VRH conduction is dominant at low temperatures and the application of the magnetic field results in the shrinkage of the wavefunctions of electrons and consequently in the reduced hopping probability as mentioned in § 2.8.4. As the current density increases, the positive MR is depressed and the negative one appears. Nguyen *et al.* pointed out for the first time that the interference of different hopping paths between initial and final states leads to the negative MR [52]. In this experiment, however, the electric field most likely forces electrons to excite into higher energy states, resulting in a change of the electron distribution and its mobility, and thus produces the negative MR.

The MR in ohmic region above 3.5 K is shown in Fig.4.1.13. The negative MR is not observed at these temperatures. This experimental fact means that the results induced by the high electric current density are considered due to the hot electron effect. The positive MR is smaller as the temperature increases. From the temperature dependence of the conductivity in the absence of magnetic field, we conclude that the MR arises from the hopping at low temperature and ϵ_2-conduction at higher temperatures.

According to Mott-Hubbard mechanism, the impurity band consists of the LHB and UHB, which are strongly localized states but both contribute to the electric conduction. Assuming the presence of the LHB and the UHB merged with the conduction band in the higher energy, we can determine the carrier concentration and the mobility in respective band [53]. For simplicity, we assume that all the electrons are excited into the UHB at a maximum current density. Let's make the resistivity and the Hall coefficient in that case to be ρ_c and R_c, respectively. Thus the resistivity ρ and Hall

coefficient R_H based on the two-band model can be expressed with eqs.(93) and (95) in § 2.10;

$$\frac{\rho}{\rho_c} = \frac{(1+x)b}{(1+xb)} \tag{96}$$

and

$$\frac{R_H}{R_c} = \frac{(1+x)(1+xb^2)}{(1+xb)^2}, \tag{97}$$

where x is n_u/n_l, b μ_u/μ_l. n_u, n_l, μ_u and μ_l are the concentration and the mobility in the respective band and the subscript u and l denote the UHB and the LHB, respectively. ρ_c is $1/n_u e\mu_u$ and R_c is $1/n_u e$. Moreover, we employed $\mu = (n_u\mu_u + n_l\mu_l)/(n_u + n_l)$ for the mobility obtained from experiments μ.

The results of the above analysis for n_l and n_u are shown in Fig.4.1.14 for sample A and Fig.4.1.15 for sample B. It is found that (1)as the electric current density increases, the carrier concentration of UHB n_u increases, (2)the lower the temperature is, the more remarkable these phenomena are. Especially, for sample B at 4.2K, $n_u \approx 10^{16}$ cm^{-3} and $n_l \approx 10^{18}$ cm^{-3} are obtained in the ohmic region. The carrier concentration in the UHB increases to above 2×10^{17}cm^{-3} with the increase of the electric current density. At low current densities most of the electrons are in the LHB and some electrons are excited into the UHB as the current density increases. Moreover, the mobility in the UHB, μ_u, decreases with the increases of current density, whereas the mobility in the LHB, μ_l, demonstrates an opposite tendency as shown in Fig.4.1.16. This effect is qualitatively explained as follows; the ionized donors increase with the increase of current density, resulting in the decrease of μ_u due to the increase of the scattering rates and the increase of μ_l due to the increase in the empty donor states and the increase in the possibility for electrons to hop into another sites.

From the experimental data we try to estimate the energy required for electrons to be excited to the higher lying energy states using the model by Sclar *et al.* [54]. The model assumes that the breakdown phenomenon of the I-V characteristics in the electronic system occurs when the rate of energy gain from the electric field becomes equal to the rate of energy loss by collision with phonons. According to this model

the critical field E_c for the onset of breakdown is expressed as follows:

$$E_c = \frac{2v_s}{\mu_u}[\frac{\overline{\epsilon}}{2k_BT} - 1]^{\frac{1}{2}} \tag{98}$$

and

$$\overline{\epsilon} = \beta I. \tag{99}$$

where β is the numerical coefficient, $v_s = \sqrt{k_BT/M}$ the velocity of sound, M the mass associated with the lattice vibration, $\overline{\epsilon}$ the average energy of electrons and I means ϵ_2. Fig.4.1.17 shows the electric field dependence of the resistivity and the breakdown phenomenon of the I-V characteristics observed in this experiment. Substituting the experimental values, $E_c = 2.04$V/cm, $\mu_u = 38.0$cm^2/Vs and $I = \epsilon_2 = 2.2$meV into eqs.(98) and (99), we obtain $\beta = 0.32$ and $\overline{\epsilon} = 0.72$meV. It is found that $\overline{\epsilon}$ is smaller than I. It is concluded that electrons are not directly excited to the conduction band, but to the low energy tail of UHB.

In the next step we will focus on the current density dependence of the MR at 4.2K. The analysis based on the two-band model motivates us to the idea that these phenomena originate from the rise in electron temperature and the negative MR at high electric current densities results from the transfer of electrons into the localized states of the UHB which are assumed to be weakly localized. Consequently, these data are regarded as composed of two effects, i.e., the reduced hopping probability in the LHB and the weak localization effect in the lower tail of the UHB. The band tail should overlaps with LHB at the Fermi level allowing for the transition of Anderson type. We employ eqs.(41), (42) in § 2.5.2 and (84) in § 2.9.4 for the analysis of experimental data. In eq.(42), $F(\delta)$ has been expanded with the Euler-MacLaurin development in a series for several functions used in the least squares method with an accuracy better than 0.1 % [64]. The above consideration leads to the following expression for the Magnetoconductivity (MC) with eqs.(41), (42) and (84) as :

$$\Delta\sigma(B) = c_1 exp(-c_2B^2) + c_3[2(\sqrt{2+\delta} - \sqrt{\delta}) - \{(\frac{1}{2}+\delta)^{-\frac{1}{2}} + (\frac{3}{2}+\delta)^{-\frac{1}{2}}\} + \frac{1}{48}(2.03+\delta)^{-\frac{3}{2}}], \tag{100}$$

where $\Delta\sigma(B) = \sigma(B) - \sigma(0)$, c_1, c_2 and c_3 are the fitting parameters, and $\delta = 0.176/B$ was derived from data in this experiment. The first term describes the decrease of the

conductivity due to the reduced hopping probability and the second one describes the increase due to the suppression of interference effect in the weakly localized states. The results of the numerical calculation after eq.(100) with proper parameters are shown in Fig.4.1.12 (solid lines). The best fits are obtained by properly choosing the numerical values of c_1, c_2 and c_3, which are shown in Table.4. c_3 increases with the increase of the current density. The weak-localization effect becomes more remarkable as electrons are excited into the UHB. The arrow in Fig.4.1.18 indicates the characteristic magnetic field where $\delta = 1$ holds. The slope of the MC against the magnetic field undergoes a change at the critical field as predicted by the weak localization theory. This fact suggests that the application of the weak localization theory is appropriate.

Table 4: Numerical values of c_1, c_2 and c_3 in eq.(100) at various electric current densities.

Electric Current Density (A/cm^2)	c_1 ($\Omega^{-1}cm^{-1}$)	c_2 (T^{-2})	c_3 ($\Omega^{-1}cm^{-1}$)
0.38	0.902	1.66×10^{-3}	8.89×10^{-4}
0.75	0.901	1.77×10^{-3}	5.78×10^{-3}
1.5	0.925	2.64×10^{-3}	5.54×10^{-2}
3.8	0.932	2.56×10^{-3}	1.90×10^{-1}
7.5	0.955	7.29×10^{-4}	4.60×10^{-1}

From the analysis based on the two-band model as shown in Fig.4.1.19, it was found that the conductivity in the respective bands, σ_u and σ_l, increase with an increase of the electric current density. The conductivity in the LHB is increased to 3 times in magnitude of the value in ohmic region and one in the UHB to 6 times. It is considered that the parameters c_1 and c_3 are in proportion to the carrier concentration in the respective bands. Nevertheless, c_1 is almost constant and c_3 increases to 500 times. In the present stage we have no answer for the above contradiction. We can guess that the problems originates from the analysis based on the too simple model, where we assume that all the electrons are excited into the UHB at the maximum

electric current density ignoring electrons excited into the conduction band. Above contradiction should be solved if we analyze the experimental data according to the three-band model taking account of LHB, UHB and conduction band. However the analysis is extremely troublesome because it includes six ambiguous parameters. It has been proven that the parameter c_2 becomes smaller as the electric current density increases. This means that the localization length becomes larger and the hopping probability of electrons in the LHB increases as clear from the experimental results on the mobility of the LHB μ_l illustrated in Fig.4.1.16.

Finally we give a few comment on the MR in ϵ_2-conduction region. In the case of ϵ_2-conduction, the magnetic field dependence of the activation energy is empirically expressed as [55]

$$\epsilon_2(B) = \epsilon_2(0) + \gamma B^2, \tag{101}$$

where γ is a constant. This formula is derived from the change of the Hubbard gap by the application of the magnetic field. The change is induced by a shrinkage of the D^- and D^0 wavefunctions and a reduction of the band width. In appearance the magnetic field dependence of the resistivity for ϵ_2-conduction has the similar formula to eq.(84) related to the MR in VRH conduction. The value γ is usually very small, so the MR is smaller than that of VRH.

In summary, it is made clear that the transport characteristics at low temperatures for the sample employed in the present experiment are dominated by the ES-type of VRH for sample B with the impurity concentration proximate to the critical one for the MI transition, even in the presence of magnetic field. A crossover from the positive to negative MR has been observed as the electric current increases. We could estimate the average energy $\overline{\epsilon} = 0.72$meV required for electrons to be excited to the higher lying energy states with using the model by Sclar *et al.* This value emphasizes that electrons concerning the conduction are not excited to the conduction band, but to the low energy tail of the UHB. The current density dependence of the MR originates from not the rise in the lattice temperature, but the rise in the electron temperature. It is the vital force for transfer of electrons from the strongly localized

states (hopping regime in the LHB) to the weakly localized states (diffusive regime in the low energy tail of the UHB).

4.1.2 Results for the sample with the impurity concentration near MI transition

Figure 4.1.20 shows temperature dependence of resistivity for sample C under various electric current densities. The data have peculiar behavior, which are different from the insulating samples A and B and the metallic samples D and E. Firstly, as the temperature decreases, the resistivity increase and have a maximum around at 80K. And then they decrease and have a minimum, after that, begin to increase again. The same tendency was reported by Sasaki [56] using some Ge samples with Sb above the metal-insulator transition. And Kurosawa *et al.* has theoretically interpreted the data [57]. They pay attention to the temperature T_M where the maximum in resistivity appears. The temperature T_M is proportional to Fermi temperature T_F, thus, the anomaly in the scattering relaxation time exists around the Fermi surface, i.e. the scattering time decreases near Fermi surface. As for the sample C, T_F is 83K and T_M is 83K, and they are coincident.

The scattering processes we have to consider are acoustic phonon (deformation potential) scattering and ionized impurity scattering. Generally the temperature dependence of relaxation time is $\tau_{ac} \propto T^{-3/2}$ for acoustic phonon scattering and $\tau_{ion} \propto T^{3/2}$. However, for heavily doped semiconductors screening effect is important and the relaxation time for ionized impurity scattering has $T^{1/2}$-dependence, taking the logarithmic factor of Brooks-Herring's formula [58] into account

$$\frac{1}{\tau_{ion}} = \frac{Z^2 e^4 N_I}{2^{15/2}\pi^{1/2} m_e^{1/2} (\epsilon\epsilon_0)^2 (k_B T)^{3/2}} [\ln(1+x) - \frac{x}{1+x}] \tag{102}$$

and

$$x = \frac{24 m_e \lambda_{TF}^2 k_B T}{\hbar^2}, \tag{103}$$

where N_I is the number of ionized impurities, ϵ the dielectric constant and λ_{TF} the Thomas-Fermi screening length. When λ_{TF} is large enough, electrons are scattered by the long-range Coulomb potential. On the other hand, when λ_{TF} is small, electrons

need to approach the ionized impurity to be scattered by the short-range one.

$$\frac{1}{\tau_{ion}} \propto \begin{cases} T^{-3/2} & (\lambda_{TF} \gg 1) \\ T^{1/2} & (\lambda_{TF} \ll 1). \end{cases} \tag{104}$$

When temperature of the system is high enough, electrons gain kinetic energy and come near the ionized impurities, then they can be scattered by the short-range Coulomb potential. When the Fermi energy is in the region where the scattering time changes from $T^{-3/2}$ to $T^{1/2}$, the resistivity has a maximum.

As shown in Fig.4.1.20, we have found that T_M shifts toward lower temperature with increasing the electric current densities. Figure 4.1.21 shows the relation between the electric current density and T_M. Electrons gain energy from the electric field and the electron temperature rises, the maximum of the resistivity appears at the lower temperature than that in the ohmic region. In Fig.4.1.22 the calculation result is shown using eq.(102). It is confirmed that the peak of the resistivity shifts into lower temperature as the electron temperature rises. As for acoustic deformation potential scattering, the formula has been given by [59],

$$\frac{1}{\tau_{dp}} = \frac{3}{2^{3/2}\pi^{1/2}} \frac{m_e^{3/2} E_1^2 (k_B T)^{3/2}}{\hbar^4 c_l}, \tag{105}$$

where E_1 is the deformation potential constant and c_l the longitudinal elastic constant. Using various parameters $1/\tau_{dp} = 4.71 \times 10^8 T^{1.5}$ is obtained. However, if the acoustic deformation potential scattering is taken into account, the peak of resistivity is not explicable with two formulas.

Next we will focus on the transport properties at low temperatures. On the metallic side of the metal-insulator (MI) transition, negative magnetoresistance (MR) is often observed at low fields and positive MR at high fields. Theoretical investigations have clarified the importance of both effects of localization and electron-electron (e-e) interaction. For the latter, Altshuler and Aronov [31] have developed the theory including the density of states (DOS) correction to the conductivity σ under the condition $k_F l > 1$, where k_F is the Fermi wavenumber and l the mean free path. This behavior leads to $T^{1/2}$-dependence of conductivity due to the DOS correction.

Experimental studies under a magnetic field give useful information about the

MI transition. For example, the result on Si:As [60] was interpreted as the magnetically induced change in the critical concentration as well as the correlation-localization-length exponent. It is in this donor concentration region that Long and Pepper have reported the low-temperature anomaly of the resistivity [9].

The donor concentration derived from the Hall coefficient at 300K is just $1.0N_c$ (Sample C). However, the donor concentration should be larger than that estimated from the Hall coefficient measurements, because electrons are not fully excited into conduction band even at 300K.

The variation of MR, $\rho(B)$, at 4.2K with the current density is shown in Fig.4.1.23. The positive MR is observed in the low current region. As the current density increases, the positive MR is depressed and the negative one appears as well as sample B in the insulating regime. However the steep change of both the resistivity and the Hall coefficient is not observed for sample C. The tendency of the electric current density dependence of MR is similar to that of the insulating sample. In the metallic regime, the electric current density dependence of MR exhibits the opposite tendency, which we will describe in the next section.

Temperature dependence of conductivity is shown in Fig.4.1.24. In the absence of a magnetic field, the differential coefficient of the conductivity with respect to temperature $d\sigma/dT$ is negative. As the magnetic field increases, a crossover to positive $d\sigma/dT$ is observed, which is shown in the inset of Fig.4.1.24. This behavior demonstrates the effect of magnetic tuning of the critical concentration $N_c(B)$. The magnetoconductivity (MC) at various temperatures is shown in Fig.4.1.25, and is always negative. The positive MC due to the destructive quantum interference is not observed. For the sample with $N_D = 3.0 \times 10^{18}\mathrm{cm}^{-3}$ $k_F l$ is estimated at 0.44. The condition $k_F l > 1$, for which the negative MR is observed and the theory of weak localization (WL) is applicable, is not fulfilled.

In order to understand these phenomena in the critical region of the MI transition, we try to analyze our data at the start by assuming variable-range hopping (VRH) conduction. In the above section, we have observed positive MR for the sam-

ple whose donor concentration is $0.80N_c$ [14]. Shrinkage of the wavefunction by the application of the magnetic field results in a reduced hopping probability, giving rise to a positive MR. In the strong field region, $a_D(B) > l_B$ is satisfied, where $a_D(B)$ is the effective Bohr radius with a magnetic field dependence and l_B the cyclotron radius, the positive MR is expressed as [45]

$$\ln \frac{\rho(B,T)}{\rho(0,T)} \propto \begin{cases} B^{1/3}T^{-1/3} & \text{(ES's type)} \\ B^{1/5}T^{-3/5} & \text{(Mott's type).} \end{cases} \tag{106}$$

The localization length is considered to be larger than the cyclotron radius at 5T in the critical regime. So that, we try to analyze the experimental data of temperature dependence of resistivity at 5T using the relation, $\rho(B,T) = \rho_0 \exp(tB^mT^n)$, where t is the numerical coefficient. From this analysis we extract $n = 0.018$, which does not obey the VRH theory in eq.(106). Moreover, if we take the VRH into account for the conduction of this sample we meet with a big problem; The inset of Fig.4.1.24 does not show the VRH conduction in the absence of magnetic field because $d\sigma/dT$ is negative. There might be a possibility of a crossover from the metallic regime to the VRH one with increasing of a magnetic field, however, at 5T the zero temperature conductivity $\sigma(0)$, for which an extrapolation is required, is not zero, so in the range of up to 5T, the sample belongs to a metallic regime.

As seen in Fig.4.1.24, the temperature dependence of σ shows $d\sigma/dT < 0$. So far, many studies at very low temperatures have reported on $T^{1/2}$ dependence (eq.(64)) due to e-e interaction (for example [61]), as shown mentioned in § 2.7. Here we ignore the term BT for localization because the positive MC due to the WL effect is not observed.

$$\sigma(T) = \sigma(0) + mT^{1/2}. \tag{107}$$

The coefficient m results from the exchange and Hartree interaction. The Hartree term depends on the screening length as mentioned in § 2.8. We have fitted the data in Fig.4.1.24 (below 1.5K) to eq.(107). First we try to fit it to the formula $\sigma(T) = \sigma(0) + mT^p$. We find $\sigma(0) = 64.7\Omega^{-1}\text{cm}^{-1}$, $m = -2.5\Omega^{-1}\text{cm}^{-1}K^{-p}$ and $p = 0.74$. Next we try to fit to eq.(107) and get $\sigma(0) = 65.7\Omega^{-1}\text{cm}^{-1}$ and $m =$

$-3.5\Omega^{-1}\mathrm{cm}^{-1}K^{-1/2}$. The e-e interaction theory gives the expression for the coefficient m in eq.(65) of § 2.7. $m = -0.61$ is extracted from the theory. Our results show stronger temperature dependence of conductivity than that expected from the theory. The VRH conduction at low temperatures is denied as above described, and other effect such as anti-localization effect to strongly increase conductivity should exist.

From the temperature dependence of conductivity, $\sigma(0) > 0$ is extracted and the sample certainly belongs to a metallic regime. Shafarman *et al.* [62] have studied the concentration dependence of the coefficient m. When the donor concentration is extremely close to the critical concentration of MI transition, m is positive. As the donor concentration increases, m decreases and the sign changes, which results from the Hartree interaction. From the comparison of m with the experimental data and the theory, it is considered that the donor concentration of sample C is larger than that estimated from the Hall coefficient at 300K.

According to Altshuler *et al.* [32], on the other hand, the MC due to the DOS correction caused by the e-e interaction in the weak magnetic field region for a single-valley semiconductor is given in eqs.(57), (58) and (59) of § 2.7. Here we employed eq.(58) and eq.(59) with Euler-MacLaurin developed of several functions used in the least-squares fit procedures [63] [64]. The experimental data of Fig.4.1.25 are fitted using eq.(58) and eq.(59). We have tried to fit the experimental data to the expression $\sigma(B,T) = \sigma(0,T) + \Delta\sigma(B,T)$ with the parameters $\sigma(0,T)$ and α. As for the function $\varphi_3(x)$, we used the low and the high-fields approximations. The solid and dashed lines of Fig.4.1.25 represent the calculated results using the approximation of low fields ($B < 0.7$T) and the high fields ($B > 2.4$T), respectively. We found $\alpha = 3.5$ in low field region and $\alpha = 3.8$ in high field region. However, the theory predicts $\alpha = 1$ for a normal metal and $\alpha = 1/4$ in the presence of spin-orbit (SO) interaction. The field dependence of MC is stronger than that expected from the theory. Other effects to strongly increase negative MC should exist.

In Fig.4.3.26 temperature dependence of conductivity under various magnetic fields is shown for sample C#. As shown the inset of Fig.4.3.26, interestingly, the

differential coefficient of the conductivity with respect to temperature $d\sigma/dT$ at 3T is negative at higher temperature, but $d\sigma/dT$ changes the sign as the temperature decreases, which originates from the change of Hartree term. The Hartree factor F is a decreasing function of Thomas-Fermi screening length and approaches unity for short-range interaction ($2k_F/K \to 0$), where K is the Thomas-Fermi screening wave vector. Qualitatively, at higher temperatures and lower magnetic field, electrons have enough kinetic energy and they interact with short-range Hartree potential. Therefore Hartree factor F is large and m is negative. The data in Fig.4.3.26 is explicable with the change of the sign of F.

Through the experiment and the analyses we have two questions. (1)A positive MC (negative MR) due to the destructive quantum interference is not observed in the temperature region where we performed the experiments. For the sample e-e interaction is much stronger than localization effect. Therefore we do not take the localization effect into account. Why is not the localization effect observed? (2)Kaveh and Mott have suggested that the SO interaction would cause destructive interference and enhance conductivity [10]. The SO interaction might hide a positive MC.

In conclusion, we have observed the change of the sign of $d\sigma/dT$ with the increase of magnetic field in the temperature dependence of conductivity, which originates from the Hartree potential. It is found that the magnetic-field and the temperature dependence of conductivity are stronger than that expected from the theory.

4.1.3 Results for the sample with the impurity concentration above MI transition

Figure 4.1.27 illustrates temperature dependence of conductivity in the ohmic region between 10K and 300K for sample D and E. The temperature dependence is not an activated type that is characteristic to an insulating sample, but shows a metallic conduction. As shown in Fig.4.1.2, the Hall coefficient for sample D slightly decreases as the temperature decreases. The change does not result from the change of the carrier concentration. In the metallic regime the carrier concentration is considered to be unchanged below room temperature for Si, so the change of the Hall

coefficient originates from the Hall factor. Therefore, the temperature dependence of conductivity depends on the mobility. The scattering processes, which are taken into account for the sample, are ionized impurity scattering (eq.(102)) and acoustic phonon (deformation potential) one (eq.(105)). The scattering probabilities for two processes are calculated as shown in Fig.4.1.28. Comparing the experimental data as shown in Fig.4.1.27 with the result of eqs.(102) and (105), the experimental result has the smaller temperature dependence and the behavior at low temperatures is different from the experimental result. The temperature dependence of conductivity is not explicable with two formulas. In fact, electrons are multiple-scattered by screened Coulomb potential. This is a very complex problem, but Takeshima [65] has treated it with Green function method. We do not mention it in detail here.

The variation of MR $\rho(B)$ at 4.2K with the current density for sample E is shown in Fig.4.1.29. Hereafter we will focus on sample E. In the low electric current density region (ohmic region), the negative MR is observed for the weak magnetic field. As the magnetic field increases, the negative MR shows the tendency which changes direction for the positive one. It is considered that this phenomenon originates from the electron-electron (e-e) interaction. On the other hand, as the electric current density increases, the negative MR diminishes and the positive one becomes notable. Consequently, this behavior suggests the contribution of the higher lying energy states than Fermi level yield the positive MR in like manner of an insulating sample. The drastic change of resistivity in the absence of magnetic field is not observed as well as that of sample C.

Firstly we have tried to analyzed the experimental data on the low electric current density region. Here we employ Kawabata's theory (eqs.(41) and (42)) and e-e interaction theory introduced by Altshuler *et al.* [32]. $\delta = 1.35 \times 10^{-3}/B$ and $x = 2DeB/\pi k_B T = 0.280B$ were derived from the data in this experiment. Two formulas have been developed by Euler-MacLaurin series. About Kawabata's formula we described in § 4.1.1. The set of formulae for e-e interaction theory is expressed by Ousset *et al.* [63] and is corrected by Baxter *et al.* [64]. Especially, for $0.7 < x < 2.4$

$\varphi_3(x)$ is expressed as follows,

$$\varphi_3(x) = -0.03043 + 0.22616x + 0.14104x^2 - 0.10293x^3 + 0.02759x^4 - 0.0028x^5. \quad (108)$$

Taking into account both the effects of the weak localization (WL) effect (Kawabata's theory) and e-e interaction, employing eq.(41), (42), (57) and (108) the MC is written by the following relation

$$\begin{aligned}\Delta\sigma(B) &= c_1'[2(\sqrt{2+\delta} - \sqrt{\delta}) - \{(\frac{1}{2}+\delta)^{-\frac{1}{2}} + (\frac{3}{2}+\delta)^{-\frac{1}{2}}\} + \frac{1}{48}(2.03+\delta)^{-\frac{3}{2}}] \\ &\quad -c_2'\sqrt{B}(-0.003043 + 0.22616x + 0.14104x^2 - 0.10293x^3 \\ &\quad +0.02759x^4 - 0.0028x^5), \end{aligned} \quad (109)$$

where c_1' and c_2' are the fitting parameters. The first term represents the increase of the conductivity due to the suppression of the interference effect and the second term represents the decrease due to the e-e interaction. The result of the fit to eq.(109) is shown with solid lines in Fig.4.1.30. We found that experimental data are fitted by properly choosing the numerical values of c_1' and c_2'. But we have a quantitative problem. According to eq.(41), $e^2/(2\pi^2\hbar)\sqrt{e/\hbar}$ is $4.83\Omega^{-1}\mathrm{cm}^{-1}/\mathrm{T}$ ($= c_1'$). But we obtained $c_1' = 1.36\Omega^{-1}\mathrm{cm}^{-1}/\mathrm{T}$ from our fit.

Next we have tried to analyze the experimental data on the high electric current density region. For the typical semiconductors which have some isolated donors (the wavefunction between the nearest neighbor donors do not fully overlap.), a positive MR owing to Lorenz force appears. The MR is given by [66]

$$\frac{\Delta\rho(B)}{\rho(B)} = T_H(\mu B)^2, \quad (110)$$

where $\Delta\rho(B) = \rho(B) - \rho(0)$, μ is the mobility, T_H depends on the scattering process and usually shows the value of ~ 1. For example, T_H is 0.38 for acoustic deformation potential scattering and 2.15 for ionized impurity scattering. From the result of the fit to eq.(110) for the experimental data in the non-ohmic region, we have found $T_H = 0.518$. On the other hand, we tried to fit the data for the insulating sample in the low electric current density region, and could obtain $T_H = 1.37 \times 10^5$. A positive MR in the variable-range hopping regime is much stronger than that of the cause of

Lorenz force.

For a metallic sample, as well as a insulating sample, the electric current density dependence of MR originates from the rise of the electron temperature and transfer of electrons from the WL states to the conduction band (higher lying energy states than WL ones).

Temperature dependence of conductivity in the absence of magnetic field at lower temperatures is shown in Fig.4.1.31. The differential coefficient of the conductivity with respect to temperature $d\sigma/dT$ is negative. In a metallic regime, both of e-e interaction effect and localization one are important and the temperature dependence of conductivity is expressed as $\sigma(T) = \sigma_3(0) + mT^{1/2} + BT^{p/2}$ (eq.(64)). As shown in Fig.4.1.31, the component $T^{1/2}$ is not seen in the experimental data and the component in proportion to T^1 is mainly observed. Therefore the interaction effect is not considered to be important in the absence of magnetic field for the sample. The localization effect is more important and the inelastic scattering time τ_ϵ is expected to be $\sim T^{-2}$.

Figure 4.1.32 shows the correction of the MC at various temperatures for sample E. The strong temperature dependence is not observed and the characteristic feature caused by the anti-localization effect is not explicitly seen in the figure. In the range of measurement only a positive MC due to the suppression of the interference effect is observed. For this sample with $N_D = 1.1 \times 10^{19}\mathrm{cm}^{-3}$, $k_F l$ is estimated at 1.4, certainly, the condition for WL is satisfied.

The data are compared with the theoretical expression eq.(109) using the fitting parameters τ_ϵ and αg. With only a WL theory, the MC is not satisfactorily explained. For the experimental data on the electric current density dependence of MC, the different fitting parameters are employed in order to investigate the degree of the contribution to localization effect and interaction one. Here we want to evaluate the inelastic scattering time τ_ϵ. The successful fits are obtained as shown in Fig.4.1.32. The obtained value of αg is about 0.5.

The temperature dependence of the inelastic scattering time τ_ϵ is shown in

Fig.4.2.7 in the next section. The relations of $\tau_\epsilon \propto T^{-1}$ is deduced in the range of our measurement. The result contradicts the one of the temperature dependence of conductivity in the absence of magnetic field. However, according to Isawa [67], taking the inelastic scattering due to the screened Coulomb interaction into account, τ_ϵ for three dimensional system should be proportional to T^{-1} at lower temperatures as well as $T^{-3/2}$ term at higher temperatures. Our result is qualitatively agreement with the theory by Isawa and the result on n-GaAs [24]. On the other hand, $\tau_\epsilon \sim T^{-1}$ is also satisfied for a δ-doped sample, as we will mention in the following section. These results for sample E are compared with those for δ-doped sample.

4.2 Results for the δ-doped Si:Sb

Spin-orbit (SO) interaction has been shown to have a drastic influence on the weak localization (WL). In the systems with the strong SO interaction, positive magnetoresistance (MR) in the WL appears, which is known as the anti-localization (AL) effect. AL effect has been mainly studied in the metallic thin films over many years. For Si:Sb samples with the impurity concentration near the metal-insulator (MI) transition, the low-temperature anomaly of the resistivity has been reported by Long and Pepper [9]. However, no one has succeeded in the observation of the anomaly in Si:Sb thereafter. We try to observe the positive MR due to AL effect, but, as mentioned in the above section, we could not observe it for bulk Si:Sb samples, and then we employ δ-doped samples.

In δ-doped layer, a typical two dimensional (2D) electronic system is produced by the quantum confinement effect in the layer, since impurity atoms are doped in a very limited layer. In the δ-doped layer the added impurities themselves greatly influence the transport of the 2D electrons, which differs from the modulation doped heterostructures such as GaAs/AlGaAs. When heavily doped bulk semiconductors are grown by various methods, carrier densities are found to saturate. This problem might originate in the solubility ($C = 5.5 \times 10^{19}\mathrm{cm}^{-3}$ at 1200 ℃ for Si:Sb) or the segregation of dopant atoms. However, if a δ-doping method for Si:Sb is employed, it is possible to attain the greater carrier concentration. For example, sample F, whose portion of the occupation of Sb atoms in the δ-doped layer is 1.0 monolayer (ML), has the three dimensional (3D) donor concentration of N_D=$1.2\times10^{20}\mathrm{cm}^{-3}$.

So far, numerous studies of 2D electronic system on Anderson localization have been reported. Using 2D electron system in semiconductor inversion layer of Si-MOS, Kawaguchi and Kawaji [68] have observed positive magnetoconductance (MC) and fitted it with Hikami *et al.*'s theory [22], and discussed temperature dependence of inelastic scattering time and the concentration dependence of the prefactor α. Kawaji *et al.* [69] have found anomalous negative MC due to SO interaction in GaAs/AlGaAs heterostructure. Bergmann has reported on positive MR (negative MC) with thin

Mg-films covered with some amounts of Au atoms [27]. The superposition with Au increases SO scattering and the magnitude of positive MR is larger with increasing the amount of Au. The scattering probability is proportional to $(Z - Z')^4$, where Z is the atomic number of doped atom and Z' that of the matrix. In the present work, we describe the MC of the above-mentioned δ-doped sample and the various relaxation time deduced from the experimental data.

In this experiment we have used three kinds of Si samples with an Sb δ-doped layer, which is grown on Si $< 100 >$ substrate by molecular beam epitaxy method. According to Secondary ion mass spectrometry (SIMS) measurements [47], the broadening of δ-doped layer is about 20nm. The electrodes were put on the side of the sample, so electrons conduct in not only δ-doped layer but also the substrate at higher temperatures. The valley degeneracy n_v is 2 on the Si $< 100 >$ layer.

Figure 4.2.1 shows temperature dependence of resistance for three kinds of samples. Generally, the differential coefficient of the resistance with respect to temperature dR/dT for the samples tends to be negative in our range of measurement, and the dependence show a characteristic behavior for respective samples, since electrons conduct in both δ-doped layer and the substrate at higher temperatures. Temperature dependence of resistance for sample F is similar to that of sample B. Figure 4.2.2 illustrates a plot of resistance as a function of the reciprocal of the temperature T^{-1}. It is found that the resistance R is approximated by the sum of two exponential terms with each characteristic activation energy of $\epsilon_1 = 10.1$meV and $\epsilon_2 = 2.2$meV. If Mott-Hubbard type's band is assumed, ϵ_1 represents the activation energy of an electron from the Fermi level located in the lower Hubbard band (LHB) to the conduction band, and ϵ_2 corresponds to that to the extended states in the upper Hubbard band (UHB) as mentioned in § 2.3. Unexpectedly, sample F does not show metallic conduction such as sample D and E, though it includes 1.0ML. We discuss the MR for sample F later. Sample H, whose portion of the occupation of Sb atoms in the δ-doped layer is 0.06 ML, shows a complex temperature dependence, and we could not measure MR at lower temperatures because the resistance is too large. In this

thesis, we do not describe it in detail.

As for temperature dependence of resistance for sample G, whose portion of the occupation of Sb atoms in the δ-doped layer is 0.11 ML, the resistance rises with decreasing temperatures between 300K and 160K, and has a peak around 160K. At lower temperatures, the resistance gently rises as the temperature decreases, not exponentially. It is considered that electrons mainly conduct in the substrates at higher temperatures and in δ-doped layer at lower temperatures.

Especially we focus on the sample G, whose concentration corresponds to the 2D donor concentration of N_D=7.5×10^{13}cm^{-2}. Temperature dependence of the conductance below 4.2K under various magnetic fields for the sample is shown in Fig.4.2.3. As magnetic field increases, the conductance increases in the range of our measurements. In the WL regime, the conductance changes logarithmically as $\Delta\sigma = \alpha_T n_v (e^2/2\pi^2\hbar) \ln T$ for 2D system, where

$$\alpha_T = p + 1 - \frac{3}{4}F, \tag{111}$$

when the intervalley scattering is important and the electron-electron (e-e) interaction is considered [70]. In the case of the strong SO interaction, the expression of α_T is defined in § 4.3.1. Here p is an exponent when an inelastic scattering time can be expressed as $\tau_\epsilon \propto T^{-p}$. F is introduced by Altshuler *et al.* [35] as described in § 2.8. The prefactors $\alpha_T n_v$ deduced from the experimental data in Fig.4.2.3 are 0.93 for B=0T, 0.77 for B=1T, 0.68 for B=2T and B=3T, respectively. The decrease of $\alpha_T n_v$ with increasing magnetic field was observed. In the absence of a magnetic field α_T is 0.46 if the valley degeneracy n_v= 2 in the δ-doped layer is taken into account.

Figure 4.2.4 shows the MC data at various temperatures for sample G in perpendicular fields. The positive MC is observed due to the destruction of the quantum interference by the application of a moderate magnetic field. In particular, the negative MC is observed in the regime of very weak field. The negative MC is attributed to the AL effect due to the SO interaction.

The MC data at various temperatures are shown in Fig.4.2.5, where the magnetic field was applied in a parallel direction to the δ-doped layer. The MC is always

negative and specific temperature dependence is not seen in our range of measurement. The existence of negative MC in a parallel field indicates that the spin-Zeeman splitting in the interaction $g\mu_B B\cdot\sigma$ is important and the orbital motion is not effective.

Fig.4.2.6 shows the angular dependence of the ratio of the MR, $[R(2\mathrm{T})-R(0)]/R(0)$ at 4.2K and 2T for sample G. As described above, we observe negative MR in perpendicular field (θ=0°) and positive MR is observed in the parallel field to the layer (θ=90°). The anisotropy of the MR reflects a 2D nature of the electrons in the δ-doping layer.

The MC in the WL regime including SO scattering for a perpendicular magnetic field on 2D system is introduced by Hikami *et al.* [22], including the prefactors $n_v\alpha_H$,

$$\Delta\sigma_L(B) = n_v\alpha_H\frac{e^2}{2\pi^2\hbar}[\frac{3}{2}\{\Psi(\frac{1}{2}+\frac{l_B^2}{4D\tau_1}) - \ln\frac{l_B^2}{4D\tau_1}\}$$

$$-\frac{1}{2}\{\Psi(\frac{1}{2}+\frac{l_B^2}{4D\tau_\epsilon}) - \ln\frac{l_B^2}{4D\tau_\epsilon}\}], \qquad (112)$$

where various physical parameters are defined in § 2.5.2. α_H in the presence of the intervalley scattering is expressed as [70],

$$\alpha_H = 1 - \frac{F}{4}. \qquad (113)$$

The experimental data on MC are compared with the theoretical expressions, eqs.(112) and (36), using three fitting parameters $n_v\alpha_H$, τ_ϵ and τ_a. Here we ignored the e-e interaction effect because we cannot perform the fits of the experimental data without large ambiguity even though we take the interaction effect into account. Here we wish to focus on the negative MC due to the AL below 0.5T. In consequence, experimental data fit well to eqs.(112) and (36) after choosing the suitable fitting parameters.

Figure 4.2.7 shows the temperature dependence of the inelastic scattering time τ_ϵ for the sample E and sample G, and the SO scattering time τ_{so} for sample G extracted from the analyses of MC in Fig.4.2.4. If the condition $k_F l > 1$ is fulfilled, the WL theories are applied, and the value of $k_F l$ for respective sample in consideration of the valley degeneracy is estimated at 2.5 for sample G and 1.4 for sample E, respectively. As for the inelastic scattering time, the relations of $\tau_\epsilon \propto T^{-1}$ for sample G is deduced

in the range of our measurements. In the previous section, it was reported that $\tau_\epsilon \propto T^{-1}$ was obtained for sample E. The inelastic scattering is considered to be acoustic phonon (deformation potential) scattering. According to Altshuler and Aronov [71], in 2D systems, large momentum transfer processes dominate the e-e interaction and thus $p = 2$ is expected at high temperatures, whereas small momentum transfer in disordered system is dominant at low temperatures and $p = 1$. For sample G the inelastic scattering length is 120nm for T=4.2K. These are larger than the thickness of δ-doped layer $d \approx 20$nm. Although the SO scattering time is generally considered to be temperature independent, our result shows a weak temperature dependence. The ratios $\tau_{so}/4\tau_\epsilon$ of SO scattering time to inelastic scattering time are 0.75 for T=4.2K and 0.60 for T=2.9K and thus the strength of the SO interaction in our system is found to be weaker than that of the thin Mg-film covered with some amounts of Au atom reported by Bergmann [27], for example, $\tau_{so}/4\tau_\epsilon$=0.066 and 0.018 at 4.6K in the case of a Mg-film with 1% and 4% of Au, respectively.

The theory of the relaxation time related to the SO scattering τ_{so} has given by Elliot [72]. Elliott's mechanism is effective if the scattering is caused by heavy impurities.

$$\tau_{so} = \frac{\tau}{(g-2)^2 R^2 k_F^2}, \tag{114}$$

where τ is the elastic scattering time by impurities, g the g-factor of conduction electron and R the atomic radius. As the value of R, we employed a lattice constant of Si. Using τ_{so} and τ extracted from the analyses, we deduce $|g-2| = 1.3 \times 10^{-2}$. The elastic scattering times τ extracted from the conductance (conductivity) of sample G (δ-doped sample) and sample E (bulk sample) at 4.2K in the absence of a magnetic field are 3.0×10^{-15}s and 2.3×10^{-14}s, respectively. The impurity scattering rate for sample G is about eight times as large as that of the sample E. From eq.(114) we calculate τ_{so} on sample E using the value of g-factor obtained by the above-mentioned procedures, and extract $\tau_{so} = 3.5 \times 10^{-9}$s. The ratio $\tau_{so}/4\tau_\epsilon = 0.75$ for δ-doped sample and 110 for a metallic bulk sample are found, therefore, the strength of the SO interaction for a δ-doped sample is certainly stronger than that of the bulk sample.

In order to clearly observe the AL effect for a bulk sample, it is required to increase the impurity concentration and the sample has to be cooled down to very low temperatures in order to suppress the inelastic scattering rate.

In the magnetic field parallel to the layer, spin-Zeeman splitting plays an important role, and we need to take both SO interaction and the spin-Zeeman effect into account. Maekawa and Fukuyama [73] have theoretically studied the effects of spin-Zeeman splitting and SO scattering in 2D systems. The MC is expressed as

$$\Delta\sigma(B) = \frac{e^2}{4\pi^2\hbar}[2\ln(\frac{\tau}{\tau_1} + \frac{D\tau t^2}{3l_B^2}) + \frac{1}{\sqrt{1-\gamma}}\{\ln(\frac{\tau}{\tau_+} + \frac{D\tau t^2}{3l_B^2}) - \ln(\frac{\tau}{\tau_1} + \frac{D\tau t^2}{3l_B^2})\}], \quad (115)$$

where

$$\frac{1}{\tau_1} = \frac{1}{\tau_\epsilon} + \frac{4}{\tau_{so}}, \quad (116)$$

$$\frac{1}{\tau_\pm} = \frac{1}{\tau_\epsilon} + \frac{2}{\tau_{so}}(1 \pm \sqrt{1-\gamma}) \quad (117)$$

and

$$\gamma = (\frac{g\mu_B B}{2\hbar}\tau_{so})^2, \quad (118)$$

where the spin-flip scattering time τ_s is ignored. The results of fits with eqs.(115), (116), (117) and (118) are shown in Fig.4.2.5. The scattering time deduced from the data is not consistent with the results for the data in a perpendicular fields. Here we employ only the results deduced from the data in the perpendicular field.

The value of $n_v\alpha_H$ is approximately 0.4 at each temperature. With the valley degeneracy n_v=2, $\alpha_H \approx 0.2$ is extracted. Fukuyama [74] has considered that α decreases as the intervalley scattering increases, and $n_v\alpha_H$ approaches one as the ratio of the inelastic scattering time to the intervalley scattering time approaches infinity. From the temperature dependence of the conductance in the absence of a magnetic field, we extract α_T=0.5. The result of $p = 1$ deduced from the temperature dependence of the inelastic scattering time does not give a proper value of α_T. Moreover it is found that α_T decreases as the magnetic field increases. It is considered that the rate of intervalley scattering increases by the application of a magnetic field.

Temperature dependence of the resistance for sample F is illustrated in Fig.4.2.8

in the absence of magnetic field below 4.2K. The dependence does not appear to obey the formula of a hopping conduction. In order to make the hopping exponent clear, we try to plot the logarithmic derivative $w = -\partial R/\partial T$ (eq.(83)) as a function of the temperature on a double logarithmic scale. However the good result from the data is not obtained. Moreover, Fig.4.2.9 and 4.2.10 show MR data at low temperatures in the fields perpendicular and parallel to the δ-doped layer, respectively. Angular dependence of MR is not clearly observed. When a hopping conduction is dominant, it is known $\ln \rho(B)/\rho(0)$ is proportional to B^2 with eq.(84). And the MR becomes larger with decreasing temperatures, however, such a behavior for a perpendicular fields is not observed and the temperature dependence indicates an opposite tendency. Sample F might show a metallic conduction at lower temperatures. Two views on sample F are considered, (1)δ-doped layer is broadening and 2D electronic system is not achieved. (2)The upper levels in the confined potential are occupied, so electrons can easily transfer into the other layers.

In conclusion, we have observed the negative MC in weak magnetic field due to the SO interaction in the δ-doped Si. On the other hand, the negative MC caused by the AL has not been explicitly observed for sample E because of the small SO scattering rate by impurities. From the obtained result of $\tau_{so}/4\tau_{\epsilon}$, it is concluded that the strength of the SO interaction for a δ-doped sample is stronger than that of the bulk sample.

4.3 Experimental results for InSb on GaAs substrates

So far concerning the electronic properties of bulk InSb near metal-insulator (MI) transition a large number of works have been carried out [11][75][76][77]. As is well known, the effective Bohr radius of the donor in InSb is very large ($a_D \sim 650\mathring{A}$), in other words the effective Rydberg energy Ry of the donor is very small, on account of the small effective mass ($m_e = 0.014m_0$) and the large dielectric constant. Therefore the parameter γ ($= \hbar\omega_c/2Ry$) $= 1$ is fulfilled at 0.13T in n-InSb ($Ry \sim 0.67$meV), and the magnetically induced MI transition has been systematically studied. Here γ characterizes the effective strength of the magnetic field. Recently InSb is expected as high-speed devices and magnetic sensors, because the electron mobility is higher than that of any other III-V semiconductors. In order to utilize it as application devices, InSb thin layers are grown on semi-insulating GaAs using molecular beam epitaxy (MBE) method. However, a large mismatch of lattice constant between InSb and GaAs induces high density misfit dislocations at the InSb/GaAs interface, which causes the degradation of crystal quality and electrical properties of n-InSb layers. Recently, a carrier accumulation model based on some experimental results and an estimated band diagram of InSb/GaAs hetero-interface have been proposed, and it is found that the electron concentration in the accumulation layer depends on the surface orientations of substrates [78]. As another example, Hermans *et al.* have reported that the large mismatch between InSb layer and semi-insulating InP also causes carrier accumulation [79]. These studies show the strikingly different transport properties from bulk InSb.

For thin film InSb on GaAs (100) substrate, two kinds of carriers are expected to exist in the InSb thin layer and in the interface, and the transport properties depend on the respective carrier concentration and mobility. Especially we are interested in the localization effect of electrons at the interface. The Hamiltonian which describes the spin-orbit (SO) interaction is given by

$$\mathcal{H}_{so} = \frac{\hbar}{4m_e^2c^2}(\nabla V(\vec{r}) \times \vec{p}) \cdot \vec{\sigma}, \tag{119}$$

where c is the light velocity and $\vec{\sigma}$ the Pauli spin matrix. Indium Antimonide consists of heavy elements, which results in the stronger SO interaction arising from the band structure. Accordingly, anti-localization (AL) effect is expected for InSb analogous to Si:Sb.

Figure 4.3.1 shows the temperature dependence of the resistivity for two samples in the absence of magnetic field. For the undoped sample we found that the resistivity significantly increases with decreasing temperatures. The resistivity of Sn-doped sample at 8.6K is just 1.3 times as large as that at 300K. The resistivity for the undoped sample is shown in Fig.4.3.2 as a function of T^{-1}. Between 300 and 200 K the resistivity changes almost two orders of magnitude, but at lower temperatures the change becomes gentle.

Figure 4.3.3 shows the temperature dependence of Hall coefficient for undoped sample. Strangely enough, the peak of the Hall coefficient is observed around 140K, and the Hall coefficient remains steady as the temperature decreases. The feature reminds us of the existence of two types of carrier [53]. The fixed Hall coefficient at low temperatures suggests that the metallic conduction should exist. The temperature dependence of the intrinsic carrier concentration shown in Fig.4.3.4 is expressed by the following formula

$$n = AT^{3/2} \exp(-\frac{E_g}{2k_B T}). \tag{120}$$

$A = 1.8 \times 10^{15}\text{cm}^{-3}$ and the bandgap $E_g = 0.23\text{eV}$ was derived from the data. The typical bandgap of InSb at 300K is 0.24eV [13]. At high temperatures the intrinsic region is clearly seen for thin film InSb. On the other hand, the temperature dependence of the Hall coefficient for Sn-doped sample is shown in Fig.4.3.5. The Hall coefficient at 8.6K is 1.4 times as large as that at 300K. This experimental observation agrees well with the variation of the resistivity. The Hall coefficient remains constant below 50 K analogous to the result for undoped sample. Figure 4.3.6 shows the Hall resistivity ρ_{xy} as a function of magnetic field at 4.2 K. It is found that the Hall resistivity is almost linear for magnetic field in the range of the experiment. In the case of bulk InSb with low impurity concentration, the magnetic freeze-out effect is

predominant by application of the magnetic field and more or less the Hall coefficient should depend on the magnetic field. The result, however, hardly shows the magnetic field dependence. This experimental fact suggests that carriers mainly contributing to the conduction at 4.2K do not originate from the primary InSb thin film. These phenomena mean that two kinds of carriers with different mobilities exist in thin film InSb and at the interface between InSb and GaAs.

4.3.1 Magnetoresistance for undoped sample

Figure 4.3.7 shows the amount of change in the transverse magnetoresistance (MR) for the undoped sample at various temperatures above 4.2 K. At 4.2K the MR gives a steep rise up to 0.3T and has a maximum at 0.3T. After that it gradually decreases, taking a minimum at 1.3T and finally increases with increasing magnetic field. At all events the MR is always positive. The absolute value of MR becomes smaller as the temperature increases. On the other hand, the MR below 4.2K is shown in Fig.4.3.8, and the amount of change in MR slightly rises with decreasing temperature. From the temperature dependence of MR, we found that the transport properties for the undoped sample show a metallic conduction rather than a hopping conduction. It is found that the positive MR has the angular dependence as shown in Fig.4.3.9. The peak of MR shifts to higher magnetic field as the angle θ increases. Here θ is the angle between the magnetic field and the normal line of the InSb thin film. This feature seems to be a typical two dimensional (2D) nature.

The MR data for the undoped sample above 4.2K is shown in Fig.4.3.10, where the magnetic field was applied in a parallel direction to the film surface. In this case the drastic change of the positive MR is not observed, even if the magnetic field increases. This feature should be compared with results of the perpendicular case. At 4.2 K the MR once rises in the weak field, becomes almost constant up to 7.5T, and finally the MR increases again. Surprisingly, the MR at 77K in parallel configuration shows negative one in the weak field suppressing the MR which behaves as B^2 due to the orbital effect. Figure 4.3.11 shows the MR for perpendicular and parallel config-

uration at 4.2K and 77K again.

When the condition $g\mu_B B > k_B T$ is fulfilled, the spin-Zeeman effect starts to work. The g-factor for InSb is 51.3 and the relation $g\mu_B B = k_B T$ at 4.2 K holds at 0.12T in the system. For bulk InSb the spin-Zeeman effect is important, and the effect related to the interaction does not depend on the direction of the magnetic field. So far Morita *et al.* have reported that the effect appears in the temperature dependence of conductivity [80]. In the case of GaAs, on the other hand, g-factor is small and thus the orbital effect is dominant. However, it was found through the MR measurements at high magnetic field in perpendicular field configuration for InSb that the spin-Zeemen effect is not predominant and the orbital effect is much stronger. In the parallel field configuration, the orbital effect is not so effective. From these experimental results it is concluded that carriers in the primary InSb hardly contribute to the electrical conduction and ones in the accumulation layer at the InSb/GaAs interface mainly carry the electrical current. The positive MR in the perpendicular field configuration at 40K and 77K are essentially different from that at lower temperatures. It originates from Lorenz force and the MR behaves as $\rho(B) \sim B^2$.

Judging from the temperature dependence of the resistivity and the Hall coefficient as shown in Fig.4.3.1 and 4.3.3, and from the angular dependence of MR, we conclude that the accumulation layer exists in the interface and accumulated carriers dominate the electrical conduction at low temperatures. With using two-carrier (band) model in § 2.9, the carrier concentration and the mobility in primary thin film InSb and in the interface are discussed. By rewriting eqs.(93) and (95), the conductivity σ and the Hall coefficient R_H can be expressed as follows

$$\sigma = e(n_B\mu_B + n_I\mu_I) \tag{121}$$

and

$$R_H = \frac{1}{e}\frac{(n_B\mu_B^2 + n_I\mu_I^2)}{n_B\mu_B + n_I\mu_I}, \tag{122}$$

where n_B, n_I, μ_B and μ_I are the concentration and the mobility and the subscript B and I denote the bulk and interface, respectively. From the experimental data at low temperatures $n_I = 1.9 \times 10^{16}\text{cm}^{-3}$ derived from the Hall measurements is assumed to

be constant for various temperatures, and $n_B = (1.8 \times 10^{15})T^{3/2}\exp(-0.23eV/2k_BT)$ is expressed in eq.(120). The results of above analysis for μ_B and μ_I are shown in Fig.4.3.12 for the undoped sample. In regard to the mobility of bulk μ_B, the mobility increases strikingly as the temperature decreases below 170 K, which originates from the increase of the relaxation time due to the phonon scattering at low temperatures. The change of the mobility μ_B hardly give a great influence on the transport at low temperatures, because the carrier concentration of bulk n_B becomes smaller with decreasing temperatures as expressed in eq.(120). The mobility expressed by μ_I still continues to decrease in the temperature range below 180K, but the change is not so large. It is considered that the mobility μ_I is mainly affected by the interface roughness scattering and thus does not sensitively depend on the temperatures.

The observation on the temperature dependence of the Hall coefficient and the analysis based on the two-carrier model motivate us to the idea that MR at low temperatures is not caused by the carriers in the primary InSb thin film. At first we will provide further insights into the dimension of the electronic system in the light of theory related to the 2D and to the three-dimension (3D). In any events, the concerned theories include the SO interaction. The theory proposed by Hikami *et al.* [22] is introduced in eqs.(35) and (36) of § 2.5.2. The theory for 3D has been studied by Fukuyama and Hoshino [81] including the SO interaction, which is ignored in the theory by Kawabata [23]. It is expressed as follows,

$$\Delta\sigma(B)/A = \sqrt{h}F(\frac{1+t}{h}) + 0.5\sqrt{\frac{h}{1-\gamma}}F(\frac{t_+}{h}) - F(\frac{t_-}{h})$$

$$-\frac{1}{\sqrt{1-\gamma}}(\sqrt{t_-} - \sqrt{t_+}) + \sqrt{t} - \sqrt{t+1}, \qquad (123)$$

where $A = (\sqrt{3}e^2/2\pi^2\hbar\lambda)\sqrt{\tau/\tau_{so}}$, $t = \tau_{so}/4\tau_\epsilon$, $\lambda = v_F\tau$ $h = (\lambda/l_B)^2(\tau_{so}/\tau)$, $t_\pm = t + 0.5(1 \pm \sqrt{1-\gamma})$. $F(z)$ is introduced in § 2.5.2 by Kawabata. $\gamma = (\hbar\kappa B)^2$ and $\kappa = (3m_e/8m_0)|g|/E_F\tau$. For simplicity, another effects are not taken into account. Figure 4.3.13 and 4.3.14 show the comparison between experimental results for the magnetoconductance (magnetoconductivity) at 4.2K and theories on the 2D and the

3D systems, respectively. We have confirmed the good coincidence for fitting with the theory on 2D system. For the fitting with the theory on 3D system, the large discrepancy is found. It is confirmed that the observed negative magnetoconductance (MC) in weak magnetic field is explicable with the theory for 2D system, and the electronic properties of carriers in the interface are the 2D nature at low temperature beyond mistake.

Temperature dependence of conductance (2D) and conductivity (3D) at low temperatures are shown in Fig.4.3.15 and 4.3.16, respectively. In the WL regime, the conductance changes logarithmically as $\Delta\sigma = \alpha_T(e^2/2\pi^2\hbar)\ln T$ for 2D system (eq.(69)). As shown in Fig.4.3.15 the conductance represented as a function of $\ln T$ has two slopes. Extrapolating the slope at high temperature to T=0, it is found that σ approaches to zero. Thus we make out that in the temperature range investigated the system does not necessarily obey to the WL regime. On one hand, the pre-factor α_T deduced from the low temperature data is 0.55. With this value of α_T we will analyze various experimental results in the latter paragraph. For 3D system it is known that the conductivity changes as $\sigma(T) = \sigma_3(0) + mT^{1/2} + BT$ as shown in eq.(64) of § 2.7, where the second and the third terms are due to the Coulomb interaction and the localization effects, respectively. The temperature dependence of conductivity (3D) is not explicable with the above equation (eq.(64)), and Fig.4.3.15 seems to be the better fit compared with the fits of Fig.4.3.16.

In the next step we will discuss on the inelastic scattering and SO scattering time. The MR in perpendicular field configuration at 77K has the B^2 dependence in the weak field. At low temperatures it also shows the B^2 dependence except for the low field anomaly. At present we cannot identify whether the origin of the MR is the Lorenz force or the electron-electron interaction expressed in eq.(63) of § 2.7. The steep rise of the MR in the weak field at low temperatures is most certainly due to the SO interaction in the WL region as above mentioned. Consequently, the MR as shown in Fig.4.3.7 is considered to consist of the anti-localization (AL) effect arising from the SO interaction and the normal B^2-type component. Employing eqs.(35) and (36)

set out by Hikami *et al.* for the analysis of experimental data, the MC is expressed as,

$$\sigma(B) = \Delta\sigma(0) + \alpha_H \frac{e^2}{2\pi^2\hbar}[\frac{3}{2}\Psi(\frac{1}{2} + \frac{l_B^2}{4D\tau_1}) - \ln\frac{l_B^2}{4D\tau_1}$$

$$-\frac{1}{2}\Psi(\frac{1}{2} + \frac{l_B^2}{4D\tau_\epsilon}) - \ln\frac{l_B^2}{4D\tau_\epsilon}] - cB^2 \tag{124}$$

and

$$\frac{1}{\tau_1} = \frac{4}{\tau_{so}} + \frac{1}{\tau_\epsilon}, \tag{125}$$

where α_H and c are the prefactors, the second term describes the AL effect and the third one describes the normal B^2-type MR due to the orbital motion of carriers. The fitting parameters are α_H, τ_a, τ_ϵ and c. In case that the SO interaction is strong, following relations are proved, i.e.,

$$\alpha_T = p + 1 - \frac{3}{4}F \tag{126}$$

and

$$\alpha_H = -\frac{1}{2} - \frac{F}{2}, \tag{127}$$

where p is an exponent for an inelastic scattering time expressed as $\tau_\epsilon \propto T^{-p}$. F is defined in § 2.8. For fitting of the experimental result we pay attention to the data below 0.5T. At this junction we have tried two different ways.

The approach for fitting with eqs.(124) and (125) is that α_H, τ_a, τ_ϵ and c are all used as fitting parameters and the result of fitting at 4.2K (dashed line) is shown in Fig.4.3.17. In the process of fitting, various values between 0.70 and 2.5 for α_H are obtained, but the values of α_H below 4.2K are almost same and it is 0.74 on average. Figure 4.3.18 shows the SO scattering time and the inelastic scattering time derived from the best fit. In order to evaluate these scattering times, the physical parameters of $n = 8.1 \times 10^{15}\text{cm}^{-3}$, $\tau = 6.2 \times 10^{-15}$s, $D = 8.1 \times 10^{-4}\text{m}^2/\text{s}$ and $E_F = 10.4$meV are employed with use of $m_e = 0.014m_0$. As for the inelastic scattering time the relation of $\tau_\epsilon \propto T^{-1}$ is obtained. It is found that τ_{so} does not show the stronger temperature dependence than τ_ϵ, which is caused by the temperature independence of scattering

centers. Even at higher temperatures, $\tau_\epsilon > \tau$ holds, where τ is the elastic scattering time by impurities, this system attains the WL states. The thickness of the interface region d is estimated from the MR measurement in parallel field configuration as shown in Fig.4.3.9. At 7.5T the MR in parallel field configuration begins to increase, and this indicate that the orbital motion became possible in the interface region due to the shrinkage of the characteristic length l_B, and that $2d > l_B$ is satisfied. l_B at 7.5T is 18 nm and the inelastic scattering length l_ϵ $(= \sqrt{D\tau_\epsilon})$ and the SO scattering one l_{so} $(= \sqrt{D\tau_{so}})$ at 4.2K are 130nm and 100nm, respectively. Accordingly, $2d < l_\epsilon$, l_{so} holds at 4.2 K, and the electronic system shows the 2D nature.

As the temperature dependence of the inelastic scattering time is not so strong at low temperatures, $p \simeq 0$ holds. By comparing the results obtained from the analyses with eqs.(126) and (127), we found that $\alpha_T = 1-3F/4 = 0.55$ and $\alpha_H = -1/2-F/2 = -0.74$, and $F = 0.60$ and 0.48 are obtained. They are better values compared with the results for the δ-doped Si:Sb in the previous section. The discrepancy of F comes from the reason that we put $p \simeq 0$ for latter case, or another reason should be the weak SO interaction.

What is the origin of the strong SO interaction at low temperatures? In the case of bulk InSb, the effect of SO interaction arising from the band structure is dominant, that leads to the AL effect [80][81]. However, for InSb thin film on GaAs substrate, carriers in the interface region of GaAs/InSb dominate the transport properties at low temperatures, and carriers in the primary InSb thin film hardly contribute to the transport at low temperature. There is a possibility that the SO interaction due to the lack of the inversion symmetry is effective as described above in § 2.6. The observation of complicate structures on Shubnikov-de Haas (SdH) oscillation for a doped InSb thin film suggests the zero-field spin splitting of the conduction band. The problem is discussed in the following section.

4.3.2 Magnetoresistance for Sn-doped sample

Figure 4.3.19, 20 and 21 show the MR at 4.2K for Sn-doped sample. The MR shows SdH oscillation, and the system is a degenerate semiconductor. The oscillation becomes more notable for the parallel configuration than that for the perpendicular field. The amplitude of the SdH oscillation does not sensitively depend on the temperature between 2.8K and 4.2K. Figure 4.3.22 shows the MR at 4.3K up to 8T, and Fig.4.3.23 illustrates the results as a function of B^{-1}, which subtracts MR from B^2 and differentiate MR twice with respect to B, in order to make clear the peak of oscillation. We confirmed that the oscillation has a period of $1/B$. Around $0.35\mathrm{T}^{-1}$ a peak has a shoulder in the higher field region and the second differential of MR show two dips. In the case of InSb, g-factor is large, so the spin-splitting of Landau levels is expected at higher magnetic field. The experimental result is considered to reflect it.

As is well known, the extremum of SdH oscillation appears when Fermi level E_F and one of Landau levels coincide.

$$(n+\frac{1}{2}) = \frac{m_e E_F}{\hbar e}\frac{1}{B}, \tag{128}$$

where ω_c is the cyclotron frequency. Figure 4.3.24 shows the result against the characteristic magnetic field where the extremum appear. Certainly the relation of eq.(128) is satisfied. Fermi energy E_F =45meV is obtained from the slope of the data, and the E_F corresponds to $7.3 \times 10^{16}\mathrm{cm}^{-3}$. From the Hall coefficient at low temperatures as shown in Fig.4.3.5, $n = 1.1 \times 10^{17}\mathrm{cm}^{-3}$ is obtained. The difference of carrier concentration is considered to come from the contribution of electrons in only an accumulation layer for the SdH oscillation, and both in the accumulation layer and InSb thin film for the Hall coefficient.

For Sn-doped sample, complicate structures on SdH oscillation are not observed. Therefore, electrons do not occupy some quantized levels in the accumulation layer. Moreover, the zero-field spin splitting of the conduction band, which results from the SO interaction due to the lack of the inversion symmetry, is not observed. We stress that electrical conduction for the system originates from the carriers in the accumu-

lation layer, not in the primary InSb thin film. It is considered that a steep rise of MR for undoped sample originate from the SO interaction strengthened by the strain in the GaAs/InSb interface.

5 Conclusion

In this study galvanomagnetic measurements were carried out to investigate the various kinds of electronic conduction for various types of semiconductors such as the bulk crystals and the δ-doped samples of Si:Sb, and thin film InSb, with the donor concentration close to the metal-insulator (MI) transition. The experimental results for temperature and magnetic field dependence of the resistivity and the Hall coefficient originate in the electronic states which strike up hopping conduction, weak localization (WL) effect, electron-electron (e-e) interaction and spin-orbit (SO) interaction at low temperatures.

It is made clear that the transport characteristics at low temperatures for the sample B with the impurity concentration below the MI transition are dominated by the Efros-Shklovskii type of variable-range hopping conduction. A crossover from the positive to negative magnetoresistance (MR) has been observed as the electric current increases. The current density dependence of the MR originates from the rise in the electron temperature. It is the vital force for transfer of electrons from the strongly localized states (hopping regime in the Lower Hubbard Band) to the WL states (diffusive region in the low energy tail of the Upper Hubbard Band). The results support the idea that the MI transition is Anderson type.

As for sample C with the impurity concentration near the MI transition, the change of the sign of the differential coefficient of the conductivity with respect to temperature $d\sigma/dT$ with the increase of magnetic field has been observed, which originates from the Hartree potential. It is found that the magnetic-field and the temperature dependence of conductivity is stronger than that expected from the e-e interaction effect. Other effect such as anti-localization effect to strongly increase conductivity should exist.

For a metallic sample (sample E), a crossover from the negative to positive MR has been observed as the electric current increases. The current density dependence of MR originates from the rise of the electron temperature and transfer of electrons from the WL states to the conduction band (higher lying energy states than WL ones).

The positive MR caused by the anti-localization (AL) effect has not been explicitly observed in the weak magnetic field.

On the other hand, the positive MR in weak magnetic field due to the SO interaction has been observed in the δ-doped Si. The ratio $\tau_{so}/4\tau_{\epsilon} = 0.75$ for δ-doped sample and 110 for a metallic bulk sample are found, therefore, the strength of the SO interaction for a δ-doped sample is certainly stronger than that of the bulk sample. MR shows the angular dependence. At high fields, negative MR in perpendicular field and positive MR are observed in the field parallel to the δ-doped layer. The anisotropy of the MR reflects a two dimensional (2D) nature of the electrons in the δ-doping layer. Temperature dependence of conductance changes logarithmically, resulting from 2D WL effect.

A carrier accumulation layer is formed at the InSb/GaAs interface, which result in peculiar behavior. For the temperature dependence of the Hall coefficient the anomalous peak is observed around 140K, which means the existence of two types carrier. As well as the δ-doped sample, the anisotropy of the MR reflects a 2D nature of the electrons in the interface. The MR at low temperatures is positive and shows a steep rise up to 0.3T, arising from the AL effect. $\tau_{so} < \tau_{\epsilon}$ holds for InSb thin film sample, on the other hand, $\tau_{so} > \tau_{\epsilon}$ for the δ-doped sample. The strength of the SO interaction for the InSb sample is stronger than that of the δ-doped sample, which reflects the magnitude of positive MR in the weak magnetic field.

6 Appendix

In a normal metal with the electron concentration n and the effective mass m_e the conductivity is given by the Drude formula (eq.(13)). For the impurity scattering, the scattering rate is written as follows

$$\frac{1}{\tau} = \sum_{k'} W(\boldsymbol{k}, \boldsymbol{k'})(1 - \cos\theta_{kk'}), \tag{129}$$

where $W(\boldsymbol{k},\boldsymbol{k'})$ is the scattering probability from the state $\boldsymbol{k}$ to the state $\boldsymbol{k'}$, $\theta_{kk'}$ the angle between the initial wave-vector $\boldsymbol{k}$ and the final wave-vector $\boldsymbol{k'}$. When a lot of impurities are randomly distributed, the potential $V(\boldsymbol{r})$ in the position $\boldsymbol{r}$ is given in eq. (47). The scattering rate using Born approximation is expressed as,

$$W(\boldsymbol{k}, \boldsymbol{k'}) = \frac{2\pi}{\hbar} < | < \boldsymbol{k'}|V|\boldsymbol{k} > |^2 >_{imp} \delta(E_k - E_{k'}), \tag{130}$$

where $< \cdots >$ represents the average on the impurity distribution. The matrix element for the scattering $<\boldsymbol{k'}|V|\boldsymbol{k}>$ is written with the Fourier transform of the impurity potential v_k and the volume in the system Ω

$$\begin{aligned} < \boldsymbol{k'}|V|\boldsymbol{k} > &= \frac{1}{\Omega}\int V(\boldsymbol{r}) e^{i(\boldsymbol{k}-\boldsymbol{k'})\cdot\boldsymbol{r}} d^3\boldsymbol{r} \\ &= \frac{1}{\Omega} v_{k-k'}\rho_{k-k'}. \end{aligned} \tag{131}$$

and

$$\rho_{k-k'} = \sum_i e^{i(\boldsymbol{k}-\boldsymbol{k'})\cdot\boldsymbol{R}_i}. \tag{132}$$

In order to calculate eq.(130), we need the following value

$$< |\rho_{k-k'}| >_{imp} = < \sum_i \sum_j e^{i(\boldsymbol{k}-\boldsymbol{k'})\cdot(\boldsymbol{R}_i - \boldsymbol{R}_j)} >_{imp} . \tag{133}$$

The terms on $i = j$ give the number of impurities N_i, and the terms on $i \neq j$ vanish, taking the average over the random distribution of impurities. Thus, the average of $< |\rho_{k-k'}| >_{imp}$ is given as follows

$$< |\rho_{k-k'}| >_{imp} = N_i. \tag{134}$$

These results are substituted with eq.(129)

$$\frac{1}{\tau} = \frac{2\pi n_i}{\hbar\Omega} \sum_{k'} |v_{k-k'}|^2 \delta(E_k - E_{k'})(1 - \cos\theta_{kk'}), \quad n_i = \frac{N_i}{\Omega}. \tag{135}$$

Assuming the impurity potential $v(r)$ is a short range type and ignoring the wavenumber dependence of $v_{k-k'}$, namely

$$v_{k-k'} = |v|, \tag{136}$$

then eq.(135) is expressed as

$$\frac{1}{\tau} = \frac{2\pi}{\hbar} n_i |v|^2 \rho, \tag{137}$$

where ρ is the density of state on the Fermi surface per unit volume and per spin. Eq.(137) is equivalent to eq.(13).

Though the random potential formed by impurities does not have the spatial symmetry, it is important to notice that the impurity potential eq.(47) has the time reversal symmetry. Due to this character, the matrix element for the scattering from $|\boldsymbol{k}>$ to $|\boldsymbol{k}'>$ should be the same as that for $|\boldsymbol{k}'>$ to $|-\boldsymbol{k}>$ scattering. The matrix element for the scattering from $|\boldsymbol{k}>$ to $|\boldsymbol{k}'>$ by a impurity-1 is given

$$\begin{aligned} < \boldsymbol{k}'|V|\boldsymbol{k} >_1 &= \frac{1}{\Omega}\int e^{-i\boldsymbol{k}'\cdot\boldsymbol{r}} v(\boldsymbol{r}-\boldsymbol{R}_1) e^{i\boldsymbol{k}\cdot\boldsymbol{r}} d^3\boldsymbol{r} \\ &= \frac{1}{\Omega} v_{\boldsymbol{k}-\boldsymbol{k}'} e^{i(\boldsymbol{k}-\boldsymbol{k}')\cdot\boldsymbol{R}_1}. \end{aligned} \tag{138}$$

On the other hand, the matrix element for the scattering from $|-\boldsymbol{k}'>$ to $|-\boldsymbol{k}>$ by a impurity 1 is also given as follows

$$\begin{aligned} < -\boldsymbol{k}|V|-\boldsymbol{k}' >_1 &= \frac{1}{\Omega}\int e^{i\boldsymbol{k}\cdot\boldsymbol{r}} v(\boldsymbol{r}-\boldsymbol{R}_1) e^{-i\boldsymbol{k}'\cdot\boldsymbol{r}} d^3\boldsymbol{r} \\ &= \frac{1}{\Omega} v_{\boldsymbol{k}-\boldsymbol{k}'} e^{i(\boldsymbol{k}-\boldsymbol{k}')\cdot\boldsymbol{R}_1}. \end{aligned} \tag{139}$$

Therefore, the following relation is approved, i.e.,

$$< \boldsymbol{k}'|V|\boldsymbol{k} >_1 = < -\boldsymbol{k}|V|-\boldsymbol{k}' >_1 . \tag{140}$$

The time reversal symmetry holds not only for the term derived from Born approximation, but also for all matrix elements of higher order. For example, the matrix element of the third order is also confirmed such relation as eq.(140)

$$< \boldsymbol{k}'|V|\boldsymbol{k} >^{(3)}_{1,2,3} = < -\boldsymbol{k}|V|-\boldsymbol{k}' >^{(3)}_{3,2,1} . \tag{141}$$

Assuming that the matrix elements for the respective scattering processes are V_a, V_b, V_c, $\cdots$, the total transition probability of the scattering W is expressed as

$$W \propto < |\tilde{V}|^2 >_{imp}, \tag{142}$$

where

$$\tilde{V} = V_a + V_b + V_c + \cdots. \tag{143}$$

Here the each matrix element has the phase which depends on the position of the impurity, for example, $e^{i(\boldsymbol{k}-\boldsymbol{k}')\cdot\boldsymbol{R}_1}$, $e^{i(\boldsymbol{k}-\boldsymbol{k}')\cdot\boldsymbol{R}_2}$, $\cdots$ for the term of the Born approximation. Therefore the product of the different matrix elements vanishes on the average over the random distribution of impurities and the following expression is obtained

$$W \propto (|V_a|^2 + |V_b|^2 + |V_c|^2 + \cdots). \tag{144}$$

If one puts $\boldsymbol{k}'=-\boldsymbol{k}$ into eq.(141), taking into account the time reversal symmetry as eq.(140),

$$< -\boldsymbol{k}|V|\boldsymbol{k} >^{(3)}_{1,2,3} = < -\boldsymbol{k}|V|\boldsymbol{k} >^{(3)}_{3,2,1}, \tag{145}$$

the matrix elements for two different scattering processes become perfectly equal. As $|V_a| = |V_b|$ holds for two scattering processes a and b, and the phases for the respective processes are different each other, the transition probability is $2|V_a|^2$. When $V_a = V_b$ holds such as eq.(141) in consideration of the phase, the transition probability is expressed as $|2V_a|^2 = 4|V_a|^2$. In this case two scattered waves for the reversed processes have the same phase due to the time reversal symmetry, and the interference take place.

7 Acknowledgements

I would first like to express my sincere appreciation to Professor Tyuzi Ohyama who draws attention to this area and provides me with stimulating ideas, guidance and encouragements in the process of this study. Frequent, stimulating and helpful discussions with Professor Shuichi Ishida of Science University of Tokyo in Yamaguchi are gratefully acknowledged. I am also deeply indebted to Dr. Hiromi Kobori for his considerable assistance and technical support with the experiment. I am grateful to Professor Hiroyasu Nakata for his instructive comments. I wish to sincerely thank Professor Ken-ichi Fujii for setting up ^{3}He system. I express my appreciation to Dr. Ichiro Shibasaki to provide InSb thin film samples. And this work was experimentally supported by Dr. Kazuo Satoh, Mr. Tadaoki Kusaka and Mr. Yoshiharu Kakehi who belong to Technology Research Institute of Osaka Prefecture. I am thankful to the other members of Ohyama research group for supporting me and having a great time. I was indebted to Asahi Woodtech Ltd. for the award of a scholarship.

References

[1] H. Fritzsche and K. Lark-Horovitz, Phys. Rev. **2** 400 (1955).

[2] W. Sasaki and Y. Kanai, J. Phys. Soc. Jpn. **11** 894 (1956).

[3] N. F. Mott, Metal-Insulator Transition, 2nd ed. Taylor and Francis, London, 1990.

[4] P. P. Edwards and M. J. Sienko, Phys. Rev. B **17** 2575 (1978).

[5] J. Hubbard, Proc. Roy. Soc. **A277** 237 (1964).

[6] P. W. Anderson, Phys. Rev. **109** 1492 (1958).

[7] G. Bergmann, Physics Reports, **107** 1 (1984).

[8] F. Komori, S. Kobayashi and W. Sasaki, J. Phys. Soc. Jpn. **51** 295 (1982).

[9] A. P. Long and M. Pepper, J. Phys. C **17** 425 (1984).

[10] M. Kaveh and N. F. Mott, Phil. Mag. Lett. **56** 97 (1987).

[11] S. Ishida and E. Otsuka, J. Phys. Soc. Jpn. **42** 542 (1977).; S. Ishida and E. Otsuka, J. Phys. Soc. Jpn. **43** 124 (1977).

[12] R. G. Mani, L. Ghenim and J. B. Choi, Phys. Rev. B, **43** 12630 (1991).

[13] M. Shayegan, V. J. Goldman and H. D. Drew, Phys. Rev. B, **38** 5585 (1988).

[14] A. Fujimoto, H. Kobori, T. Ohyama and S. Ishida, phys. stat. sol. (b) **210** 263 (1998).

[15] A. Fujimoto, H. Kobori, K. Fujii, T. Ohyama and S. Ishida, phys. stat. sol. (b) **218** 177 (2000).

[16] A. Fujimoto, H. Kobori, K. Fujii, T. Ohyama amd S. Ishida, Ann. Phys. **8** Spec. Issue, SI-69 (1999).

[17] A. Fujimoto, H. Kobori, T. Ohyama, S. Ishida, K. Satoh, T. Kusaka and Y. Kakehi, Physica B (to be published).

[18] Y. Yafet, R. W. Keys and E. N. Adams, J. Phys. Chem. Solids **1** 137 (1956).; R. W. Keys and R. J. Sladek, J. Phys. Chem. Solids **1** 143 (1956).

[19] N. F. Mott, Rev. Mod. Phys. **50** 203 (1978).

[20] D. J. Thouless, Phys. Rev. Lett. **39** 1167 (1975).

[21] E. Abrahams, P. W. Anderson, D. C. Licciarrdello and T. V. Ramakrishnan, Phys. Rev. Lett. **42** 673 (1979).

[22] S. Hikami, A. I. Larkin and Y. Nagaoka, Prog. Theor. Phys. **63** 707 (1980).

[23] A. Kawabata, Solid State Commun. **34** 431 (1980).

[24] S. Morita, N. Kihoshiba, Y. Koike, T. Fukase, M. Kitagawa and S. Ishida, J. Phys. Soc. Jpn. **53** 2185 (1984).

[25] S. K. Greene, J. Singleton, P. Sobkowicz, T. D. Golding, M. Pepper, J. A. A. J. Perenboom and J. Dinan, Semicond. Sci. Technol. **7** 1377 (1992).

[26] P. D. Dresselhaus, C. M. A. Papavassilius, R. G. Wheeler and R. N. Sacks, Phys. Rev. Lett. **68** 106 (1992).

[27] G. Bergmann, Physics Reports, **107** 1 (1984).

[28] F. Komori, S. Kobayashi and W. Sasaki, J. Phys. Soc. Jpn. **51** 3136 (1982).

[29] P. A. Lee and T. V. Ramakrishnan, Phys. Rev. B **26** 4009 (1982).

[30] H. Fukuyama, J. Phys. Soc. Jpn. **48** 2169 (1980).; H. Fukuyama, J. Phys. Soc. Jpn. **50** 3407 (1981).

[31] B. L. Altshuler and A. G. Aronov, Solid State Commun. **30** 115 (1979); JETP, **50** 968 (1979).

[32] B. L. Altshuler, A. G. Aronov, A. I. Larkin and D. E. Khmelnitskii, Soviet Phys. -JETP **54** (1981) 411.

[33] W. L. McLean and T. Tsuzuki, Phys. Rev. B **29** 503 (1984).

[34] R. N. Bhatt and P. A. Lee, Solid State Commun. **48** 755 (1983).

[35] B. L. Altshuler, A. G. Aronov and P. A. Lee, Phys. Rev. Lett. **44** 1288 (1980).

[36] L. Kleinman, Phys. Rev. **160** 585 (1967).

[37] D. Langreth, Phys. Rev. **181** 753 (1969).

[38] T. Ando, A. B. Fowler and F. Stern, Rev. Mod. Phys. **52** 437 (1982).

[39] A. Miller and E. Abrahams, Phys. Rev. **120** 745 (1960).

[40] D. K. Paul and S. S. Mitra, Phys. Rev. Lett. **31** 1000 (1973).

[41] R. F. Allen and C. J. Adkins, Philos. Mag. **26** 1027 (1972).

[42] I. S. Shlimak and E. I. Nikulin, Sov. Phys. Lett. JETP **15** 30 (1972).

[43] A. L. Efros and B. I. Shklovskii, J. Phys. C: Solid State Phys., **8** L49 (1975).

[44] A. G. Zabrodskii, Sov. Phys. -Semicond. **14** 670 (1980).

[45] B. I. Shklovskii, Soviet Phys. -Semicond. **6** 1053 (1973).; **8** 268 (1974).

[46] T. G. Castner, N. K. Lee G. S. Cieloszyk and G. L. Salinger, Phys. Rev. Lett. **34**, 1627 (1975).

[47] S. Fukatsu, S. Kubo, Y. Shiraki and R. Ito, Appl. Phys. Lett. **58** 1152 (1991).

[48] I. Shibasaki, J. Cryst. Growth **175/176** 13 (1997).; A. Okamoto and I. Shibasaki, J. Cryst. Growth **201/202** 765 (1999).

[49] K. Morigaki and M. Onda, J. Phys. Soc. Jpn. **36** 1049 (1974).

[50] A. N. Ionov, M. N. Matveev, R. Rentzsch and I. S. Shlimak, Sov. Phys. -JETP. Lett. **42** 406 (1985).

[51] A. N. Ionov, I. S. Shlimak and M. N. Matveev, Solid State Commun. **47** 763 (1983).

[52] V. L. Nguyen, B. Z. Spivak and B. I. Shklovskii, Sov. Phys. JETP **62**, 1021 (1985).

[53] H. Miyazawa and H. Ikoma, J. Phys. Soc. Jpn. **23**, 290 (1967).

[54] N. Sclar and E. Burstein, J. Phys. Chem. Solids **2**, 1 (1957).

[55] C. Yamanouchi, K. Mizuguchi and W. Sasaki, J. Phys. Soc. Jpn. **22** 859 (1967).

[56] W. Sasaki, Prog. Theor. Phys. Suppl. **57** 225 (1975).

[57] T. Kurosawa, M. Matsui and W. Sasaki, J. Phys. Soc. Jpn. **42** 1622 (1977).

[58] H. Brooks, Phys. Rev. **83** 879 (1951).; H. Brooks, Advan. Electron Phys. **7** 158 (1955).

[59] J. Bardeen and W. Shockley, Phys. Rev. **80** 72 (1950).

[60] T. G. Castner, W. N. Shafarman and D. Koon, Phil. Mag. B **56** 805 (1987).

[61] T. F. Rosenbaum, R. F. Milligan, M. A. Paalanen, G. A. Thomas and R. N. Bhatt, Phys. Rev. B **27** 7509 (1983).

[62] W. N. Shafarman, D. W. Koon and T. G. Castner, Phys. Rev. B **40** 1216 (1989).

[63] J. C. Ousset, S. Askenazy, H. Rakoto and J. M. Broto, J. Physique **46** 2145 (1985).

[64] D. V. Baxter, R. Richter, M. L. Trudeau, R. W. Cochrane and J. O. Strom-Olsen, J. Physique **50** 1673 (1989).

[65] M. Takeshima, Phys. Rev. B **40** 3090 (1989).

[66] K. Seeger, Semiconductor Physics, 5nd ed. Springer, Berlin, 1991.

[67] Y. Isawa, J. Phys. Soc. Jpn. **53** 2865 (1984).

[68] Y. Kawaguchi and S. Kawaji, J. Phys. Soc. Jpn. **48** 699 (1980).

[69] S. Kawaji, K. Kuboki, H. Shigeno, T. Nambu, J. Wakabayashi, J. Yoshino and H. Sasaki, Proc. 17th Int. Conf. on Physics of Semicond., ed. J. D. Chadi and W. A. Harrison p.413 (Springer-Verlag, 1985).

[70] H. Fukuyama, J. Phys. soc. Jpn, **50** 3562 (1981).

[71] B. L. Altshuler and A. G. Aronov, Electron-Electron Interactions in Disordered Systems, edited by A. L. Efros and M. Pollak, North Holland, Amsterdam p.1 (1985).

[72] R. J. Elliott, Phys. Rev. **96** 266 (1954).

[73] S. Maekawa and H. Fukuyama, J, Phys. Soc. Jpn. **50** 2516 (1981).

[74] H. Fukuyama, Prog. Theor. Phys. Suppl. **69** 220 (1980).

[75] H. J. Horostowski, F. J. Morin, T. H. Geballe and G. H. Wheatley, Phys. Rev. **100** 1672 (1955).

[76] H. Tokumoto, R. Mansfield and M. J. Lea, Phil. Mag. B **46** 93 (1982).

[77] R. Mansfield, M. Abdul-Gader and P. Fozooni, Solid-State Elec. **28** 109 (1985).

[78] T. Tanaka, M. Washima and H. Sakaguchi, Jpn. J. Appl. Phys. **38** 1107 (1999).

[79] J. Heremans, D. L. Partin, D. T. Morelli, C. M. Thrush, G. Karczewshi and J. K. Furdyna, J. Appl. Phys. **74** 1793 (1993).

[80] S. Morita, N. Mikoshiba, Y. Koike, T. Fukase, S. Ishida and M. Kitagawa, Solid-State Electronics, **28** 113 (1985).

[81] H. Fukuyama and K. Hoshino, J. Phys. Soc. Jpn. **50** 2131 (1981).

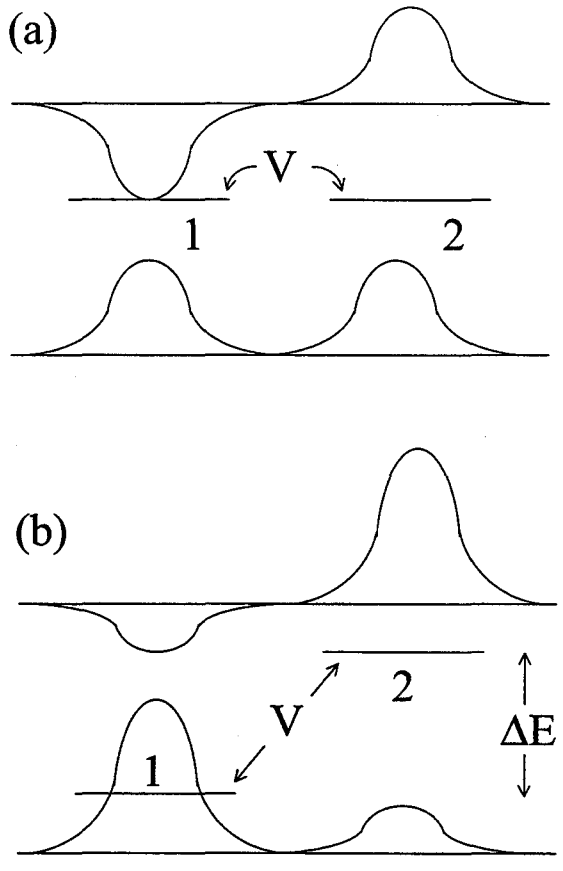

Fig.2.2.1 An electron is transfered between two levels with energy E_1 and E_2 by transfer V. The wavefunctions of stationary states are shown schematically for two cases: (a)$\Delta E = 0$ and (b)$\Delta E \gg |V|$.

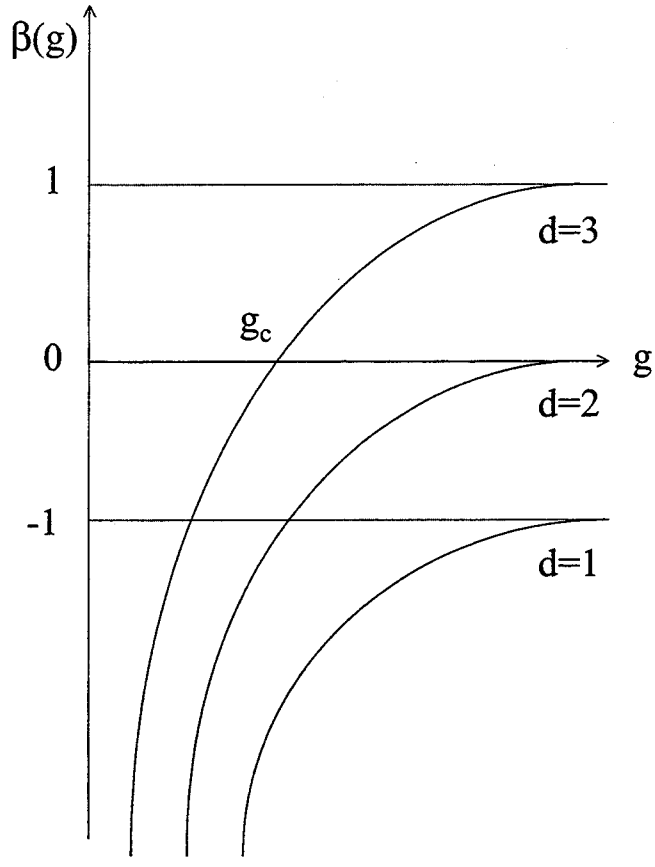

Fig.2.4.1 The behavior of $\beta(g)$ is shown schematically for $d = 1, 2, 3$.

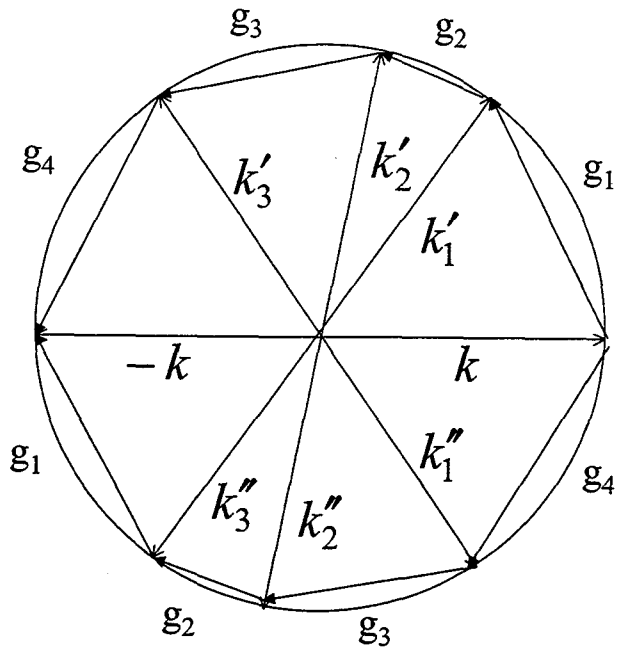

Fig.2.5.1 The electron in the eigenstate of momentum k is scattered via two complementary series. g_1, g_2, g_3 and g_4 represent the change of momentum.

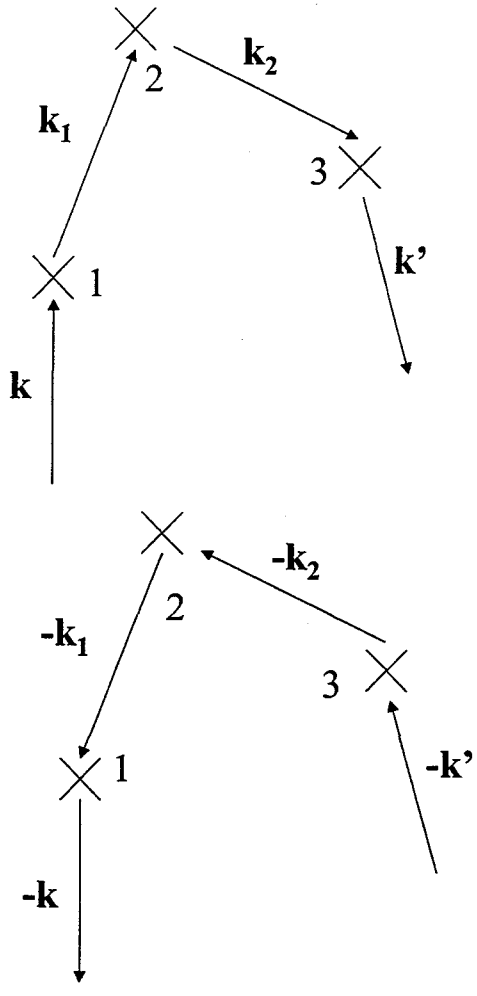

Fig.2.5.2 The third order scattering processes whose matrix elements are equal to each other due to the time reversal symmetry.

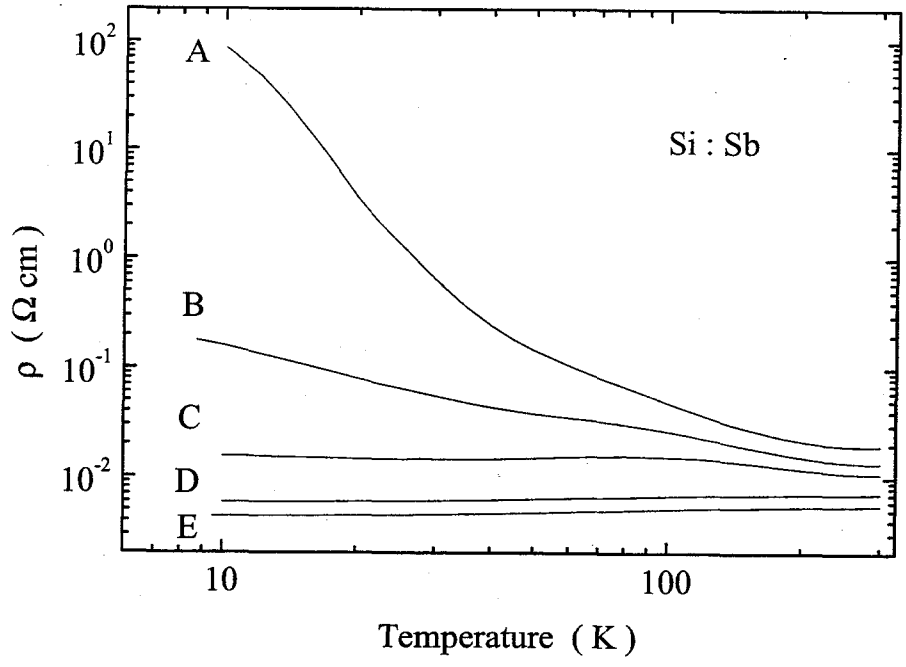

Fig.4.1.1 Temperature dependence of resistivity for five samples on Si:Sb.

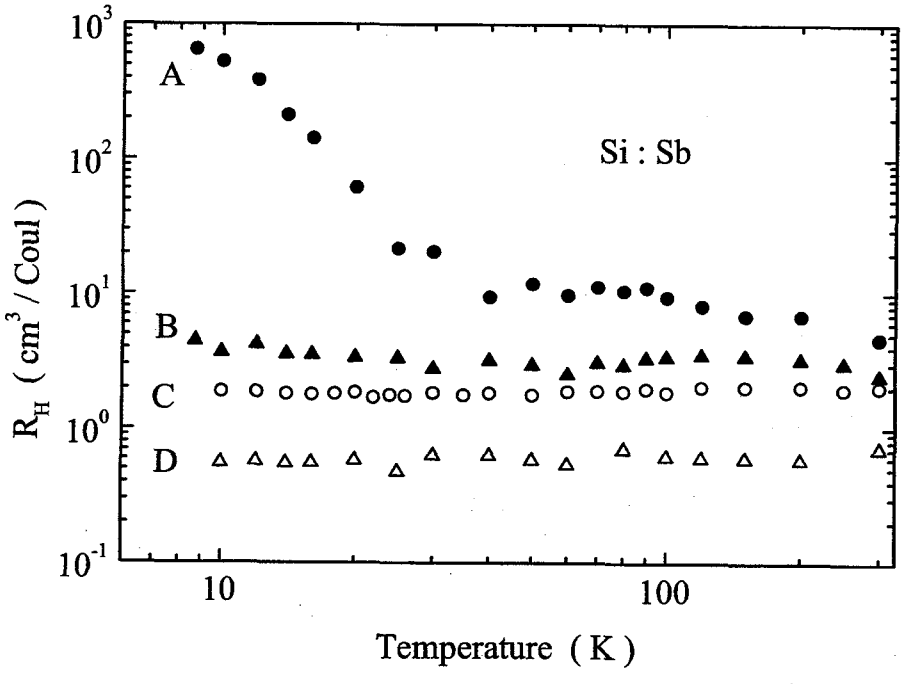

Fig.4.1.2 Temperature dependence of Hall coefficient for five samples on Si:Sb.

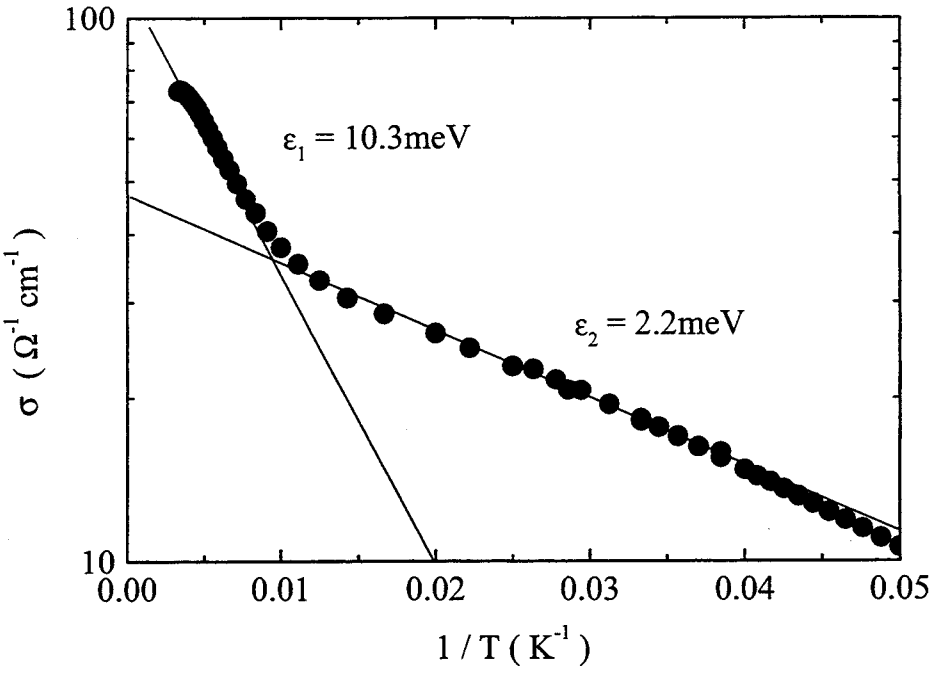

Fig.4.1.3 Conductivity above 20K as a function of T^{-1}.

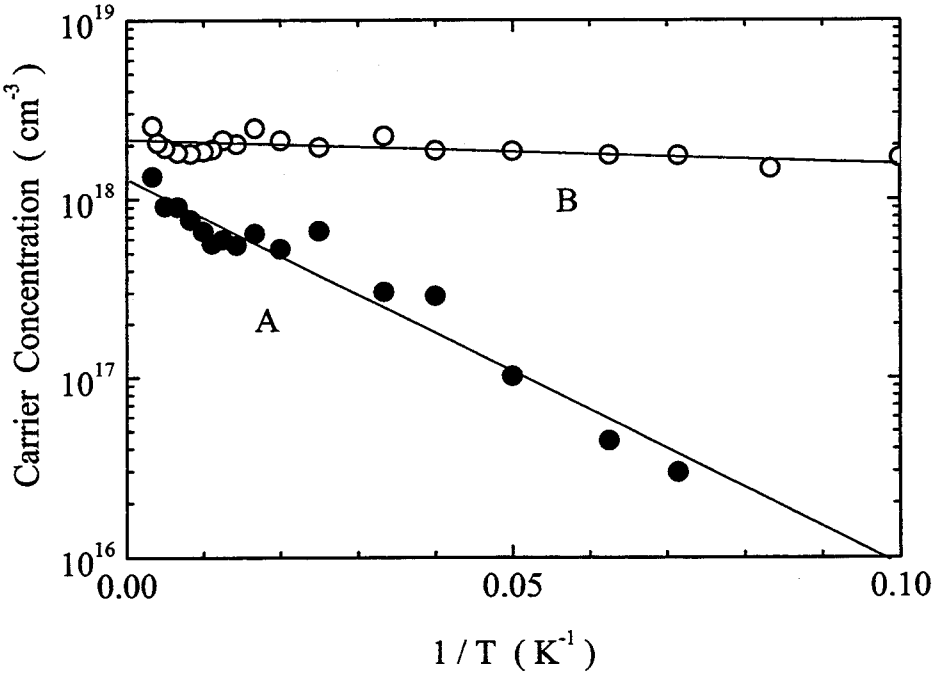

Fig.4.1.4 Carrier concentration as a function T^{-1}. Solid and open circles are for sample A and B, respectively.

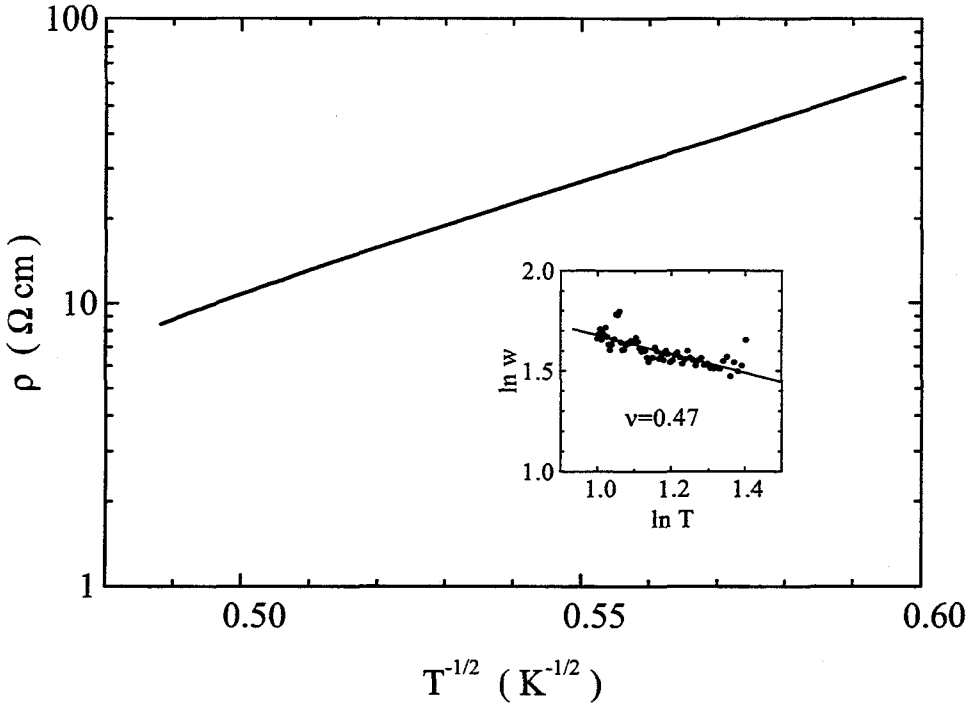

Fig.4.1.5 Resistivity between 2.8K and 4.2K as a function of $T^{-1/2}$. Inset: log-log plot of the logarithmic derivative $w = -\partial \ln \rho / \partial \ln T$. A fit to the expression $\ln w = -\nu \ln T + const.$ (solid line) yeilds the hopping exponent of $\nu = 0.47$.

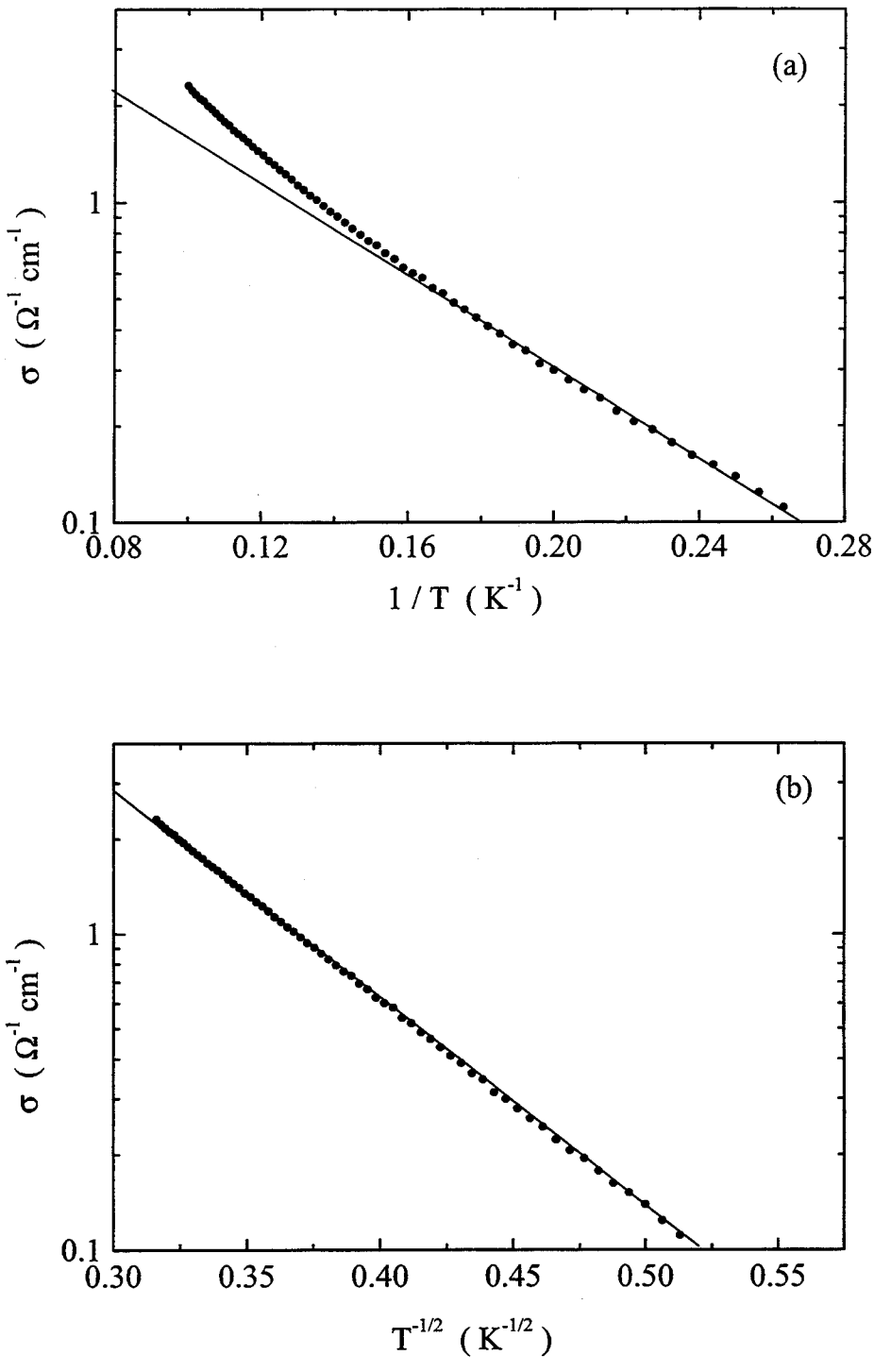

Fig.4.1.6 (a)Conductivity between 3.8K and 10K as a function of T^{-1}. (b)One as a function of $T^{-1/2}$.

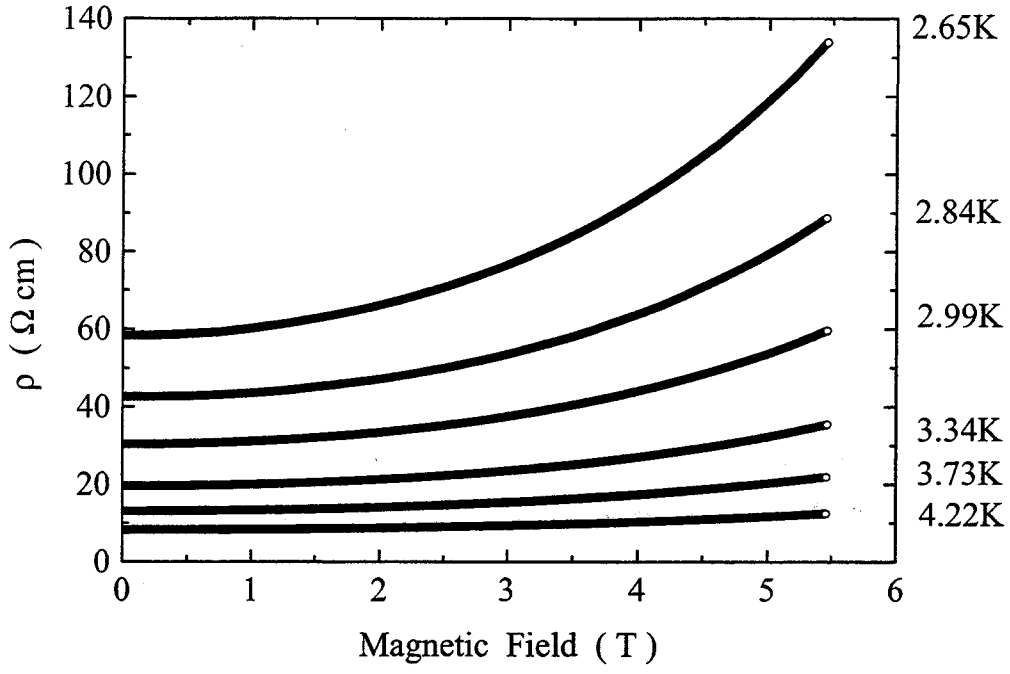

Fig.4.1.7 MR at various temperatures below 4.2K.

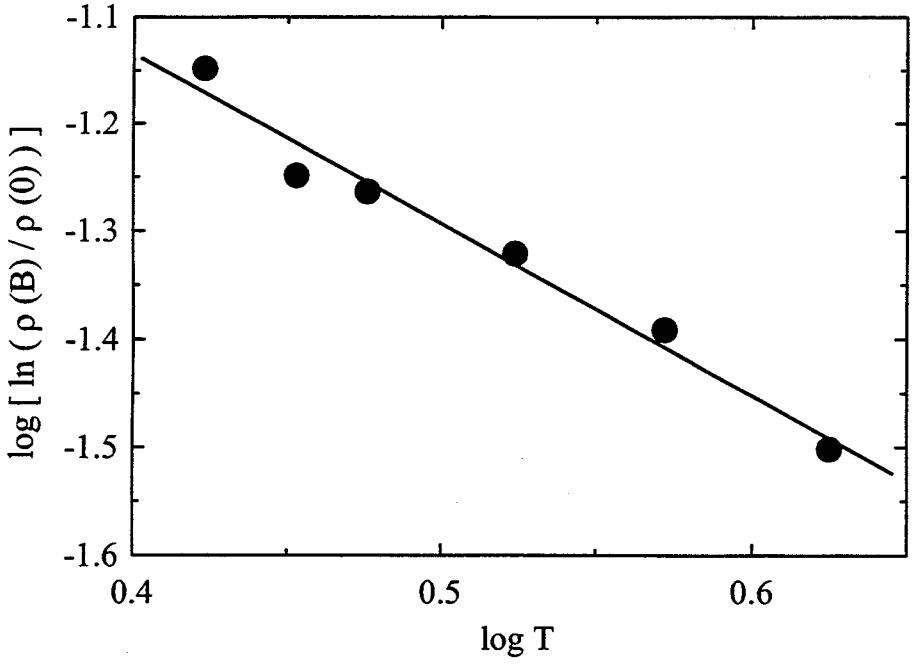

Fig.4.1.8 $\log(\ln(\rho(B)/\rho(0)))$ vs $\log T$ in the magnetic field $B = 1.5$T. The slope $y = 1.6$ indicates that ES-type of VRH conduction is predominant.

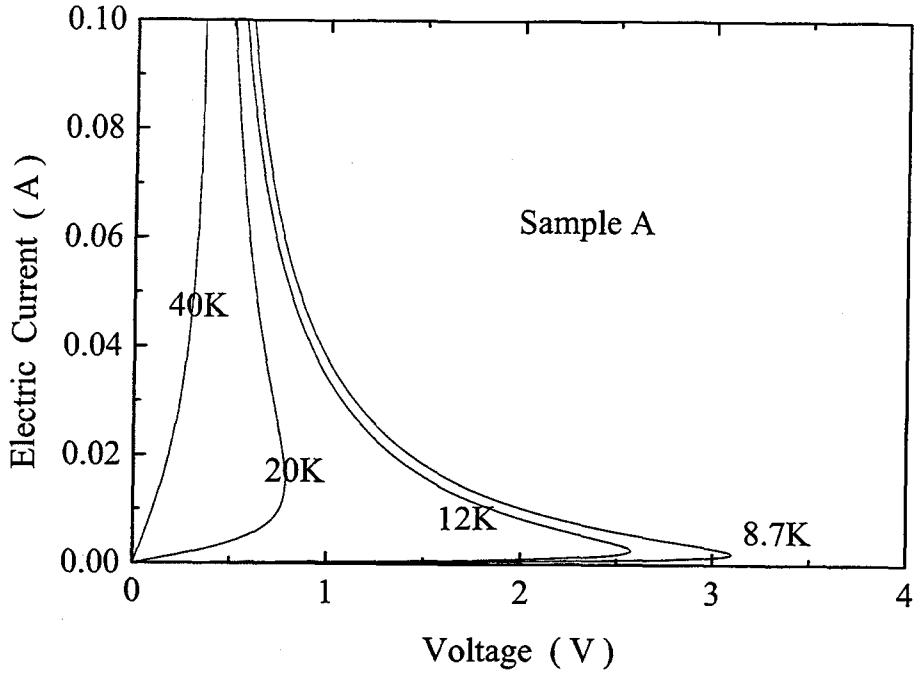

Fig.4.1.9 I-V characteristics at various temperatures for sample A.

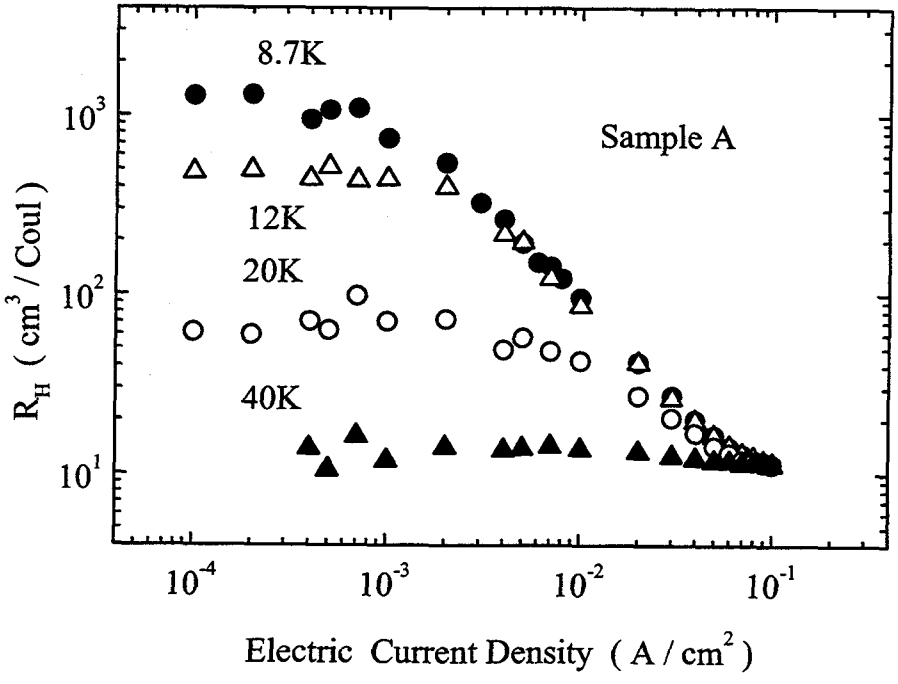

Fig.4.1.10 Electric current density dependence of Hall coefficient at various temperatures for sample A.

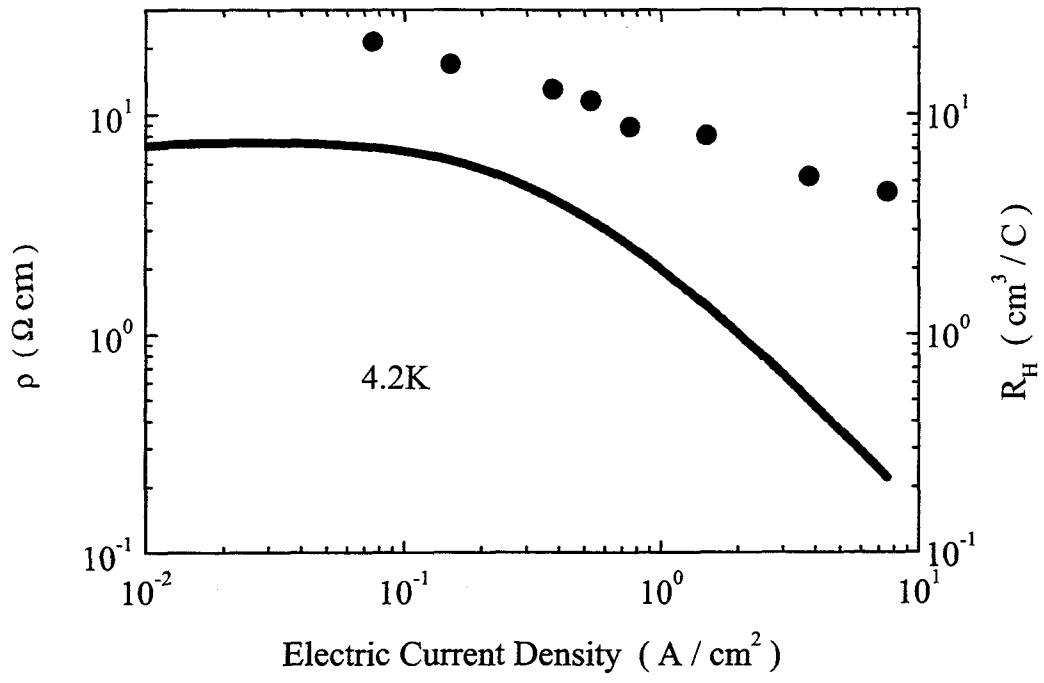

Fig.4.1.11 The dependence of resistivity (solid line) as well as Hall coefficient (solid circles) on the electric current density at 4.2K.

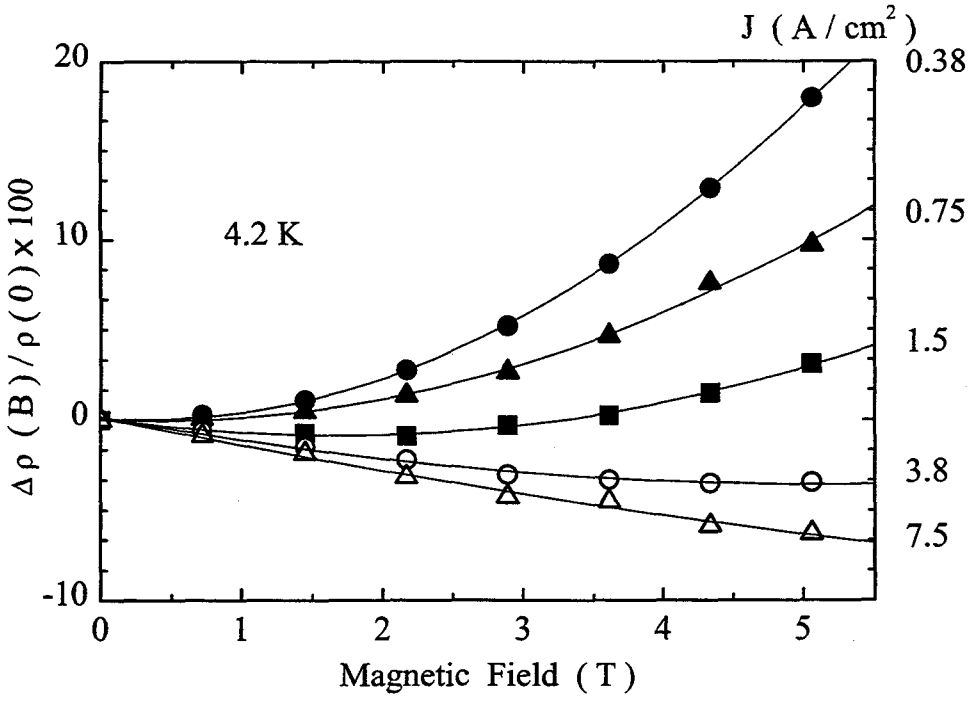

Fig.4.1.12 MR for different electric current densities at 4.2K. Solid lines are after eq.(100).

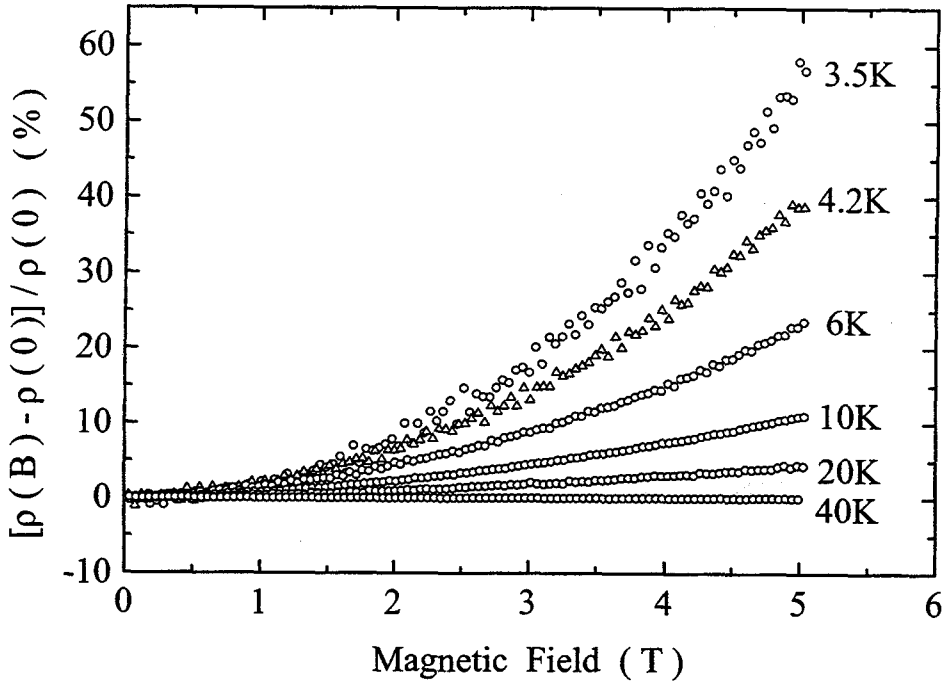

Fig.4.1.13 MR in ohmic region above 3.5K.

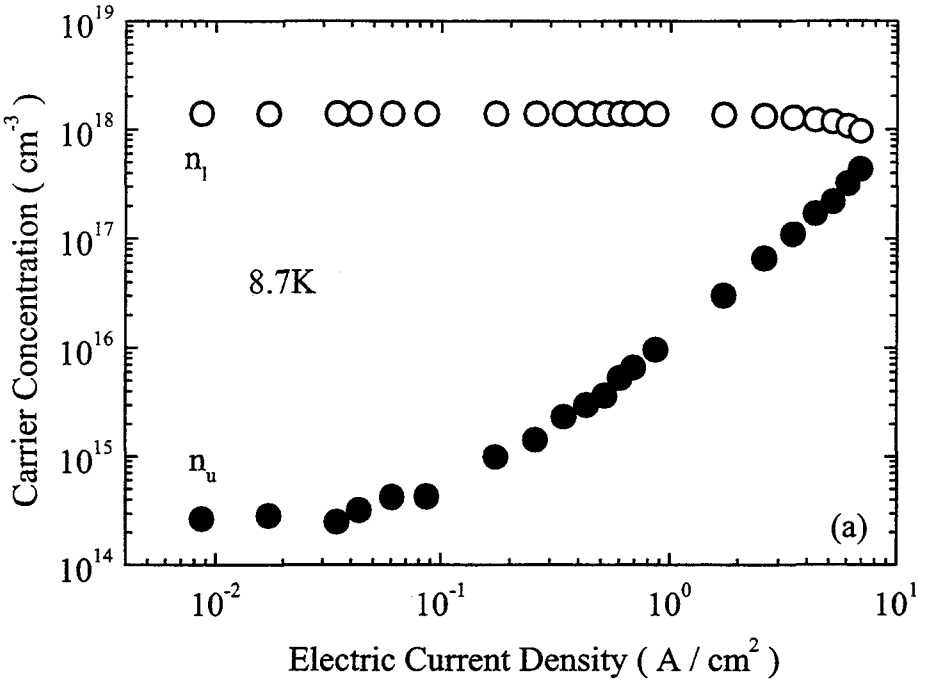

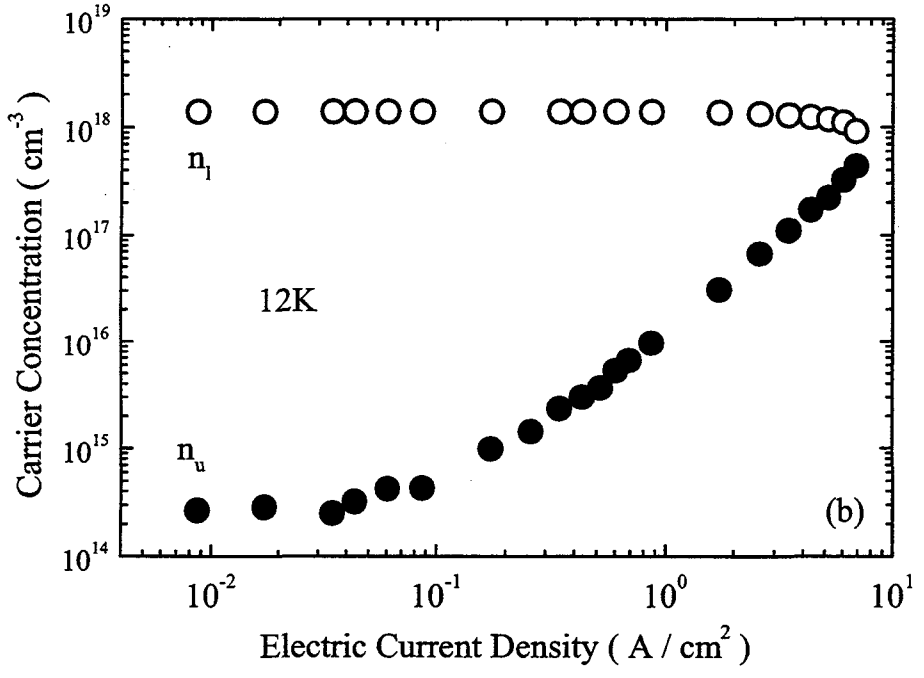

Fig.4.1.14(a), (b) n_u (solid circles) and n_l (open circles) at various temperatures derived from the two-band model at (a) 8.7K and (b) 12K.

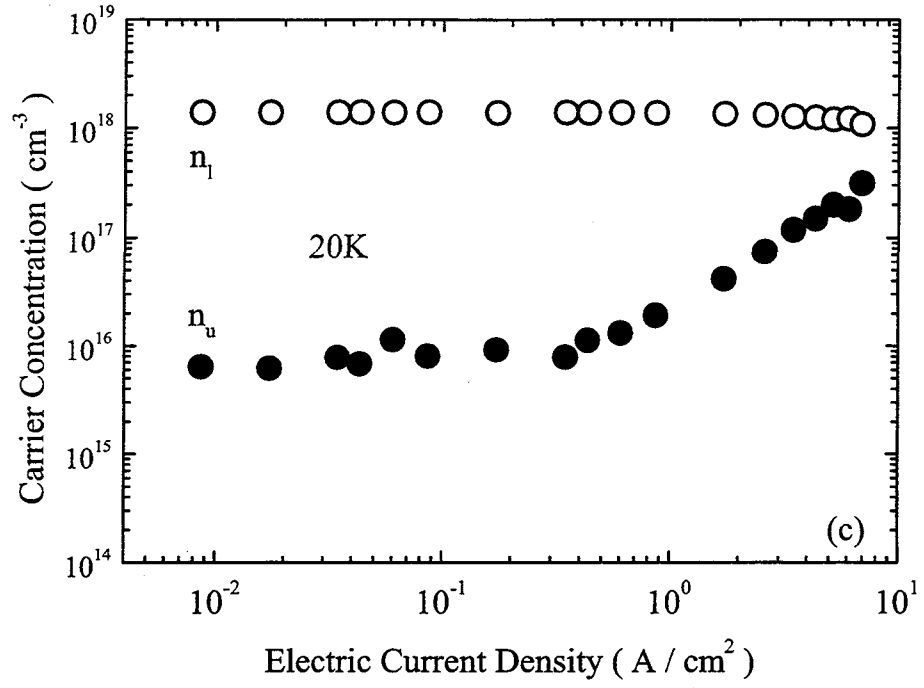

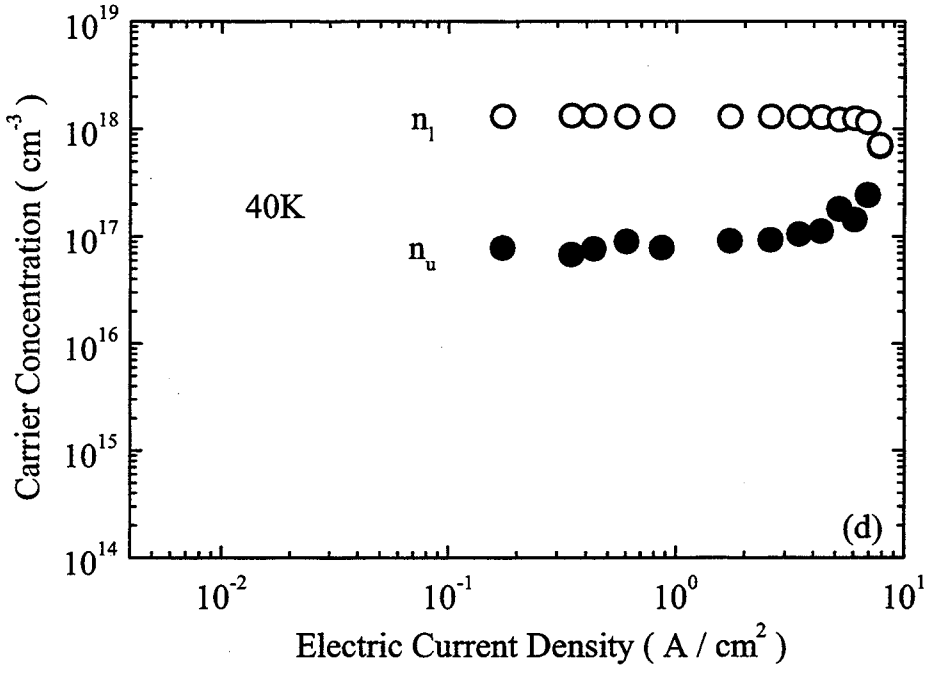

Fig.4.1.14(c), (d) n_u (solid circles) and n_l (open circles) at various temperatures derived from the two-band model at (c) 20K and (d) 40K.

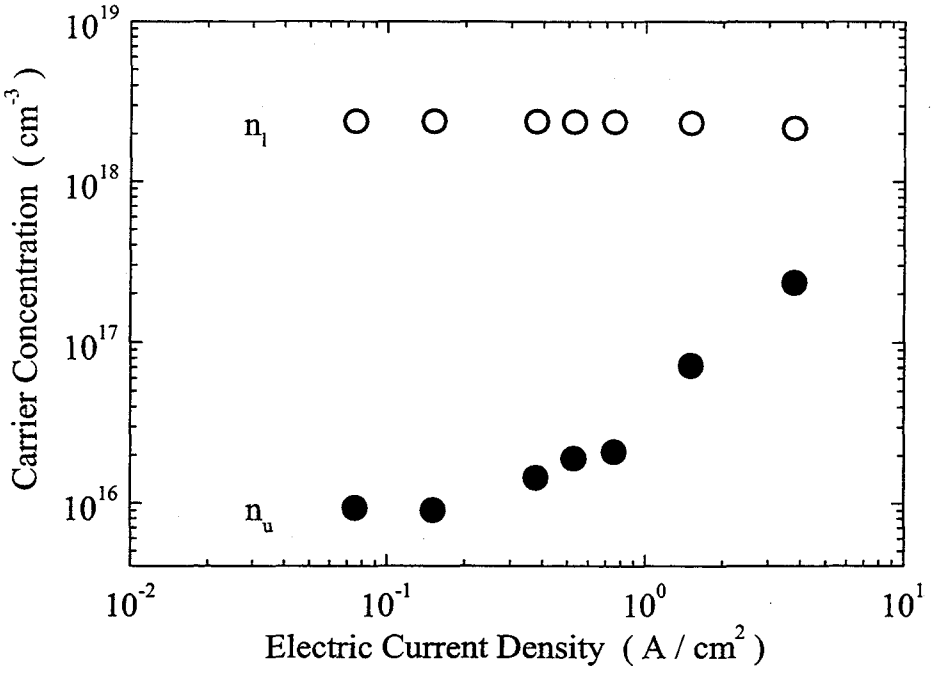

Fig.4.1.15 n_u (solid circles) and n_l (open circles) at 4.2K derived from the two-band model.

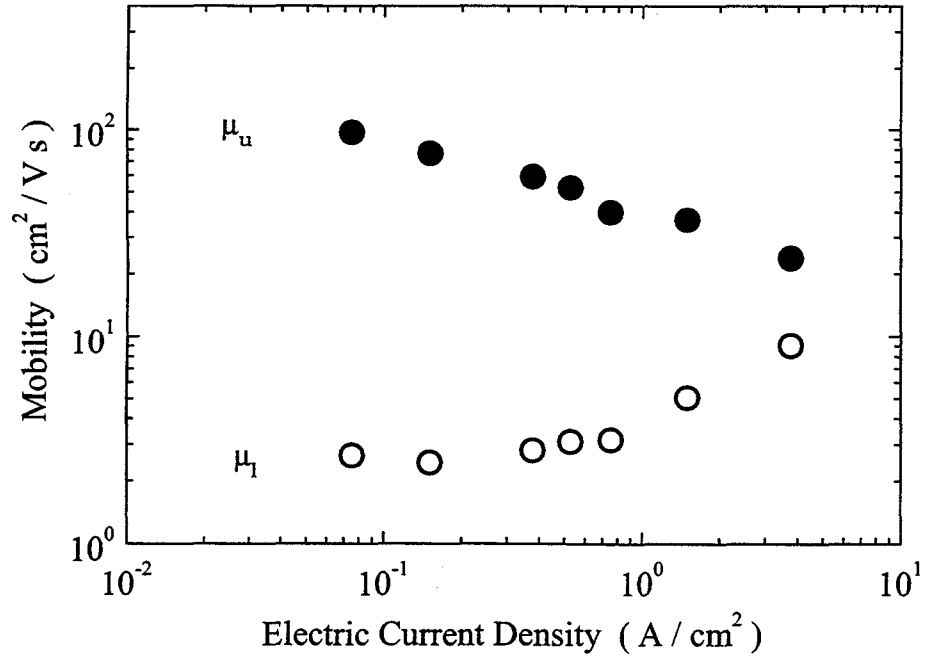

Fig.4.1.16 μ_u (solid circles) and μ_l (open circles) at 4.2K derived from the two-band model.

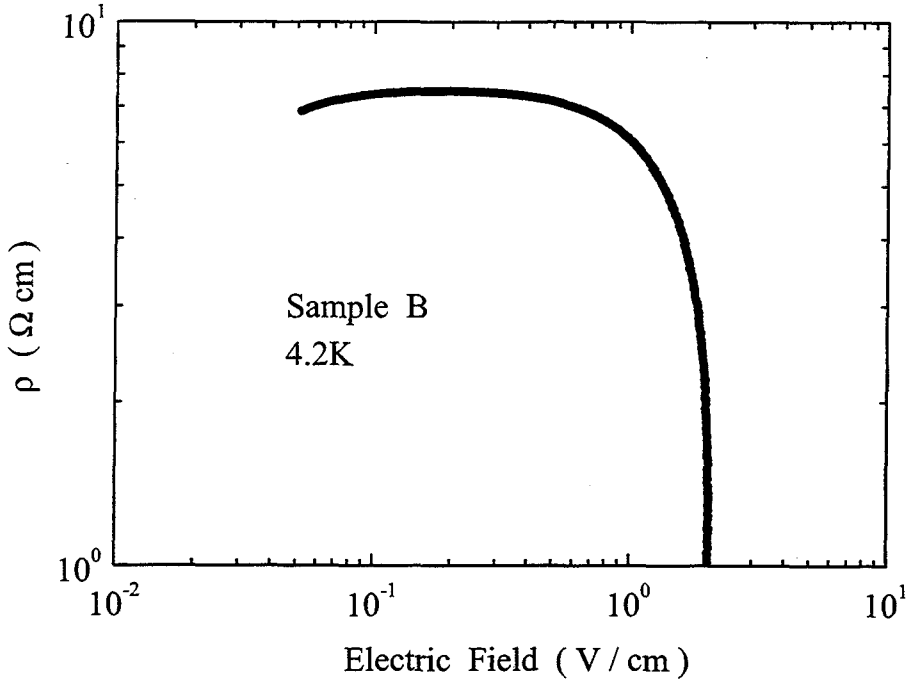

Fig.4.1.17 Electric field density dependence of resistivity at 4.2K for sample B. The critical field $E_c = 2.04$eV.

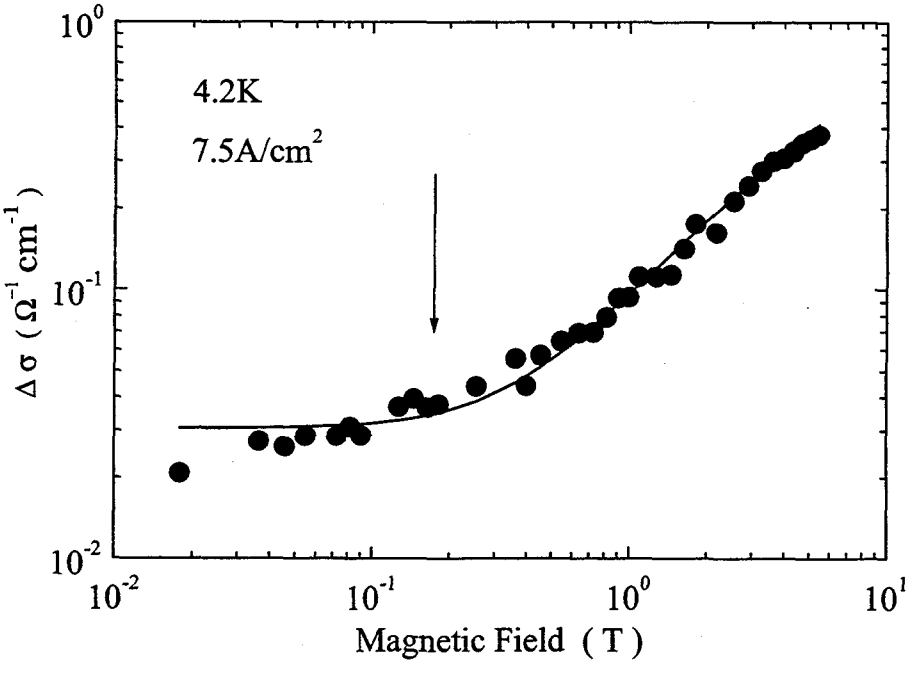

Fig.4.1.18 Magnetoconductance for 7.5 A/cm^2 at 4.2K. The arrow shows the characteristic magnetic field where $\delta = 1$ holds.

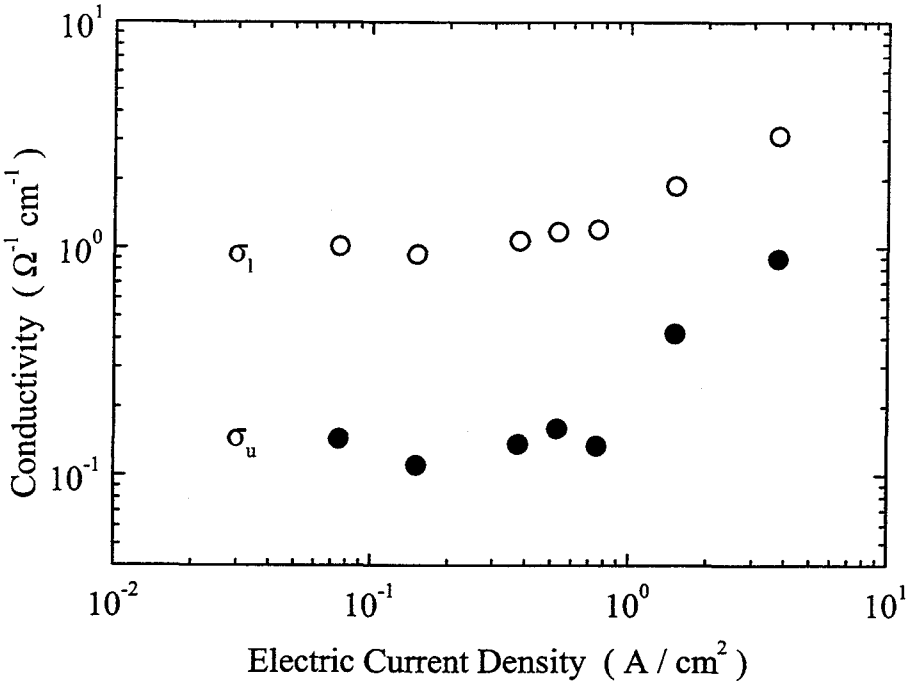

Fig.4.1.19 σ_u (solid circles) and σ_l (open circles) at 4.2K derived from the two-band model.

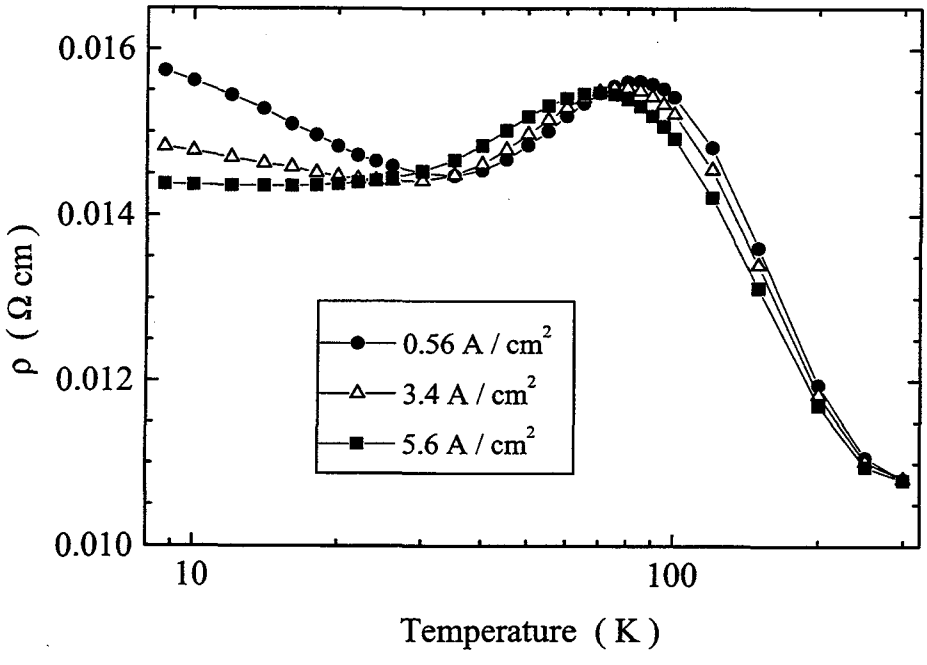

Fig.4.1.20 Temperature dependence of resistivity under various electric current densities.

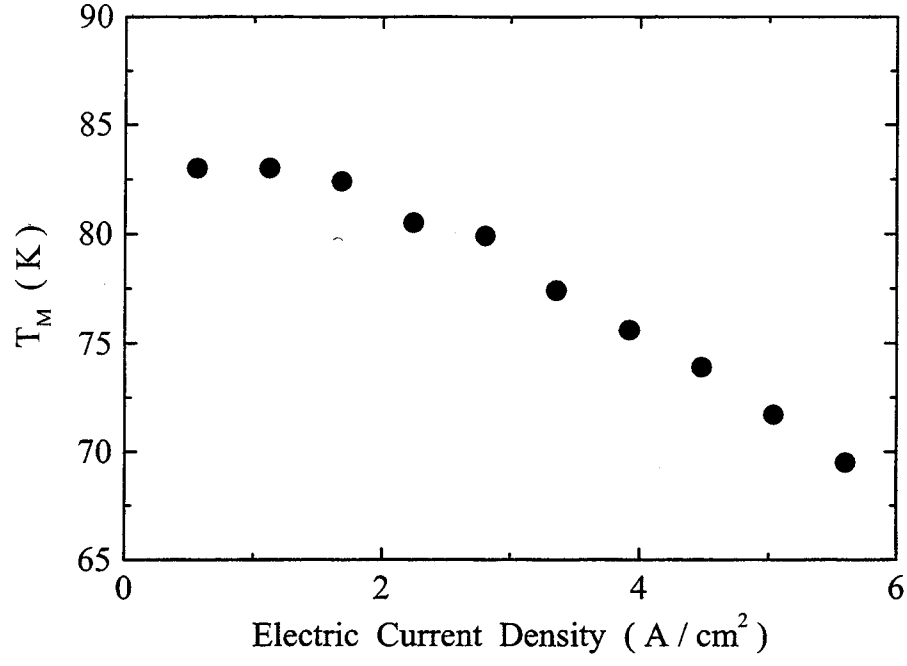

Fig.4.1.21 Electric current density vs T_M where the maximum of the resistivity appears.

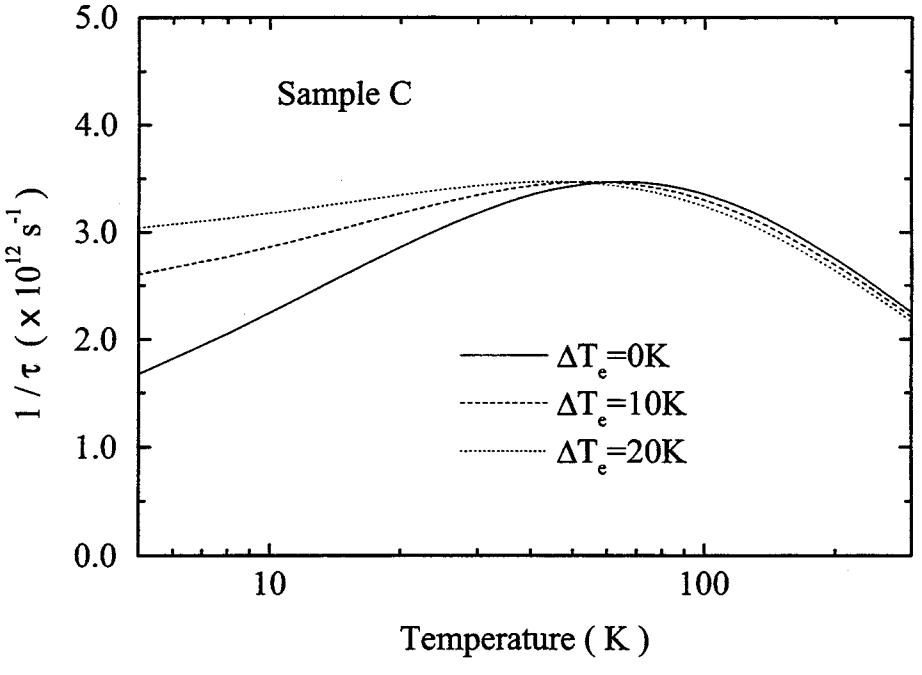

Fig.4.1.22 The results of calculation with Brooks-Herring formula. ΔT_e represents the rise of electron temperature from the lattice temperature. As the electron temperature increases, the peak shifts into lower temperature.

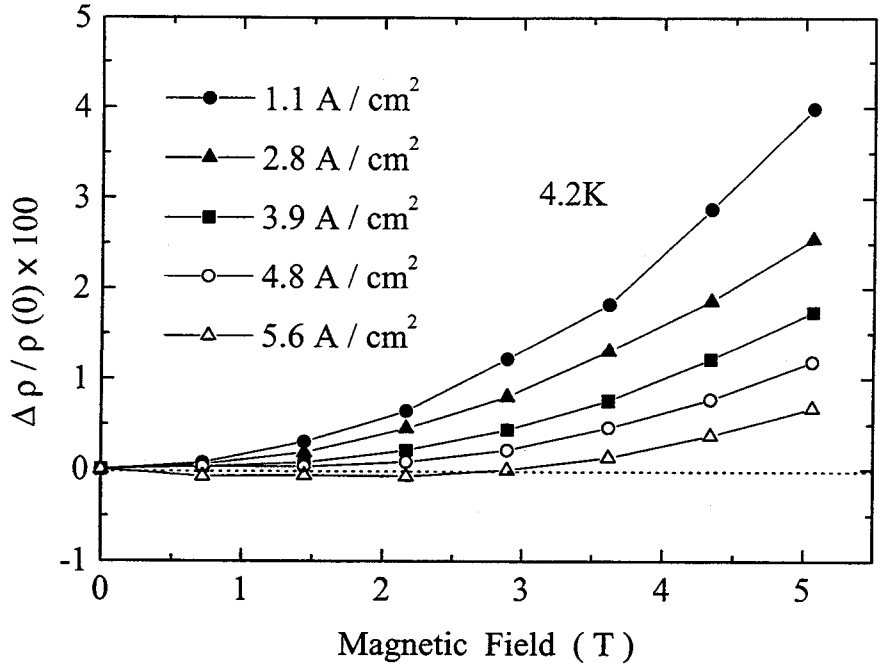

Fig.4.1.23 Electric current density dependence of MR at 4.2K.

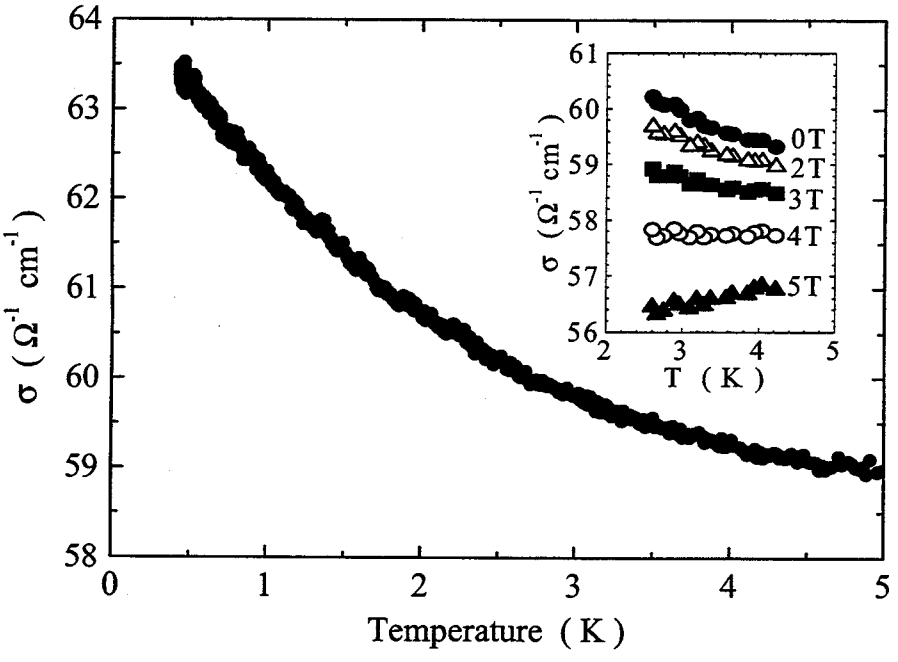

Fig.4.1.24 Temperature dependence of conductivity in the absence of a magnetic field. The inset shows the temperature dependence of conductivity under various magnetic fields.

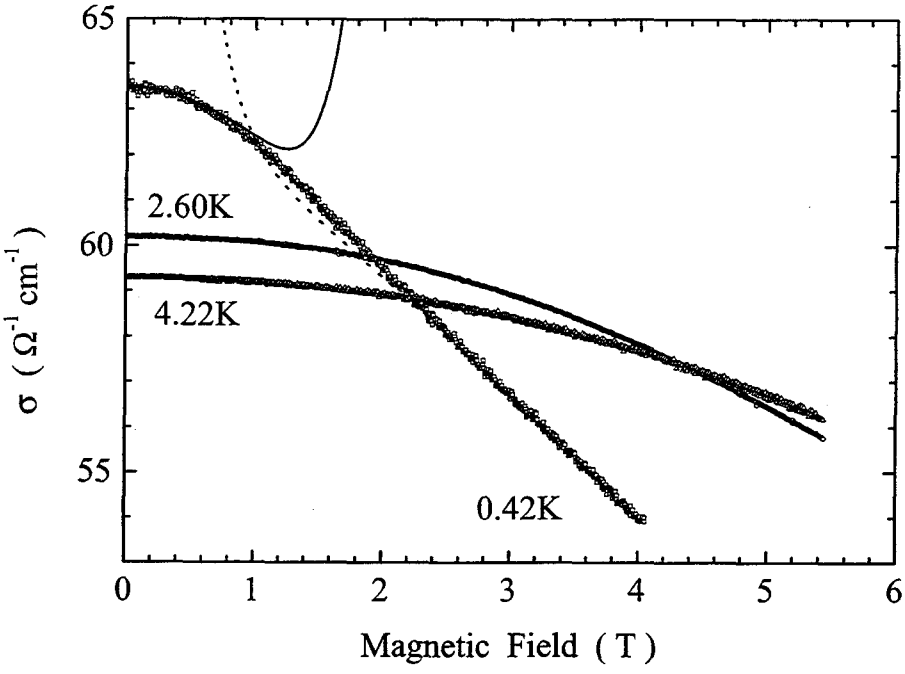

Fig.4.1.25 MC at different temperatures. The solid and dashed lines represent the result of fits using the approximation of low and high fields, respectively.

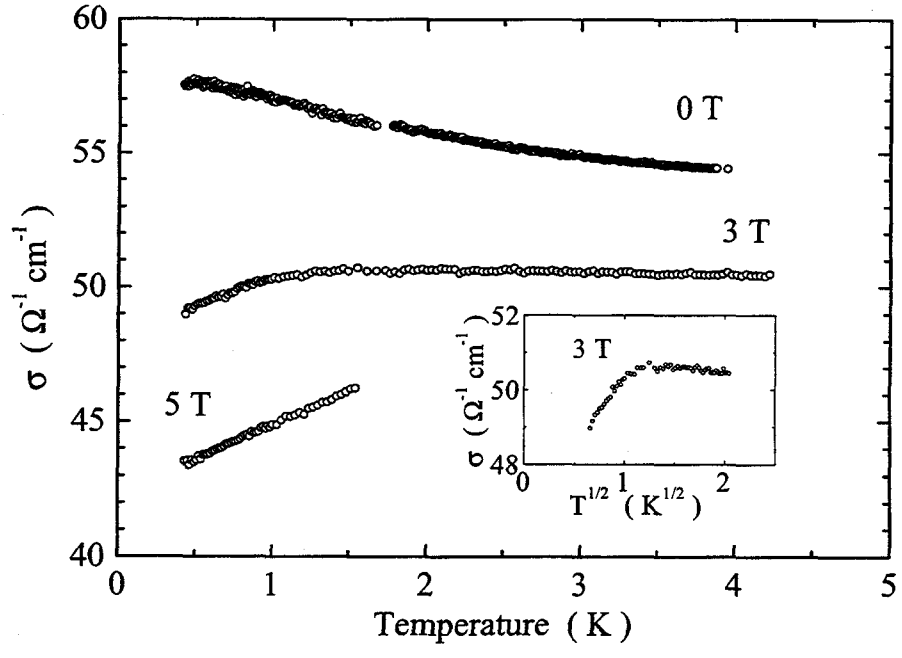

Fig.4.1.26 Temperature dependence of conductivity under various magnetic fields. The inset shows the temperature dependence of conductivity at 3T.

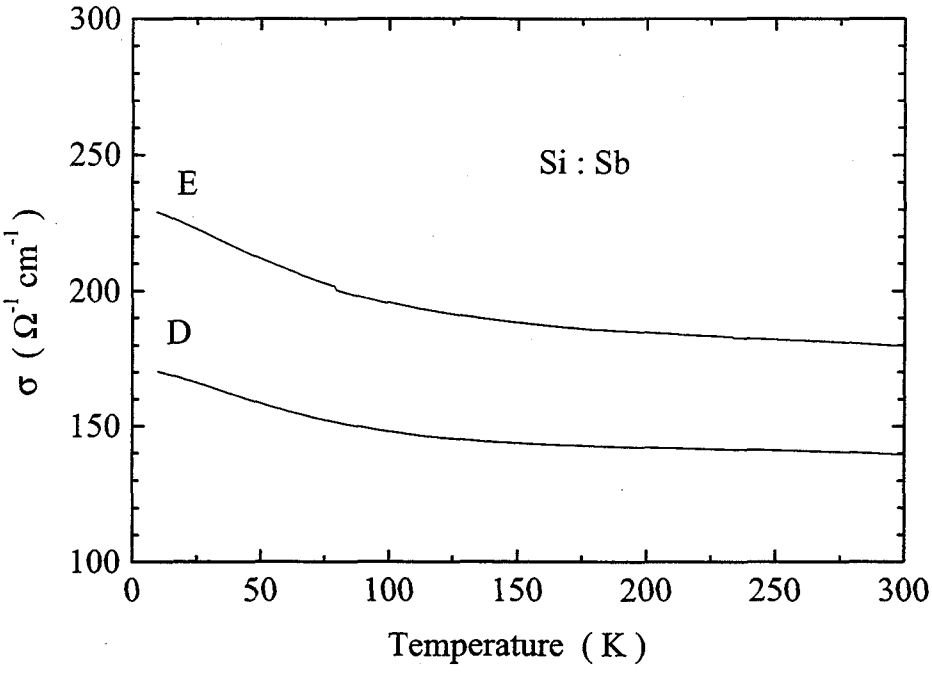

Fig.4.1.27 Temperature dependence of conductivity between 10K and 300K for sample D and E.

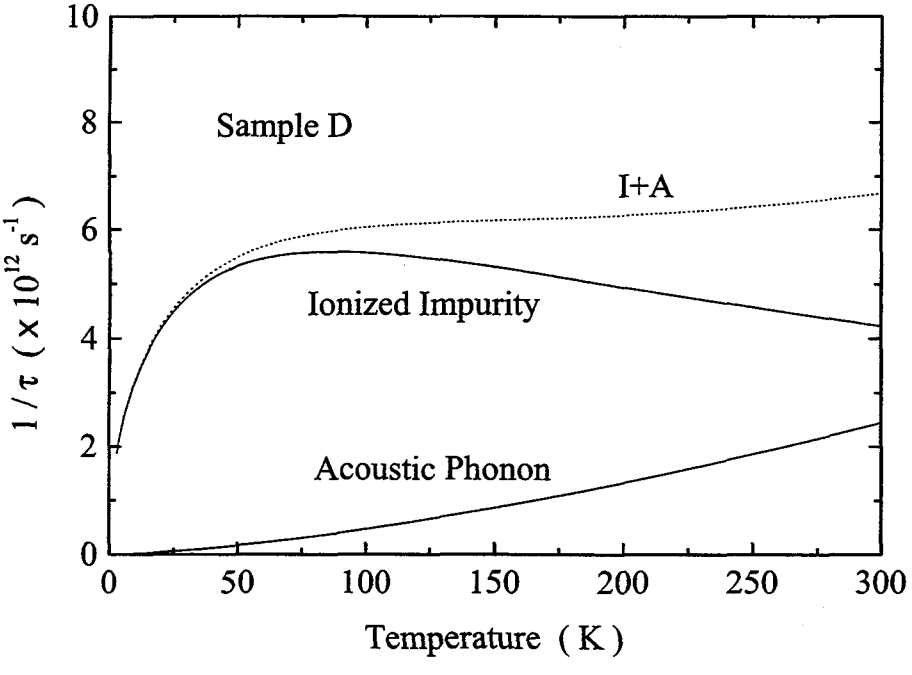

Fig.4.1.28 The results of calculation on the relaxation time due to acoustic phonon and ionized impurity scattering (solid lines). The dashed line represents the sum of two terms $1/\tau = 1/\tau_{ac} + 1/\tau_{ion}$.

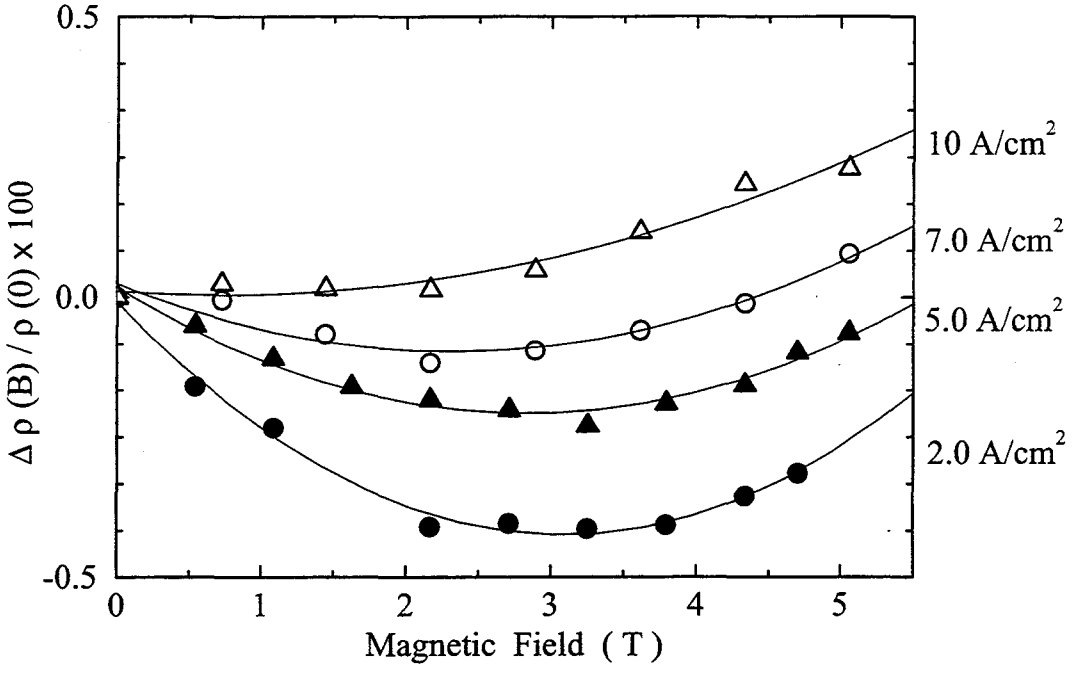

Fig.4.1.29 The variation of MR $\rho(B)$ at 4.2K under the various electric current density.

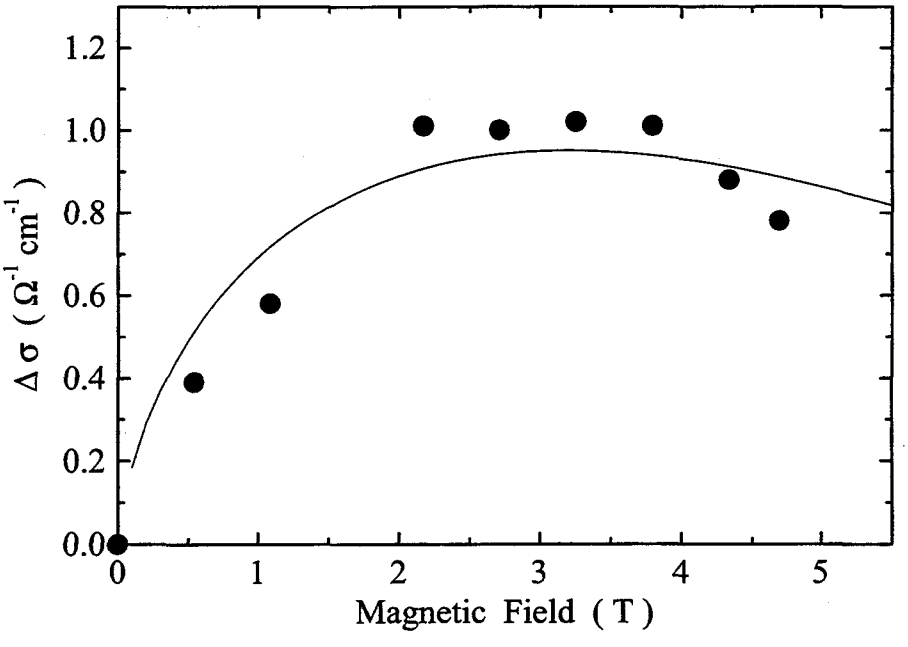

Fig.4.1.30 The MC at 4.2K in 2.0A/cm^2 (solid circles). The solid line represents the result of fit to eq.(109).

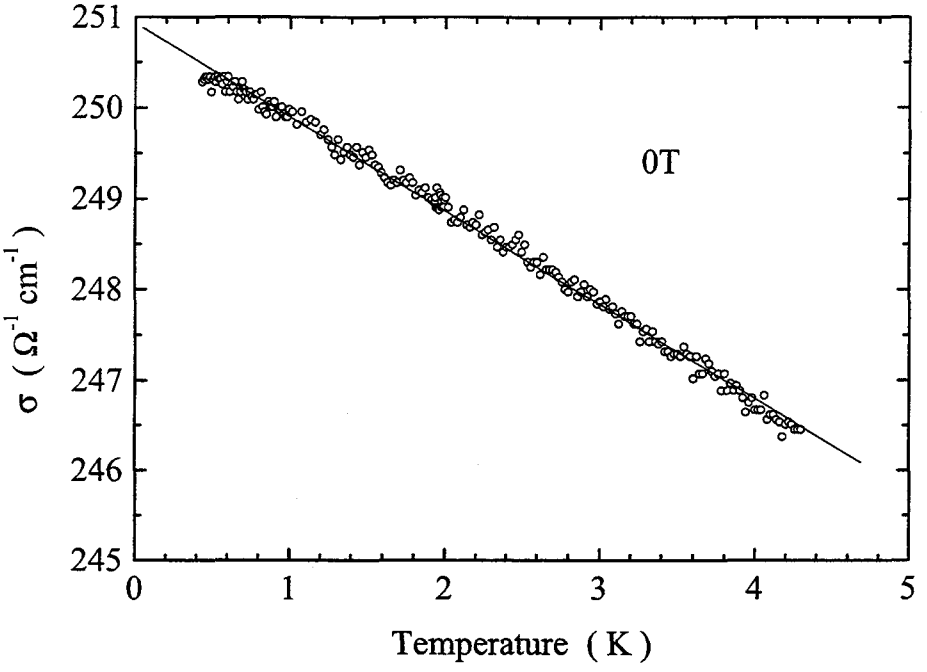

Fig.4.1.31 Temperature dependence of conductivity in the absence of a magnetic field. The solid line represents the relation $\sigma(T) = \sigma(0) + BT$.

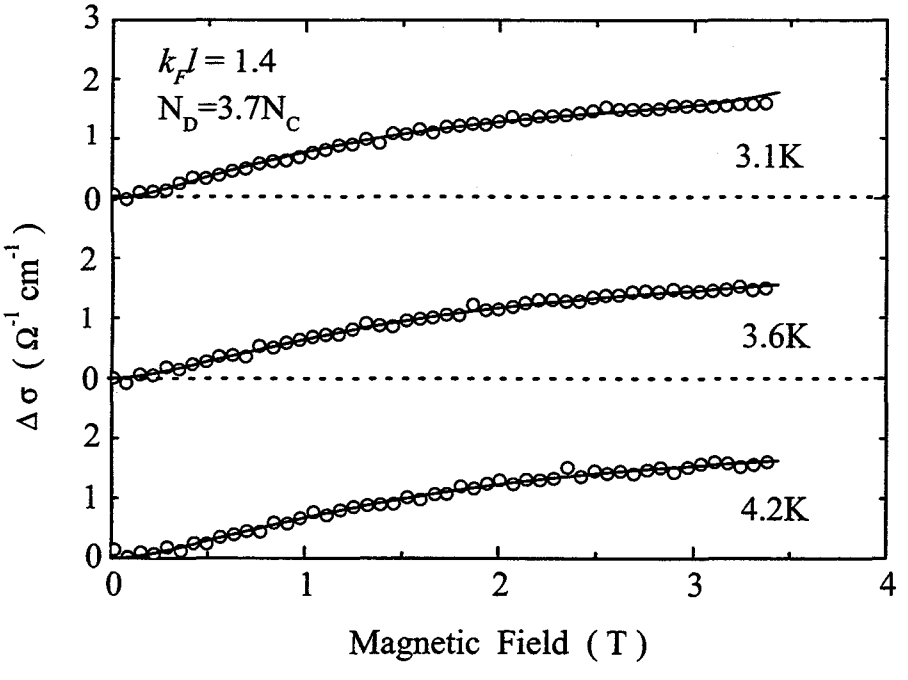

Fig.4.1.32 The correction of the MC at various temperatures. The solid circles and the solid lines are the experimental data and the fits with eq.(109). The dashed lines represent the zero of the correction for respective temperatures.

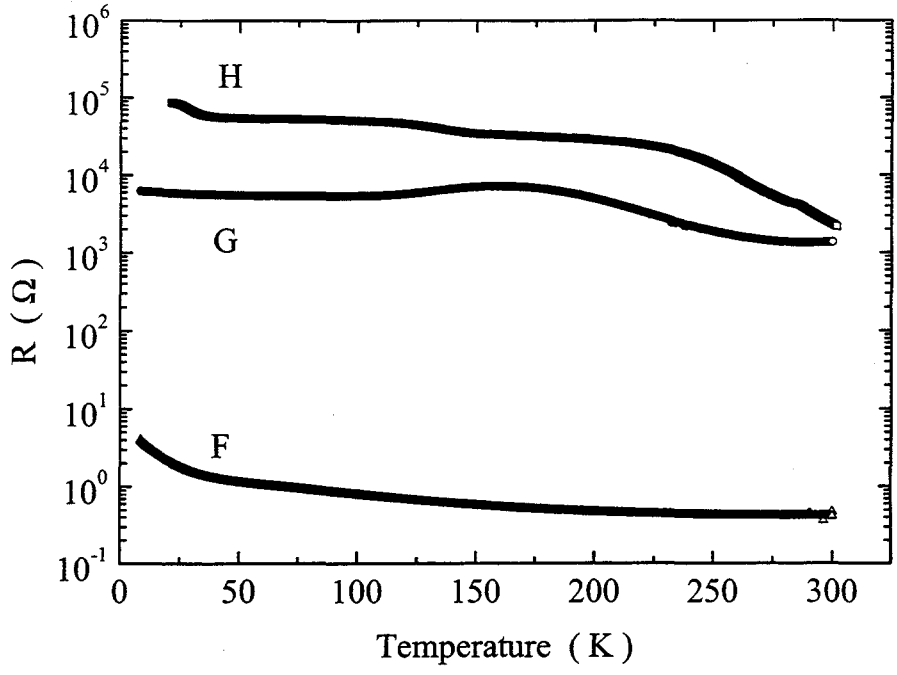

Fig.4.2.1 Temperature dependence of resistance for three kinds of δ-doped samples.

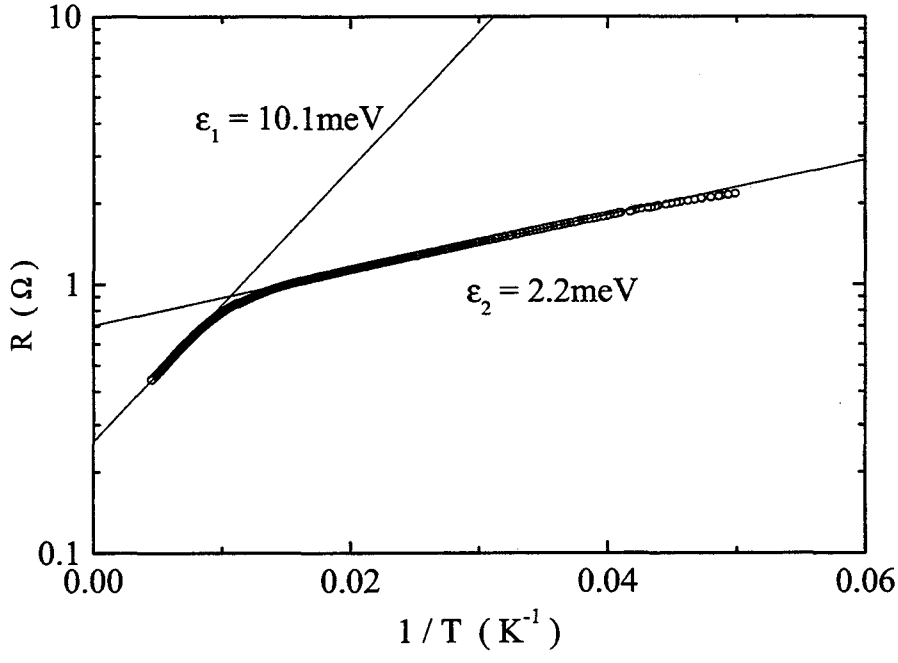

Fig.4.2.2 Resistance as a function of the reciprocal of the temperature T^{-1} for sample F.

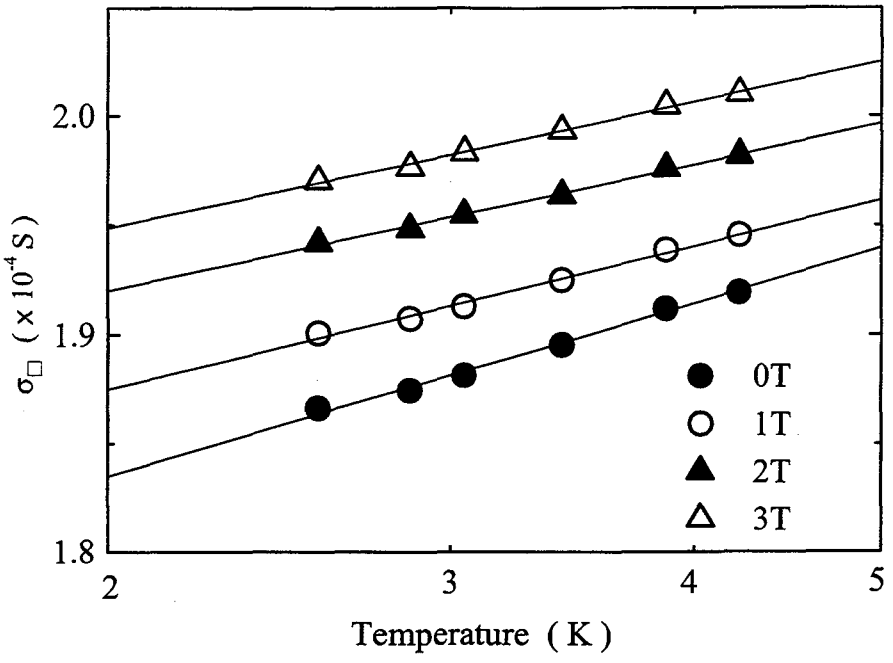

Fig.4.2.3 Temperature dependence of the conductance under various magnetic fields for sample G. The solid lines shows the fits obtained from analyses with the relation $\sigma(T) = \sigma(0) + a \ln T$.

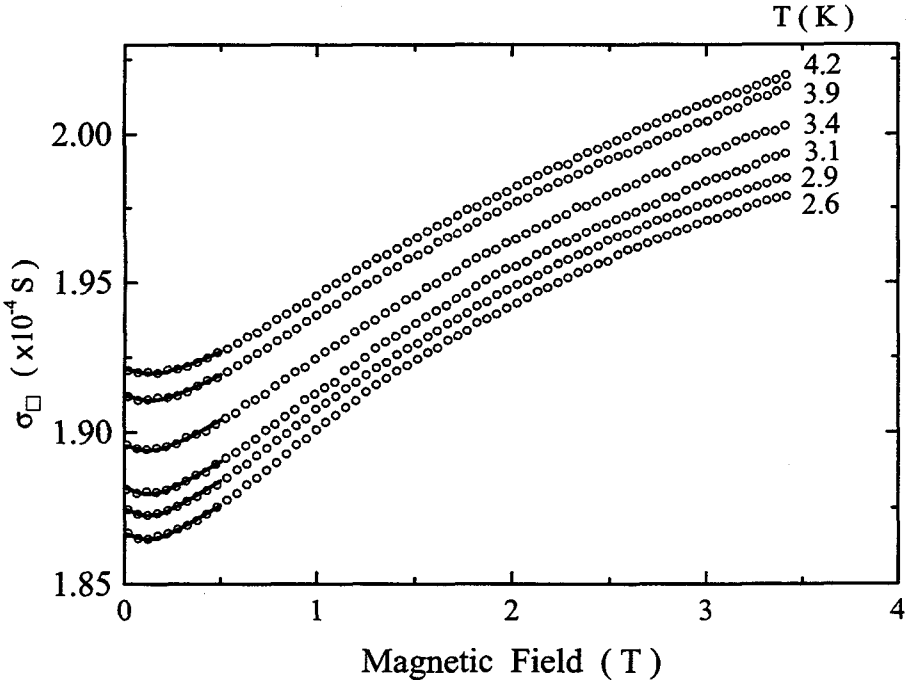

Fig.4.2.4 The MC at various temperatures for sample G in perpendicular field. The negative MC is observed in the region of very weak magnetic field. The open circles and the solid lines show the experimental data and the fits with eqs.(112) and (36), respectively.

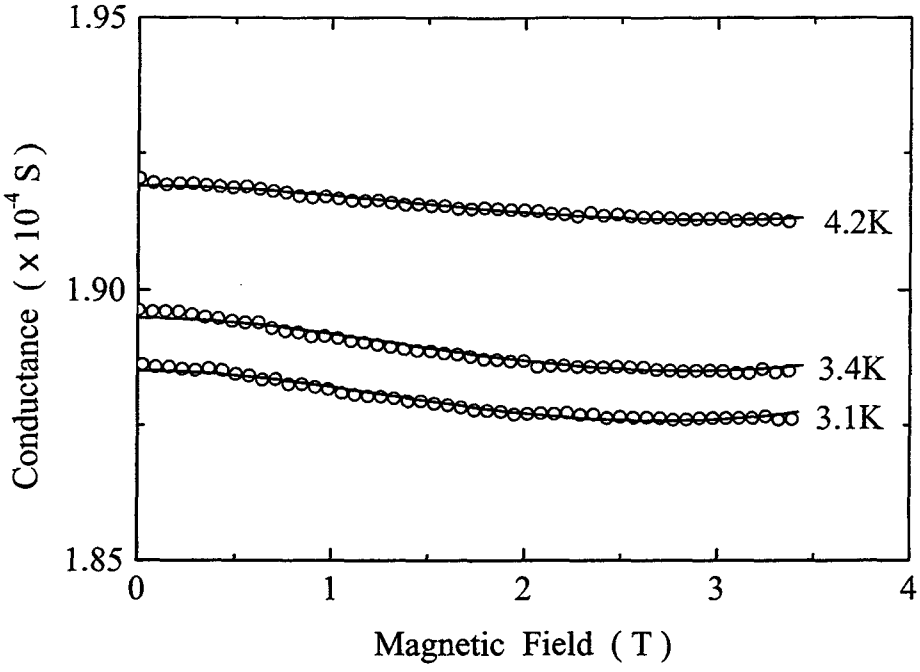

Fig.4.2.5 The MC at various temperatures for sample G in the field parallel to the δ-doped layer. The open circles and the solid lines show the experimental data and the fits with eqs.(115), (116), (117) and (118), respectively.

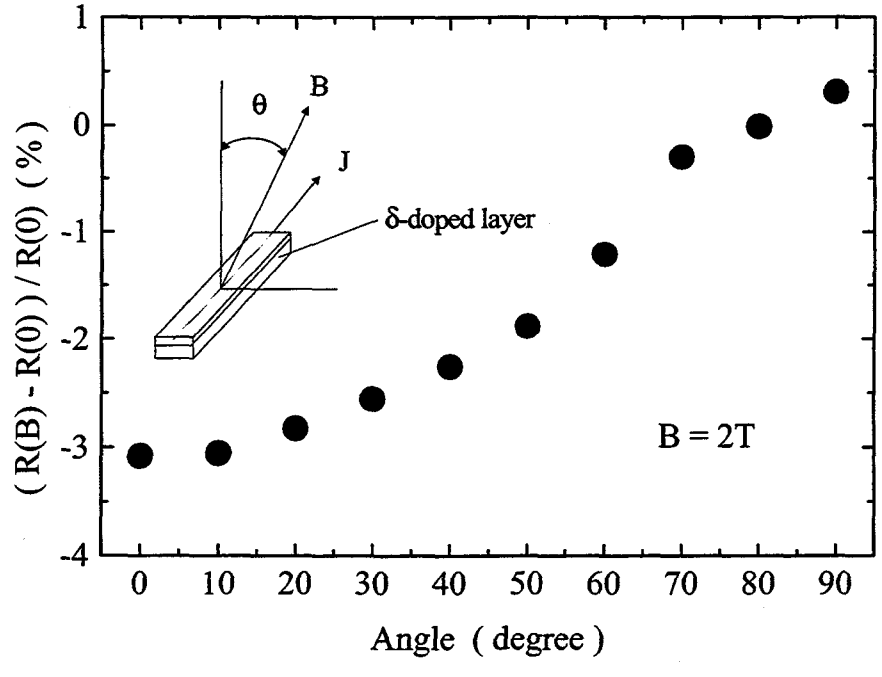

Fig.4.2.6 The angular dependence of MR, $[R(2\mathrm{T}) - R(0)]/R(0)$ at 4.2K and 2T for sample G.

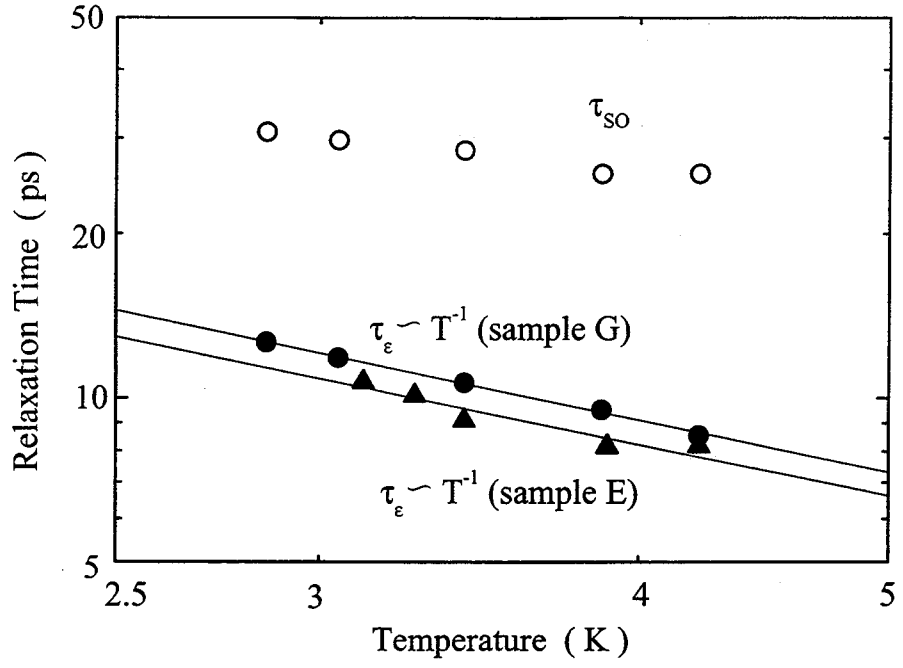

Fig.4.2.7 Temperature dependence of the inelastic scattering time τ_ϵ for sample E and G, and the SO scattering time τ_{so} for sample G derived from the analyses of MC. The relation of $\tau_\epsilon \propto T^{-1}$ for both samples is obtained.

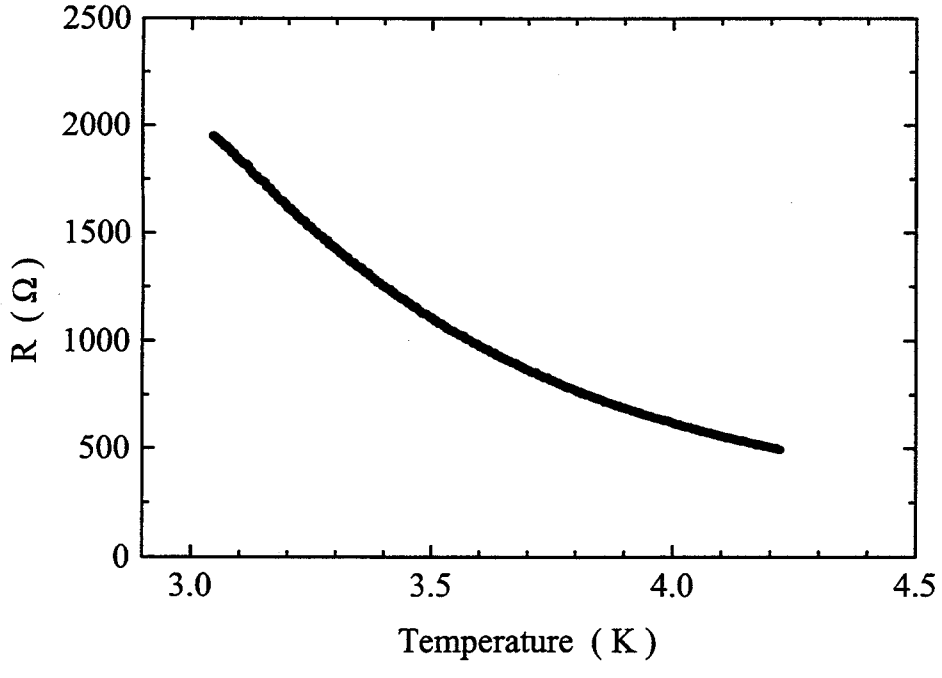

Fig.4.2.8 Temperature dependence of resistance for sample F below 4.2K.

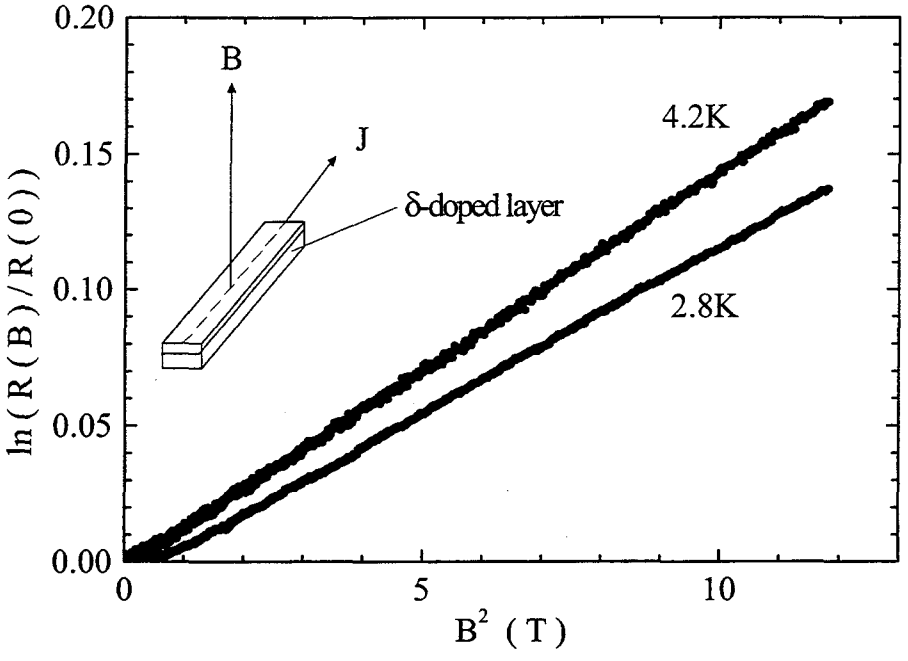

Fig.4.2.9 The MR at low temperatures for sample F in perpendicular field.

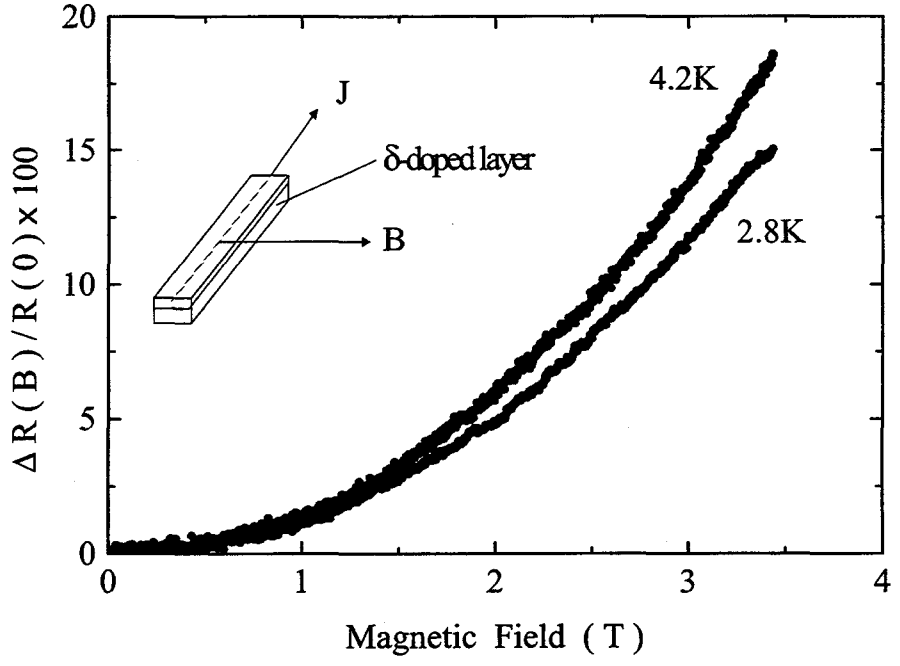

Fig.4.2.10 The MR at low temperatures for sample F in the field parallel to the δ-doped layer.

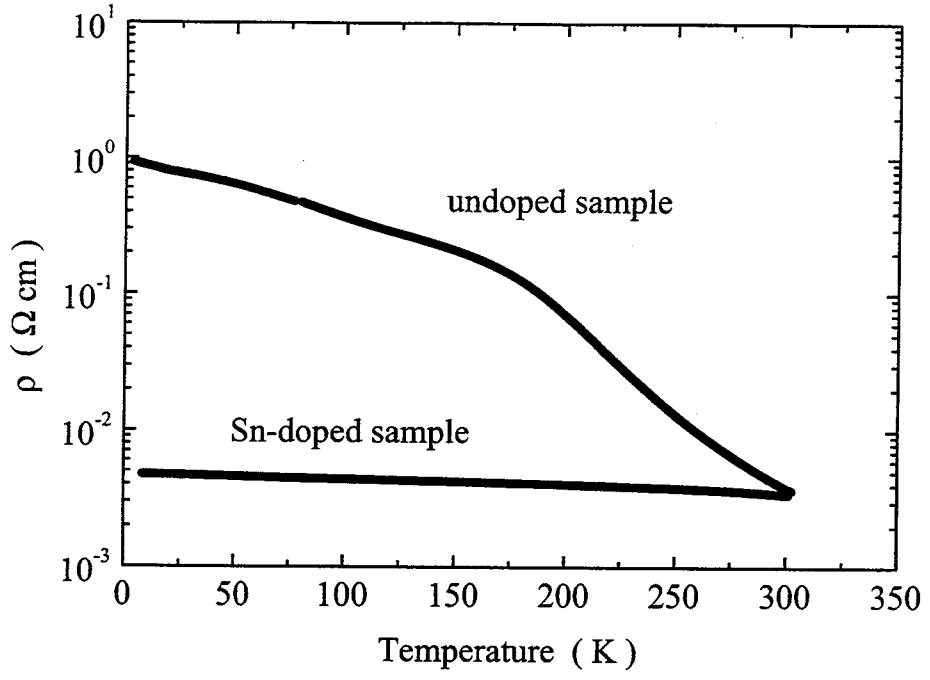

Fig.4.3.1 Temperature dependence of resistivity for two samples on thin film InSb.

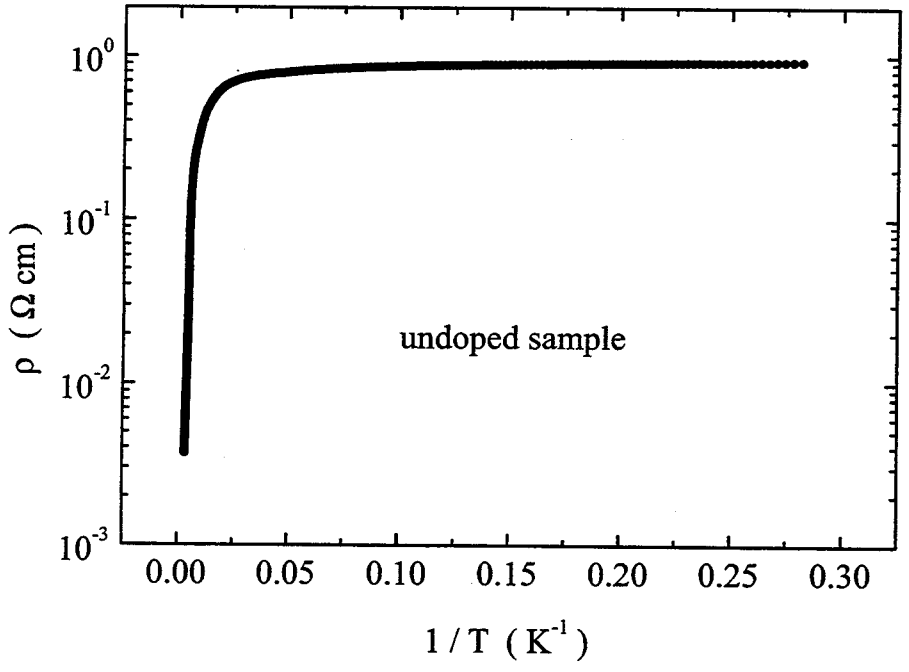

Fig.4.3.2 Resistivity as a function of T^{-1} for undoped sample.

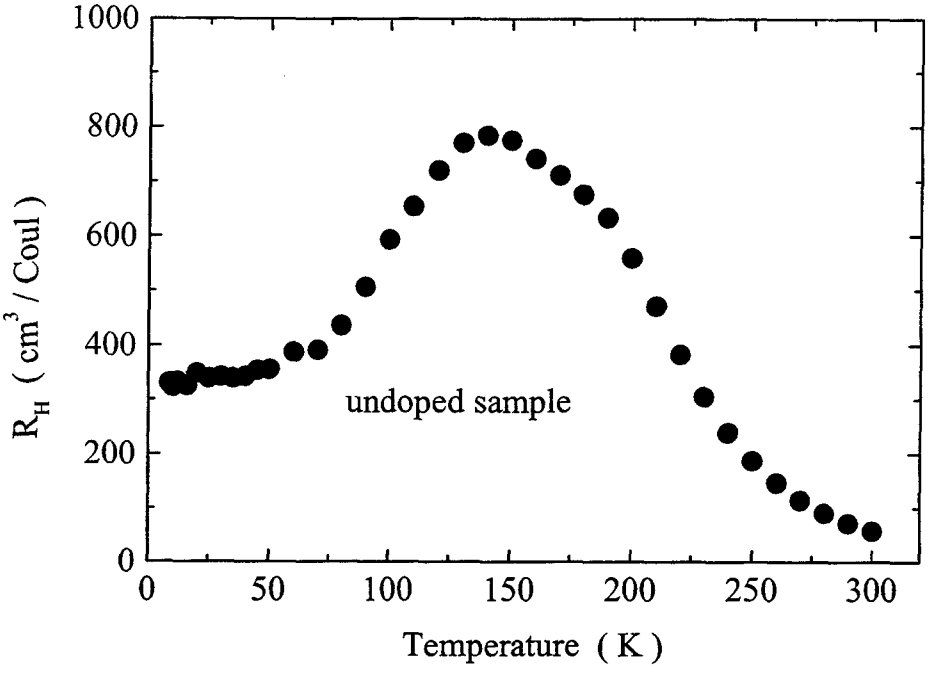

Fig.4.3.3 Temperature dependence of Hall coefficient for undoped sample.

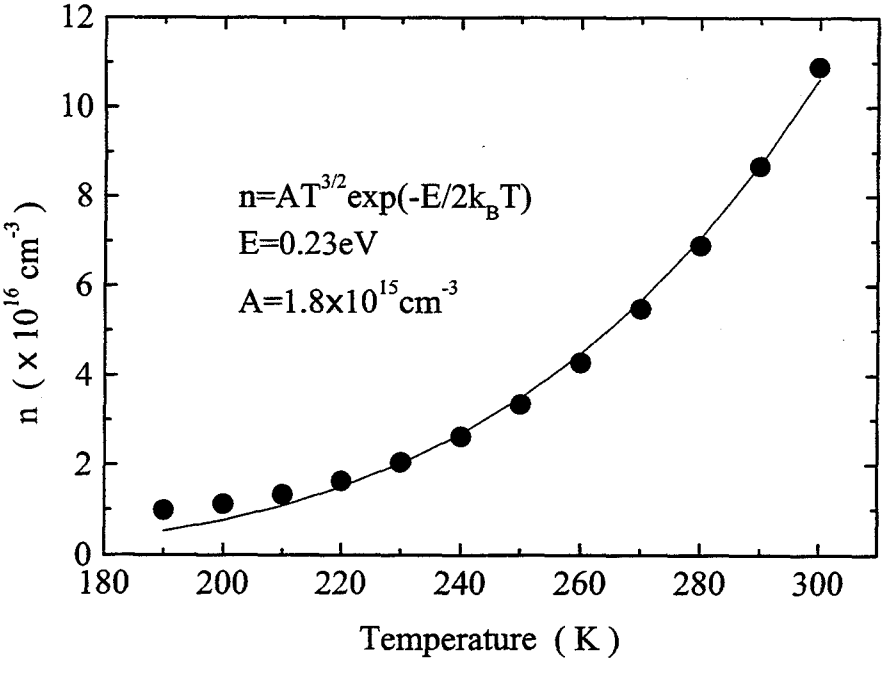

Fig.4.3.4 Temperature dependence of the intrinsic carrier concentration.

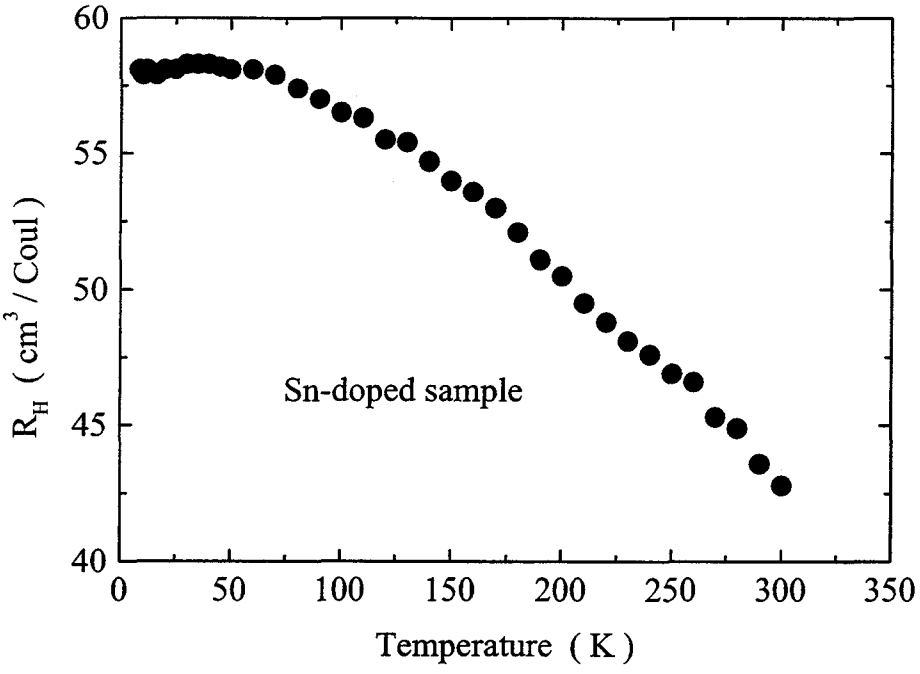

Fig.4.3.5 Temperature dependence of Hall coefficient for Sn-doped sample.

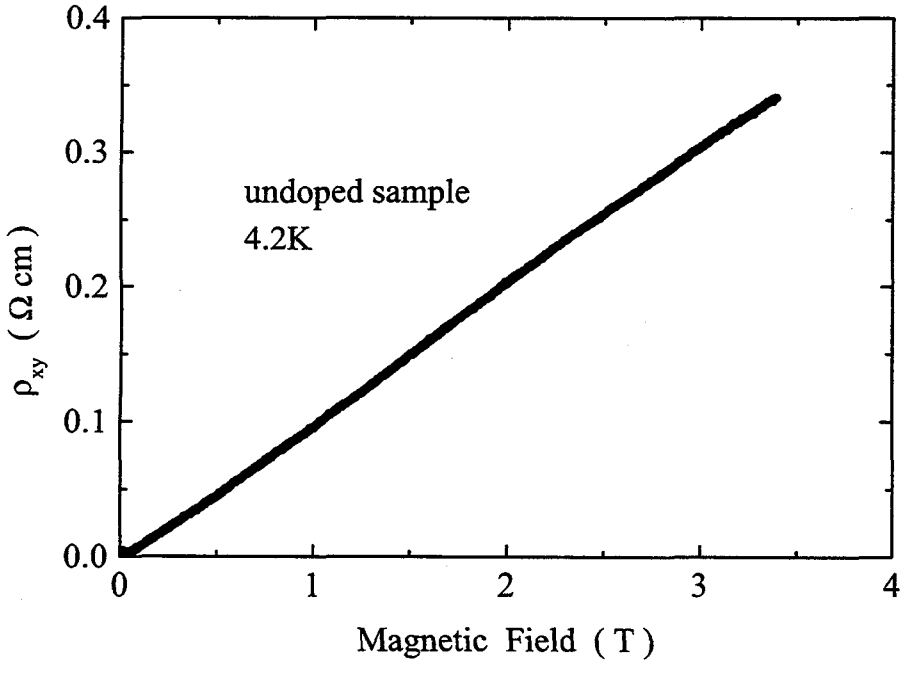

Fig.4.3.6 Hall resistivity ρ_{xy} as a function of magnetic field at 4.2K.

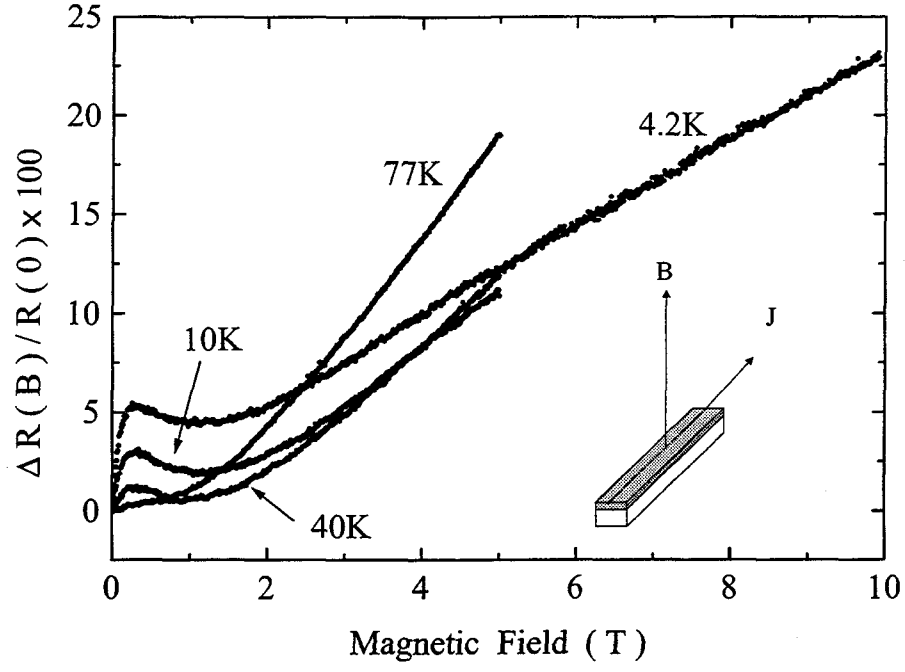

Fig.4.3.7 MR data above 4.2K in perpendicular field.

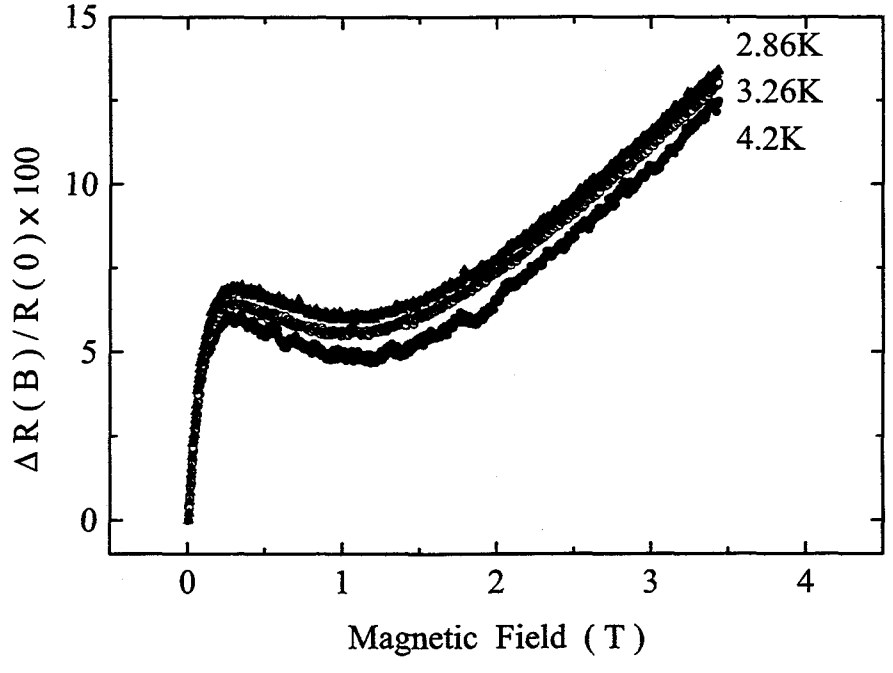

Fig.4.3.8 MR data below 4.2K in perpendicular field.

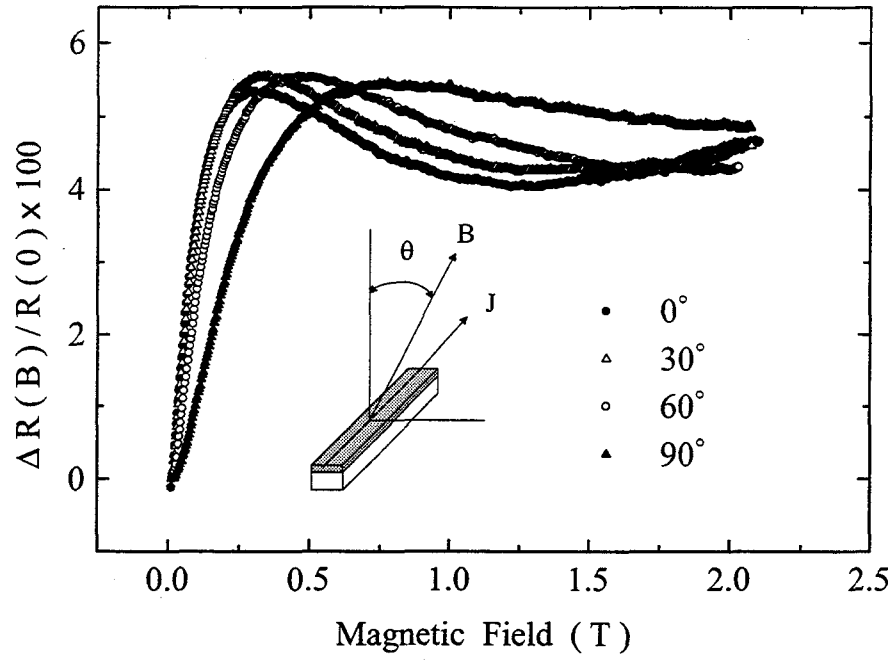

Fig.4.3.9 Angular dependence of MR at 4.2K. θ is the angle between the magnetic field and the normal line of the InSb thin film.

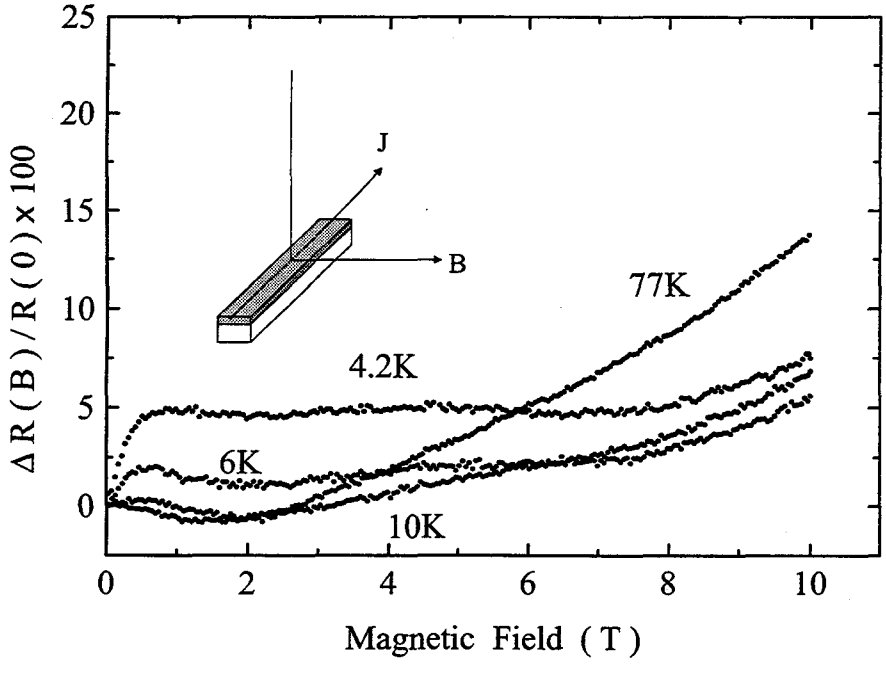

Fig.4.3.10 MR data above 4.2K in parallel field.

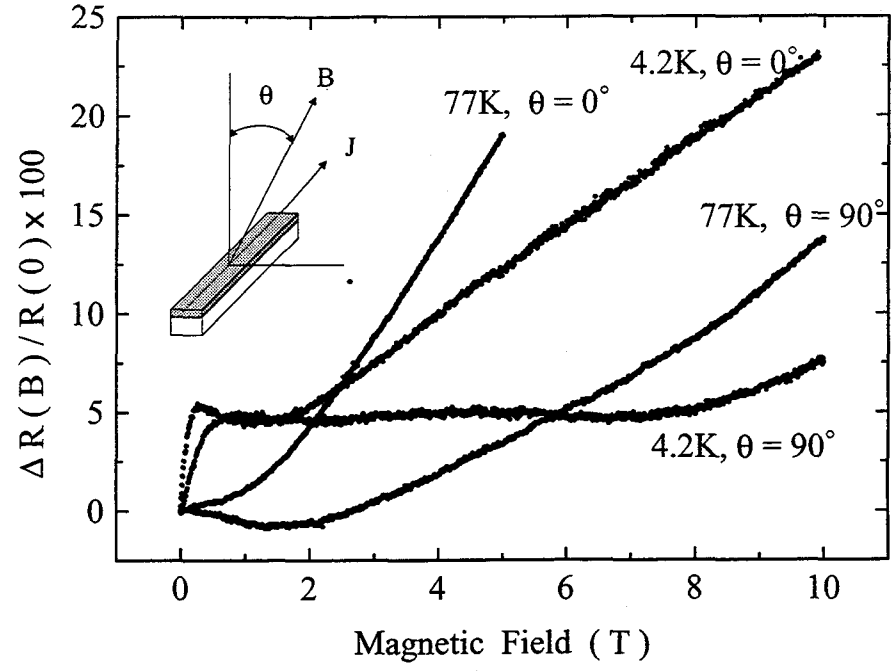

Fig.4.3.11 MR data at 4.2K and 77K for the direction of magnetic field $\theta = 0°$ and 90°.

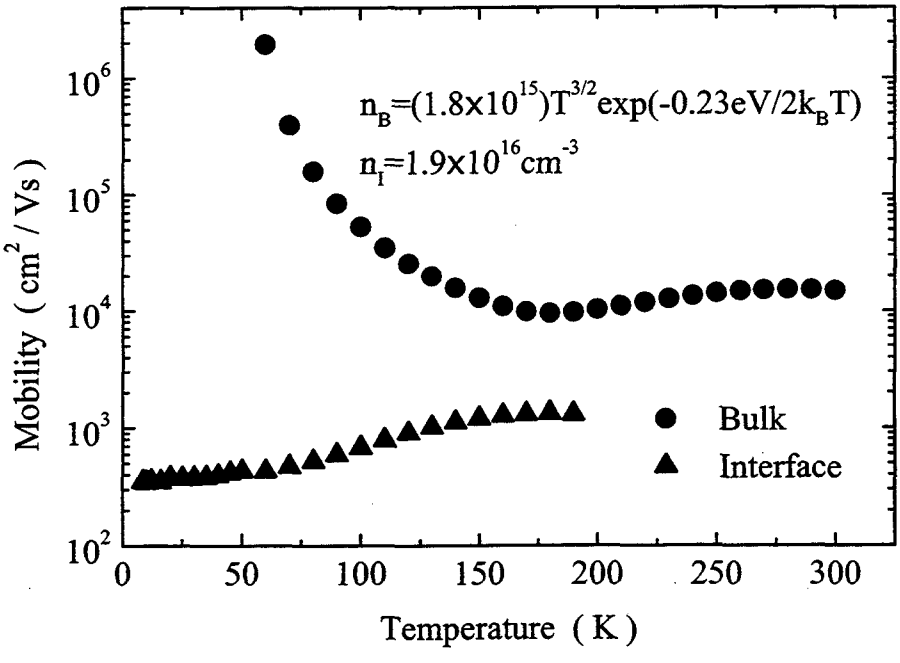

Fig.4.3.12 Temperature dependence of mobilities μ_B (solid circles) and μ_I (solid triangles) derived from the two-carrier model.

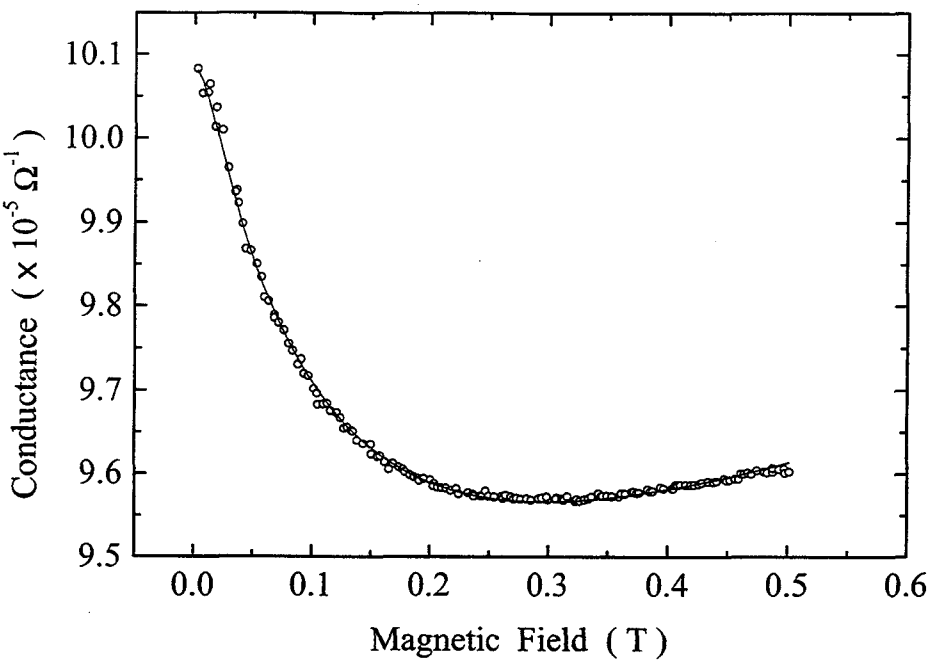

Fig.4.3.13 The fit with the theory by Hikami *et al.* for 2D systems. Open circles and solid line represent the experimental data at 4.2K and the result of fit, respectively.

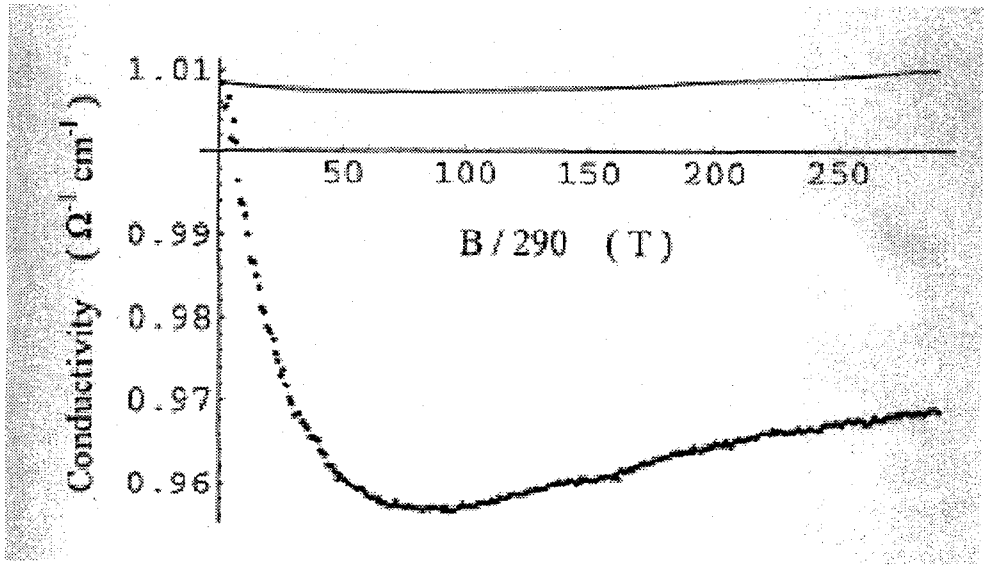

Fig.4.3.14 The fit with the theory by Fukuyama and Hoshino for 3D systems. Solid circles and line represent the experimental data at 4.2K and the result of fit, respectively.

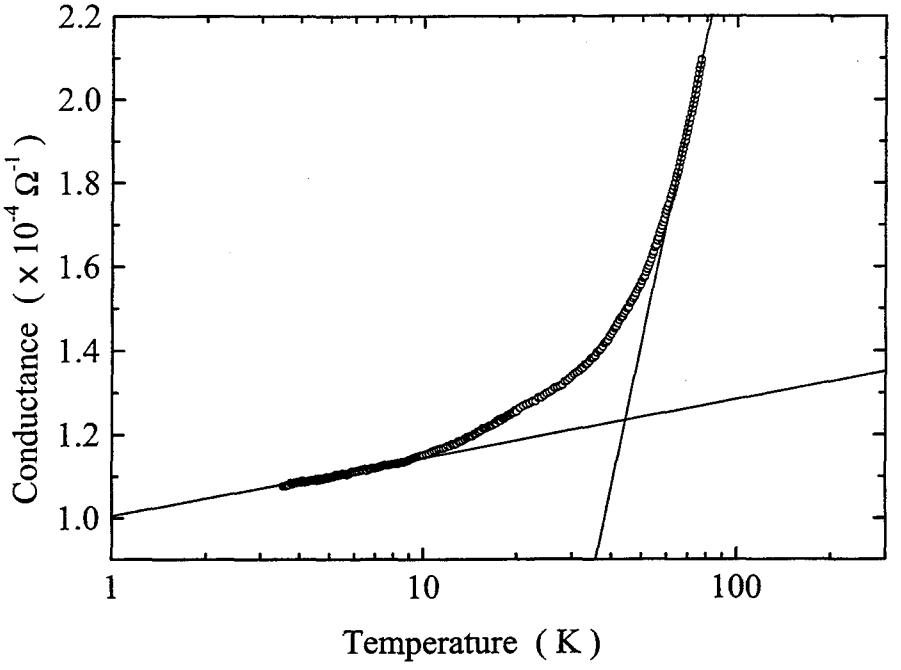

Fig.4.3.15 Temperature dependence of conductance as 2D system. The lines represent $\Delta\sigma \propto (e^2/2\pi^2\hbar)\ln T$.

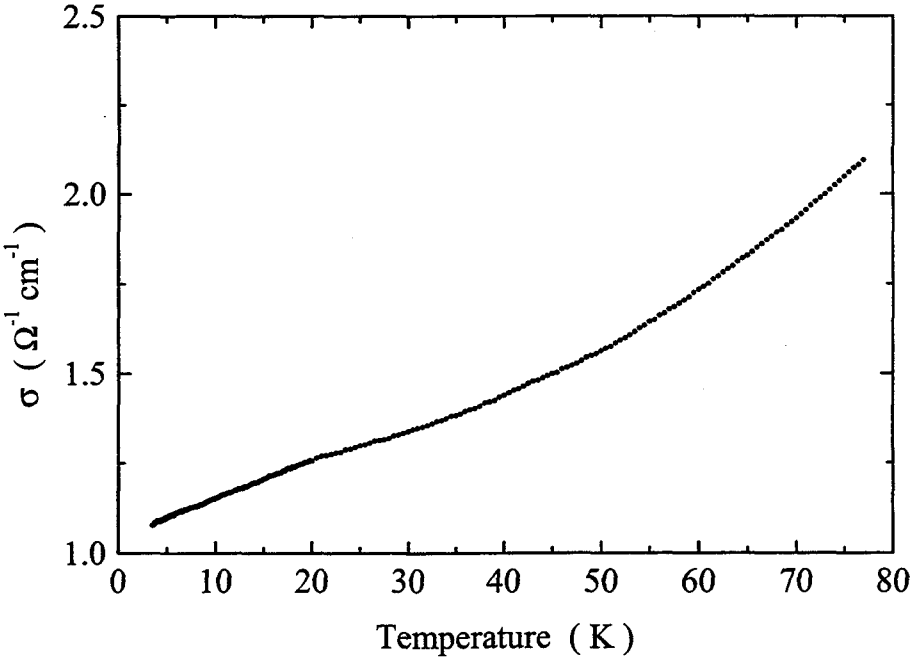

Fig.4.3.16 Temperature dependence of conductivity as 3D system.

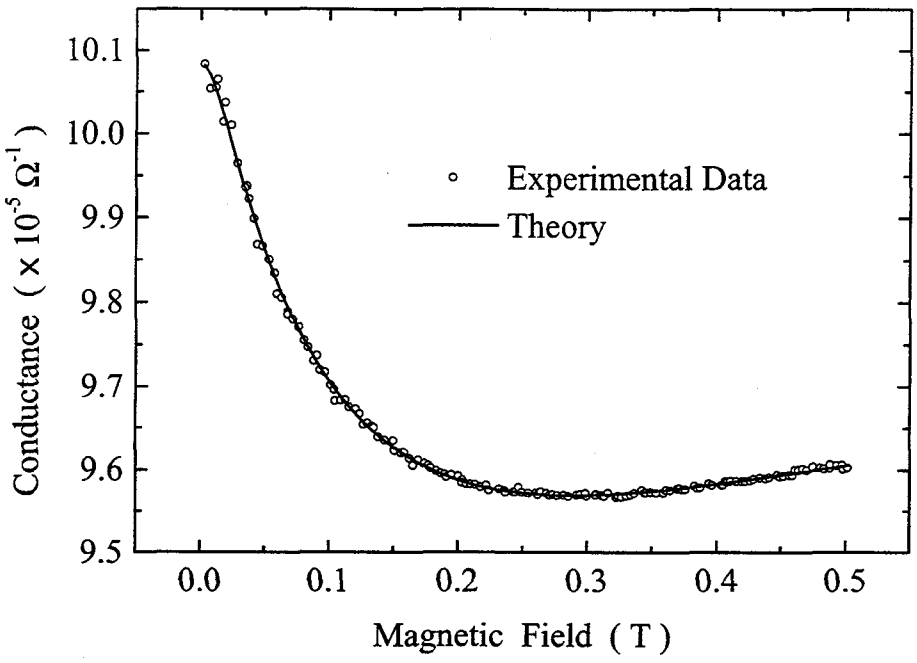

Fig.4.3.17 Magnetoconductance data (open circles) at 4.2K. The results of fit (solid line) is shown.

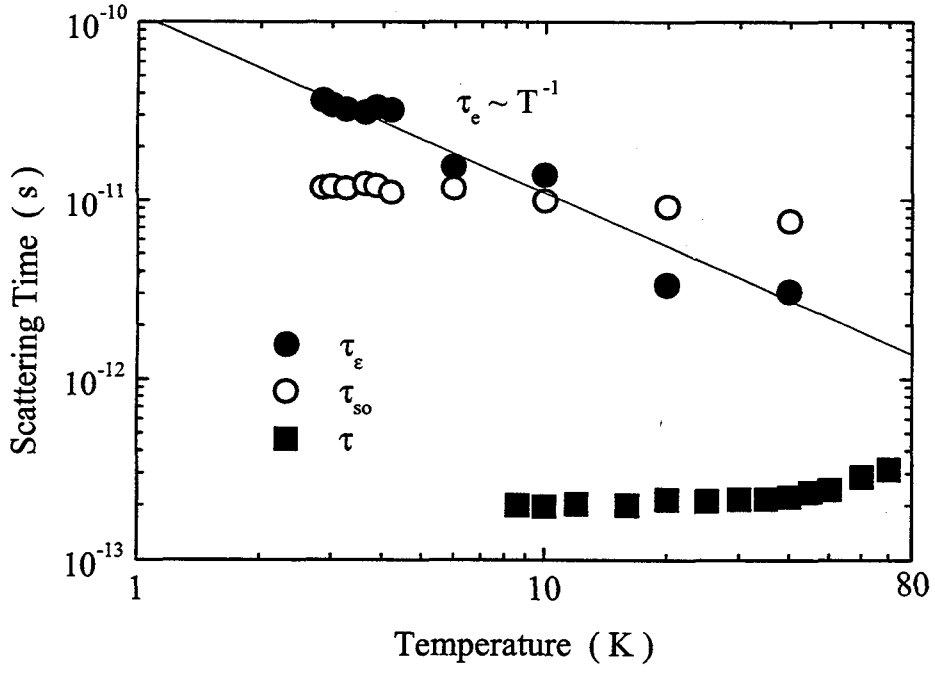

Fig.4.3.18 Temperature dependence of the inelastic scattering time τ_ϵ, the SO scattering time τ_{so} derived from the analyses of magnetoconductance. And the elastic scattering time τ deduced from the temperature dependence of conductance and Hall coefficient is shown, too.

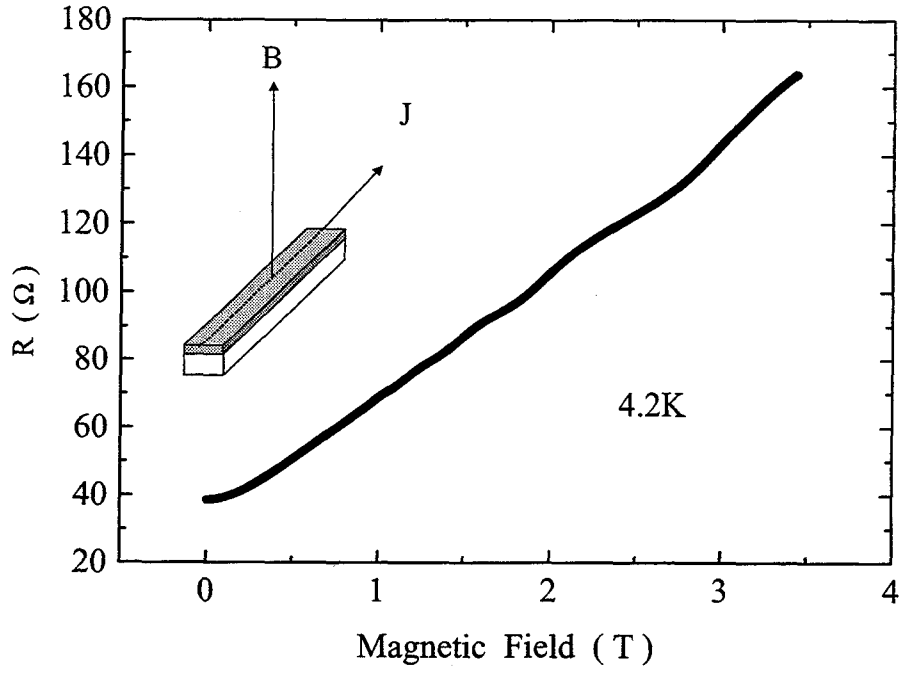

Fig.4.3.19 MR data at 4.2K for a perpendicular field.

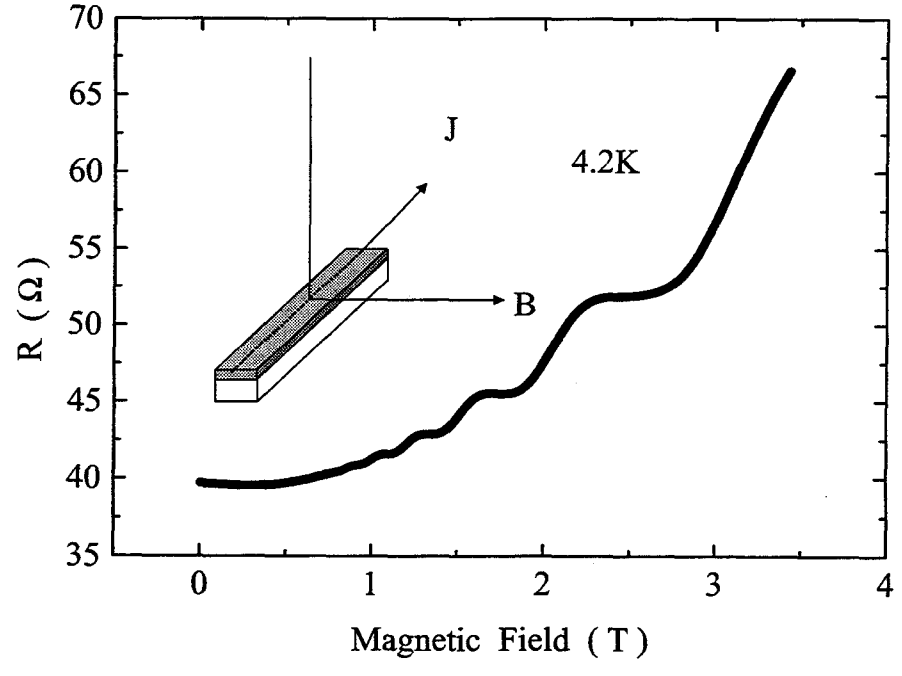

Fig.4.3.20 MR data at 4.2K. The direction of magnetic field is shown in the figure.

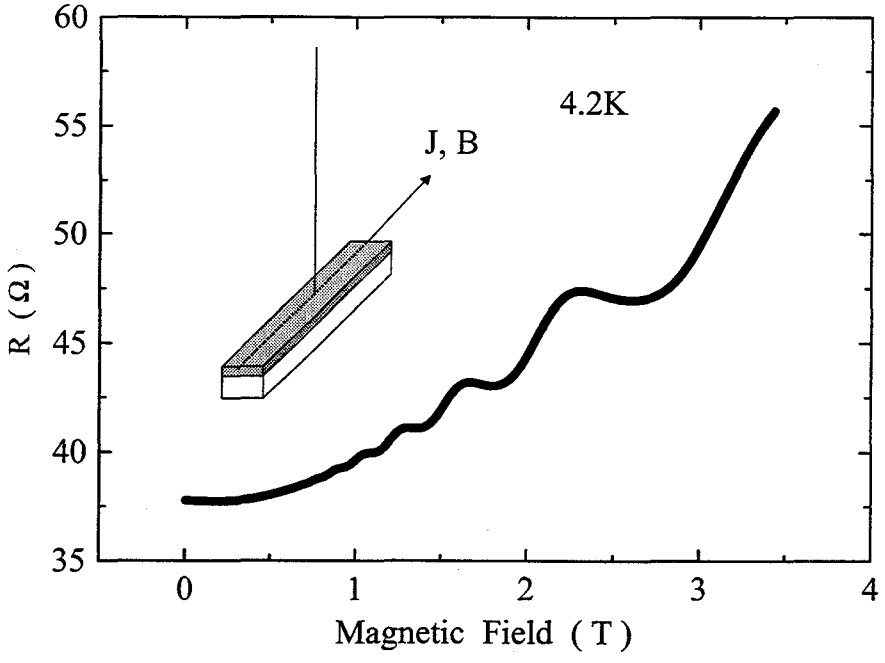

Fig.4.3.21 MR data at 4.2K. The direction of magnetic field is shown in the figure.

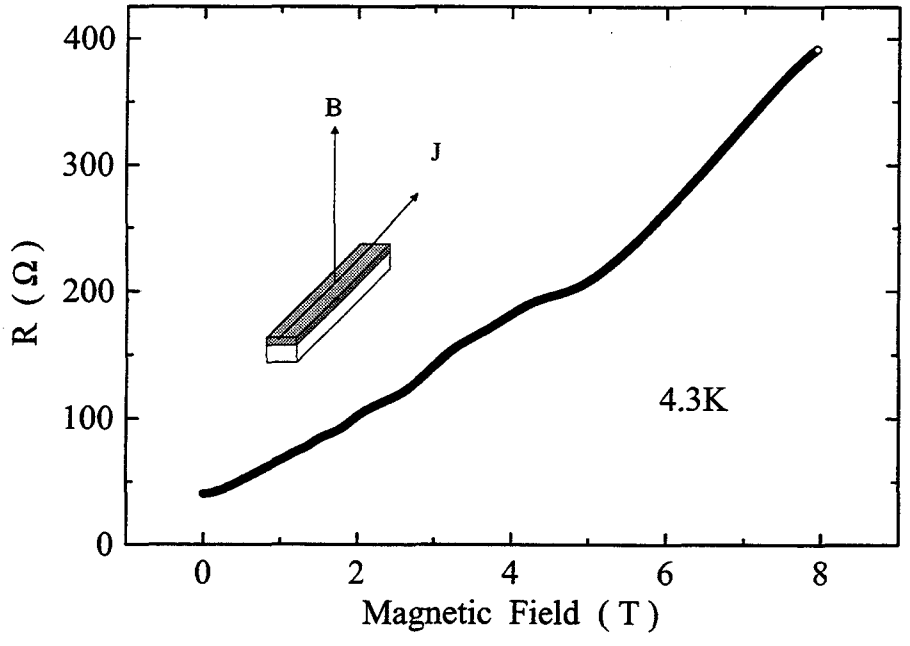

Fig.4.3.22 MR data up to 8T at 4.3K for a perpendicular field.

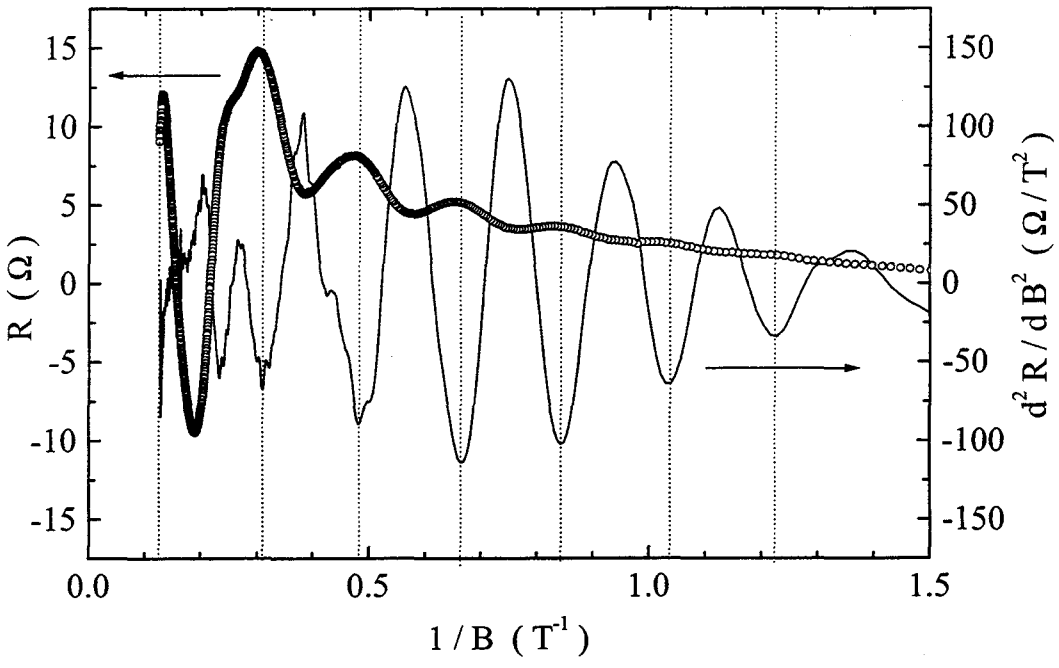

Fig.4.3.23 The results as a function of B^{-1}, which subtracts MR from B^2 (open circles) and differentiate MR twice with respect to B (solid line).

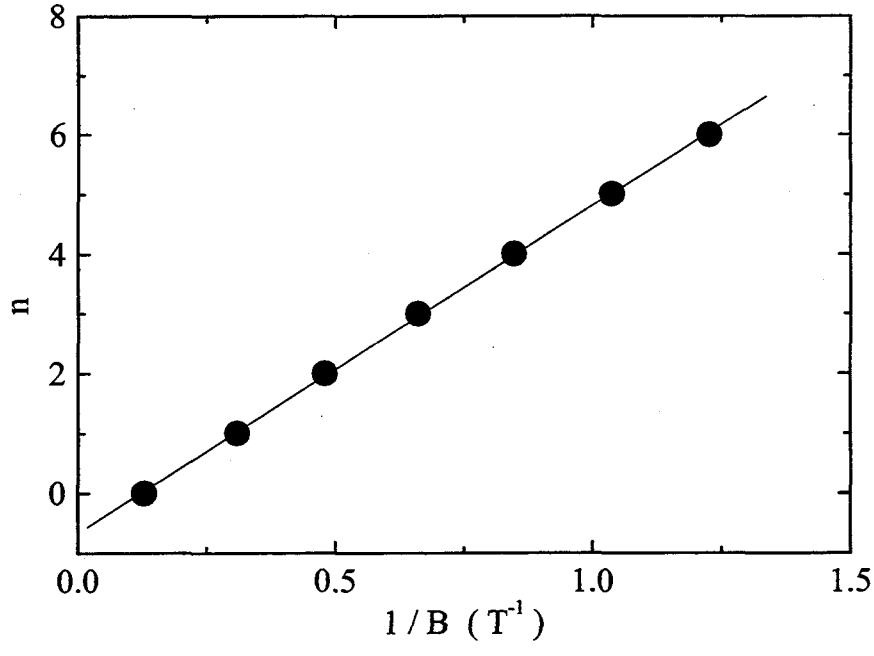

Fig.4.3.24 The result against the characteristic magnetic field where the extremum appear. The slope is in proportion to Fermi level.